Simulating Dynamic Vehicle Maneuvers Using Finite Elements For Use In Design Of Integrated Composite Structure

Nicholas A. Angelini

Thesis submitted to the Faculty of the
Virginia Polytechnic Institute and State University
in partial fulfillment of the requirements for the degree of

Master of Science
in
Mechanical Engineering

Robert L. West, Chair
Michael W. Hyer
Scott W. Case

February 20, 2014

Blacksburg, Virginia

Keywords: FSAE, Finite Elements, Vehicle Maneuvers, Composites

Simulating Dynamic Vehicle Maneuvers Using Finite Elements For Use In Design Of Integrated Composite Structure

Nicholas A. Angelini

(ABSTRACT)

Formula SAE (FSAE) chassis systems are increasing being manufactured with integrated composite structures in an effort to increase the performance of the system while decreasing weight. The increased use of composite structures requires more details of the loading conditions and evaluation metrics than the mild steel structures they are replacing. The prototypical FSAE steel space frame chassis designs are heavily structured around the mandated safety rules that doubled as mostly satisfactory structures for vehicle loads. The use of composite structures and the directionality of their material properties has created a need for more detailed loading scenarios to evaluate their ability to transfer load.

This thesis presents a framework for evaluating the chassis structure not only through the standard static twist analysis, but increased use of modal analysis and dynamic vehicle maneuvers using an attached suspension. The suspension joints and springs/dampers are modeled using Abaqus Connector Elements, allowing for the use of complex kinematic degrees of freedom definitions required to accurately model the suspension behavior. The elements used to represent the joints and springs are detailed as well as their superiority over traditional multi-point constraints in this context.

The use of modal analysis is used for a more direct comparison of not only the efficiency of stiffness in the chassis alone, but also how the chassis interacts with the suspension. The natural frequencies from the modal analysis along with the static twist distribution along the chassis are presented as a replacement for the static torsional stiffness performance metric.

By using dynamic vehicle maneuvers the chassis-suspension structure can be evaluated based on loads developed during the typical use of the FSAE vehicle. The dynamic nature of the analysis also allows for the inclusion of mass in the loading profile as well as the load variation with time that can be hard to achieve with static analysis. The framework for a bump event as well as a constant-speed-constant-radius turn are presented. The bump analysis is designed to evaluate the system's response to straight line dynamic events, while the turning maneuver evaluates the lateral components of the suspension load transfer capabilities. For the turn analysis both a spring/damper tire model using connector elements and a rolling tire model are presented. Intermediate checks on suspension and chassis behavior are evaluated to verify the modeling techniques; while the maneuver results are evaluated based on trends and overall motion rather than magnitudes due to lack of data at the time of the analysis.

Acknowledgements

I would like to thank my advisor Dr. Bob West for the opportunity to pursue this research as well as all his guidance throughout the project. I would also like to thank Dr. Mike Hyer and Dr. Scott Case for their patience and assistance throughout the many paths this project went through.

I would also like to thank Dan Lluch and the Mathworks team for their assistance throughout the project. Also, the help of the entire Virginia Tech Formula SAE team was critical to many aspects of this research.

And finally without the love and support of my girlfriend Krystina and my entire family this would not be possible.

Contents

List of Figures

List of Tables

Nomenclature

Bell Cranks Rocker arm connecting the motion of the wheel to that of the spring

Chassis Frame not including suspension

Control Arm Suspension members design to control the suspension geometry

FH Front Roll Hoop

FLCAA Front Lower Control Arm Aft

FLCAF Front Lower Control Arm Fore

FUCAA Front Upper Control Arm Aft

FUCAF Front Upper Control Arm Fore

GROUND-LF Left front ground node

GROUND-LR Left rear ground node

GROUND-RF Right front ground node

GROUND-RR Right rear ground node

LF Left front wheel center node

LR Left rear wheel center node

MH Main Roll Hoop

RF Right front wheel center node

RLCAA Rear Lower Control Arm Aft

RLCAF Rear Lower Control Arm Fore

RR Right rear wheel center node

RUCAA Rear Upper Control Arm Aft

RUCAF Rear Upper Control Arm Fore

Suspension Control Arms, springs/damper

Tie Rods Suspension member connecting the steering rack to the front uprights

Toe Rods Suspension member connecting the rear uprights to the chassis to control toe angle

Chapter 1

Introduction

1.1 Research Objective

Formula SAE (FSAE) is a competition organized by the Society of Automotive Engineers (SAE) for university students to design and build single seat open-wheel weekend race cars. Most of the chassis structure is outlined in the rules documentation [20] to specify general structure configuration and materials allowed. But, recently there has been an increase in use of composite materials among teams in the competition, requiring more sophisticated analysis by design teams to create equivalent structures to pass inspection. Until recently most of what was needed for structural equivalence was not standardized or published, but now the rules committee has outlined a static analysis to perform to make sure deviations from the standard structure meet safety requirements. With a more structured approach to validating structures, the Virginia Tech FSAE (VT FSAE) team intends to start incorporating more integrated composite structures into the chassis design.

While the new rules do provide guidance for safety concerns, they do not help with designing the structures for loads experienced during typical driving of the vehicle. The safety conditions provide a semi-standard chassis structure, but also leaves a significant portion of the structure left to be tailored to particular vehicles. It is this leftover structure the VT FSAE team has identified to drastically increase the performance of the chassis and the vehicle in general by using integrated composite structures.

In order to effectively use composite structures, composite structures need to be tailored to transfer loads in particular directions; this requires accurate loading scenarios. Currently, the method for developing loading scenarios hinges on using vehicle dynamics equations or multi-body simulation software, each considers the structures as rigid. The rigidity assumption is not fully understood, only rule of thumb assumptions for static stiffness to equate rigidity in dynamic environments.

The objective of this research is to develop a framework for simulation of vehicle maneuvers using elastic structures to test the rigidity assumptions and develop more accurate loading scenarios to design the chassis and specifically integrated composite structure.

1.2 Hypothesis

Vehicle loads are usually derived from vehicle dynamics equations assuming components are rigid bodies rather than the elastic structures they are. The equations typically over simplify most of the detailed interactions in the system. Vehicle dynamics equations are useful for evaluating suspension parameters and performance, but only when the components, chassis and suspension, are stiff enough to be considered rigid. The rigidity assumption raises the question of how to evaluate whether the component is stiff enough to be considered rigid. There are rule of thumbs for chassis stiffness, but they are not specific to a particular chassis or suspension design. The stiffness values are also evaluated statically for individual subsystems and do not account for the coupling of the dynamics between chassis and suspension.

Another option would be physical testing of existing vehicles to get loads for particular maneuvers. This is expensive both for equipment cost, but also time to run the same maneuvers over and over to get representative data. The VT FSAE team, like most teams, do not have access to professional drivers making it harder to consistently recreate the scenarios needed. There is also time to go through data collected and turn it into loading scenarios that can be used. Even then, the scenario is only good for that particular vehicle and setup. It does not provide the information needed to evaluate multiple designs.

Multi-body simulation software like ADAMS or CarSim can simulate vehicle maneuvers, but they are built on the same assumptions found in vehicle dynamics equations. Simulating vehicle maneuvers with elastic structures in finite element software will result in more accurate loading scenarios than rigid body simulation. Using finite elements will also be faster and with more detail than physical testing. Finite elements can also help to prove or disprove rigidity assumptions and provide better durability designs based on dynamic loading.

1.3 Objectives

The objectives of the research is outlined below:

1. Start with static analysis and show the shortcomings of purely static approach in general as well as reducing the chassis to a single stiffness value.
2. Move from static to modal analysis to provide a better understanding of the chassis-suspension interaction as well as the beginning step towards dynamic analysis.

3. Take a look at how attaching composite structure to existing steel structure can increase the performance metrics, static stiffness and natural frequencies, of the chassis.

4. Establish the framework for bump analysis to evaluate the straight line dynamics of the model.

5. Establish the framework for a constant-speed constant-radius turn to evaluate the non-straight line dynamics.

1.4 Scope

As there were not data available at the time of this research the vehicle maneuvers are evaluated only on trends and overall reaction. Magnitudes of spring displacements, loads at the tire contact patch, and stress/strains are not evaluated for accuracy. Also, the research focused only on the framework of developing loads for use in design of composite structure, therefore a detailed design of composite structures will not be presented here. The goal of the research is to present a framework for a chassis-suspension system to develop loads, and not present a detailed design.

Chapter 2

Background

Integrated composite structure is not new to Formula SAE or racing in general, with composite materials making up at-least 85% of a typical modern F1 race car [21] and a majority of FSAE teams using composites in some fashion or another. While composite material is a general term, encompassing many different materials, the VT FSAE team uses carbon fiber. Therefore the term composite can be taken to mean carbon fiber and other fiber-based composite materials unless otherwise stated.

2.1 Integrated Structure

Integrated structure in the context of this thesis is simply combining structures together to form one load sharing structure. The structures do not need to be made of different materials, rather originally intended for different functions but designed to work together. The aerospace industry has been using integrated structures for decades by integrating the skin into the structure to distribute load, typically called a bulkhead-shear-skin design. This involves creating a series of bulkheads that are responsible for the attachment of other components, loads normal to the structure, compressive loads, and outlining the overall shape of the structure. These bulkheads are generally made from and connected together using classical materials. The openings left are then closed by attaching composite panels that are responsible for tension and shear loads [17]. Integrated structure does not have to be permanently attached through welding or bonding, but they are the more efficient method as there is less compliance than using bolts, rivets, and other less permanent methods.

2.2 Composites

"A composite material is any material that consists of at least two constituents" [12]. Alloys can be considered composite materials, but are generally not grouped with composites since alloys mix at a molecular level whereas composites are considered to mix at the macro or physical level. Examples of composite materials include reinforced concrete, wood, fiber glass, and carbon fiber. Here composite material will be used to describe fiber composites in general and specifically carbon fiber since that will be the material of choice for the work to follow.

Carbon-fiber reinforced polymers, also called graphite reinforced polymers (GRP), are strands of carbon mixed with a matrix material that keep the fibers aligned in the direction needed and parallel to the other fibers. This is important because fiber composites only have desirable stiffness in the direction the fibers are oriented. This is different from homogeneous isotropic materials where the stiffness of the material does not vary with orientation a statistically significant amount. This is one reason that knowing not only the load magnitudes, but directions as well is extremely important when designing composite structures. Figure 2.1 shows a simple example of a composite panel with a load applied in one direction, and how the strains are affected by the direction the fibers are pointing. The calculations were done using Classical Lamination Theory equations found in Hyer [9].

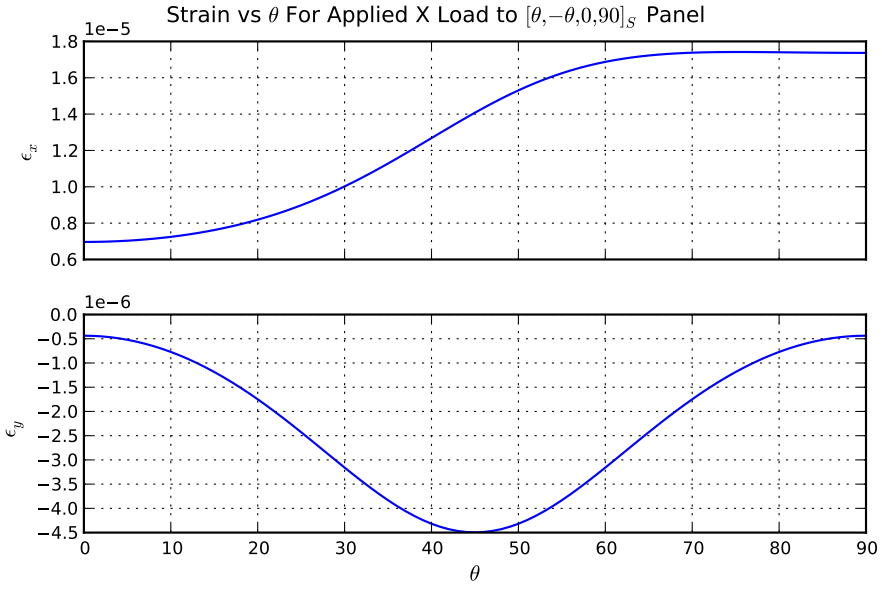

Figure 2.1: Plot of strains for applied load in global X direction.

Figure 2.1 shows that as the fibers move farther away from the axis of applied load the strain increases, reinforcing the idea that the fibers need to be aligned with the axis of applied load to be most effective. The order in which the layers of carbon fiber are stacked also plays a

role in the overall stiffness of the structure. By moving fibers farther from the neutral axis of the structure the bending and torsional natural frequencies will increase. Figures 2.2 and 2.3 show the effect of panel layup on natural frequencies and the effect of increasing the core size on natural frequency. Adding core material to the carbon fiber structure is an effective way of moving fibers farther away from the neutral axis without increasing the weight significantly. In Figures 2.2 and 2.3 the models were run with the symmetric layups listed on the y-axis. For Figure 2.2 a $[45/-45/0]$ symmetric layup would be $[45/-45/0/0/-45/45]$ and in Figure 2.3 $[45/-45/90]$ would be $[45/-45/90/\text{core}/90/-45/45]$. The panels are based on geometry from the floor panels on the Virginia Tech 2012 FSAE chassis.

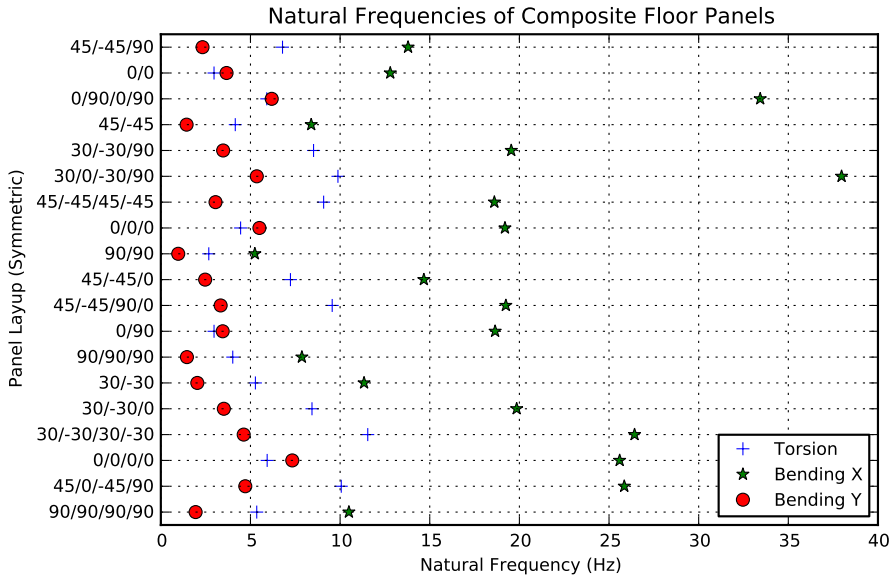

Figure 2.2: Plot of natural frequencies for different floor panel layups.

Another reason the load scenario is so important is that the manufacture of composite structures can be significantly more expensive than typical metal alternatives. Not only can the raw materials for composites be more expensive to acquire and manufacture, but the other materials needed for building the structure as well as the time needed to build the structure all contribute to the cost of the structure. Of these costs, the time required for building the structure, placing the fiber plies in their correct orientation, applying the matrix material, assembling the bagging materials for placing the structure under vacuum to cure is the most expensive for most FSAE teams. If the structure is not designed correctly from the beginning, making a new structure or repairing the original is an expensive and time prohibitive process.

So why use composites if they are more expensive and harder to design for? It mainly comes down to the stiffness to weight ratio of the composites. In racing and other ventures lighter and stronger is almost always the performance goal. With racing and aerospace in

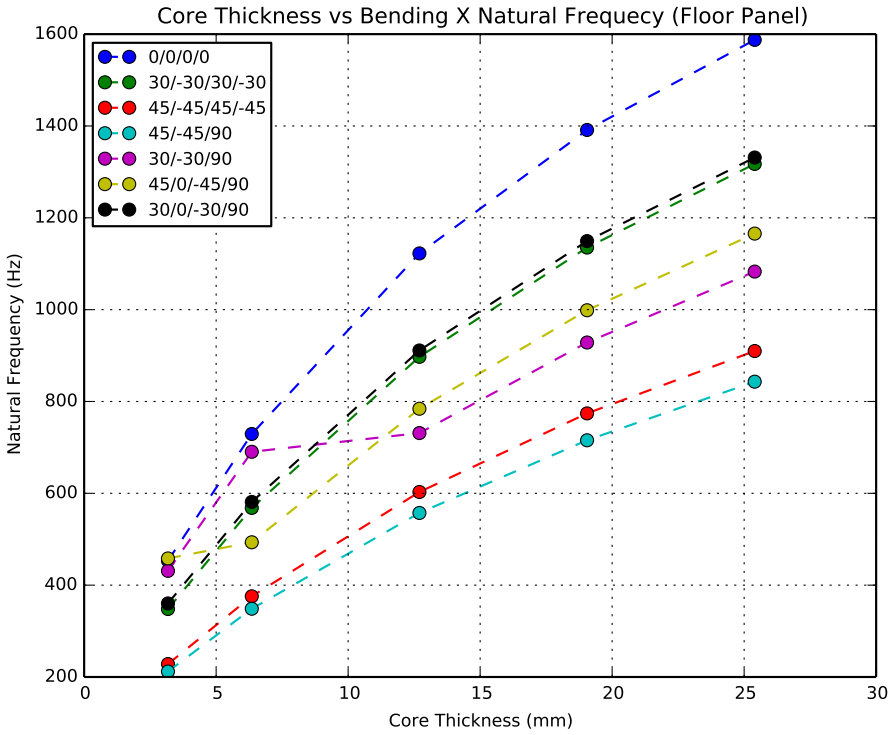

Figure 2.3: Plot of natural frequencies for different floor panel core thicknesses.

particular, the industry is willing to pay a premium for lightweight. Table 2.1 below shows typical material properties for composites and metals where E1, E2, and E3 are the elastic moduli in the 1, 2 and 3 (through thickness) direction as defined in Figure 2.4. As Table 2.1 shows, a typical GRP composite has superior stiffness properties in the fiber direction with more than double the elastic modulus of aluminum, and half the density.

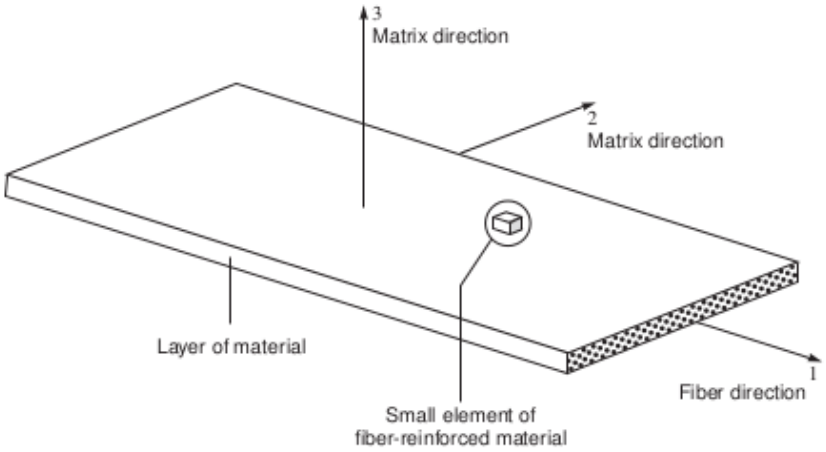

Figure 2.4: Figure showing the direction definitions for the elastic moduli. Reprinted from Stress Analysis of Fiber-Reinforced Composite Materials, by Michael Hyer, Copyright 2009, Lancaster, PA: DEStech Publications, Inc. [9]

With superior properties in the fiber directions of the composites, the designer can begin to tailor the composite structure to align the fibers in the best direction(s) to transfer the applied load(s). This is where the carbon fiber composite structures become most useful, being able to use less material and align the stiffness where it is needed.

As stated previously, along with the preceding figures, when building composite structures it is extremely important to have accurate loading scenarios. The structures need to be tailored to have stiffness in particular directions to resist the loads. If the composites are designed to have equal stiffness in all directions, the benefits and uniqueness of the composite may not effectively utilized.

Table 2.1: Typical engineering properties of several materials. Reproduced from Stress Analysis of Fiber-Reinforced Composite Materials, by Michael Hyer, Copyright 2009, Lancaster, PA: DEStech Publications, Inc. [9]

	Graphite-polymer composite	**Glass-polymer composite**	**Aluminum**
E_1	155.0 GPa	50 GPa	72.4 GPa
E_2	12.10 GPa	15.20 GPa	72.4 GPa
E_3	12.10 GPa	15.20 GPa	72.4 GPa
ν_{23}	0.458	0.428	0.3
ν_{13}	0.248	0.254	0.3
ν_{12}	0.248	0.254	0.3
G_{23}	3.20 GPa	3.28 GPa	27.8 GPa
G_{13}	4.40 GPa	4.70 GPa	27.8 GPa
G_{12}	4.40 GPa	4.70 GPa	27.8 GPa

2.3 FSAE Chassis Design and Analysis

Most FSAE teams use some variation of the methods presented by Riley [18, 19] to design and analyze their chassis. "Most teams" should be taken to mean teams that have published their process/results. The number of teams and the amount of resources, both monetary and technical, vary widely across the teams and would not be wise to group them all together.

Literature on the FSAE chassis design and analysis process usually only entails static analysis of the chassis and is mostly concerned with the static torsional stiffness of the frame. Most papers only present the relationship between chassis stiffness and other aspects of the vehicle like roll stiffness or camber stiffness. Riley's SAE paper [19] looks at how torsional stiffness of the chassis affects the apparent overall system stiffness. Crocombe [3] looks at how the torsional stiffness of the chassis affects the vehicle dynamics. Thompson [26] looks at chassis stiffness and roll stiffness of the suspension. These papers evaluate the chassis as purely a spring in series with the suspension. While this approach does have value when considering vehicle dynamics equations they only provide rough rule-of-thumb design parameters and only for torsional stiffness.

Riley's thesis [18] does do a good job of presenting and summarizing the ideas found in Costin [14] related to load paths and the process that goes into designing a chassis and adapts them to the FSAE framework. Riley also presents looking at the modal characteristics of the

chassis and suspension system separately and together, recognizing that it is an important part of the chassis design. Though he does report the calculated natural frequencies, he does not discuss the importance of natural frequencies. It is important to design the chassis with natural frequencies that are sufficiently separated from suspension modes to prevent interaction. While this still seems like the rule of thumb associated with torsional stiffness, natural frequencies do provide mass information and provide a stepping stone to full dynamic analysis as well as an experiment that is easier to reproduce. With a free-free modal analysis there are no boundary conditions to calibrate a model to. While Riley does go into detail on modal analysis in the thesis, there is still no mention of loading scenarios to evaluate stresses, strains, and failure.

Steed [24] states that the Cincinnati FSAE team started out using natural frequencies as a measure of stiffness for the chassis. He also makes sure to include non-rigid suspension members in his static torsion analysis and used beam elements for modeling the suspension arms. In most of the other literature, suspension members are modeled as truss elements because the assumption is that they are two force members. Borg [2] showed, when considering suspension member loads bending should be taken into account. In order to model bending, beams need to be used instead of trusses.

The decision to use elastic geometry is important because great effort is put into designing a fixture to be able to do the static torsion test. There is also a lot of effort made to correlate boundary conditions in the finite element models with the experiment. Not including elastic suspension members, and modeling the joints correctly, can result in poor experimental correlation. When trying to line up experimental data with calculated data it is important to model as much of the real system as possible, otherwise it becomes more difficult to assess where the error is coming from.

The literature also tries to establish a torsional stiffness goal, 8-10 times the roll stiffness of the suspension, to achieve when designing the chassis, but do not mention anything of bending stiffness, longitudinal or lateral. This is mainly because according to Miliken [15] "... a chassis that has good torsional stiffness also has adequate bending stiffness." Both the literature and RCVD recommend a stiffness factor above the suspension's roll stiffness. This idea is rooted in the idea of adding springs in series, that given a large enough chassis stiffness the system will only see the suspension spring. This is a static design criteria that does not take into account the natural frequencies.

The most common method for measuring torsional stiffness of the chassis is some variation of what is found in Riley's work. It involves fixing one end of the vehicle, while applying a known force to one of the hubs on the other end thus producing a torque. One can then calculate the stiffness from the measured deflections. The assumption is that with rigid springs in place of real ones, perfect suspension joints, and rigid suspension members all the load is transmitted into the chassis and that all the deflection in the chassis is due to torsion. But given that the load applied does not create a pure torque and as shown in Peery [17] pure torsion occurs about the elastic axis of the structure it is not likely the deflection of the

chassis are due to pure torsion. The axis of twist, in general, passes through the shear centers of the different cross-sections. Despite the limitations and caveats for the static torsion test, it is still considered an adequate method for determining static stiffness.

While at the time of this writing there does not seem to be published literature of teams using loading scenarios to design their chassis, such analysis is likely being done. The current state of these loading scenarios, like some of the Virginia Tech scenarios, are most likely based in vehicle dynamics models assuming rigid components or pure experimental data. Teams like Texas A&M [16] are doing full vehicle models in software like Adams, and other teams simulating vehicle dynamics with other methods based in rigid-body dynamics.

Though not an FSAE system, Hellman [7] begins to simulate vehicle dynamics in finite elements as well as in Adams. His work in Abaqus begins to show how to incorporate the suspension components into finite element software and begin to simulate vehicle maneuvers. Hellman found good correlation between Abaqus and Adams spring force/displacement results in straight-line dynamics and bump analysis. Due to lack of tire models he did not consider turning maneuvers. Hellman's goal was to show that vehicle maneuvers could be simulated using finite element code for consolidation of simulation software for small companies. By simulating the maneuvers in finite element code the companies likely already have there would not be a need to purchase multi-body simulation software. While Hellman uses elastic components in his models, his primary goal and future goals centers on using Abaqus as an Adams alternative. Abaqus, using rigid bodies, can effectively represent Adams simulations the power of using Abaqus would be the ability to evaluate the elastic response of the components during the simulations.

2.4 Modal Analysis

Modal analysis is the evaluation of structures and systems and their response to known frequency dependent input [5]. While there are other values and information to be obtained from modal analysis and modal testing, the primary goal is to obtain the natural frequencies and mode shapes of the system or structure. Ewins [5] defines natural frequencies as "the frequencies at which free vibration of the system can take place." These are usually evaluated numerically from solving an eigenvalue problem using the relationships between the system's stiffness and mass/inertia characteristics. This relationship is called the frequency equation. In Abaqus the frequency equation is typically written as in Equation 2.1 [25]:

$$(-\omega^2[M] + [K])\{\phi\} = 0 \tag{2.1}$$

where $[M]$ is the mass matrix, $[K]$ is the stiffness matrix, ω is the eigenvalue, cyclic frequency in rad/s, and ϕ is the eigenvector. From the eigenvalue solution, the analyst can obtain the natural frequencies (eigenvalues) and the mode shapes (eigenvectors), a scaled displacement

field of the system.

The eigenvalue problem, along with the eigenvalues and eigenvectors, is a mathematical transformation of the problem in an effort to decouple a complex coupled multiple-degree-of-freedom system into simpler single-degree-of-freedom system. The modal transformation forces the mass and stiffness matrices to become diagonal. The eigenvalues and eigenvectors from the solution do not represent the true shape of the structure, but rather an idealized mathematical scaled representation of the free vibration of the modes of vibration.

In the real response, the structure experiences resonance, a large amplitude response to specific input frequencies, around the frequencies. This resonance does not occur at one particular frequency as in the eigenvalue problem, but rather a range of frequencies around the "natural frequencies". The frequencies are unique to the structure and dependent on geometry, materials, and boundary conditions. The actual vibration deformed shape, also referred to as operational shape, will also be representative of the mode shape near the resonant frequencies. If the mass and stiffness representations in the eigenvalue problem are representative, the natural frequencies should be close to the range in the tests and the operational shape should resemble the mode shape from the eigenvectors.

2.5 Elastic Dynamic Vehicle Maneuvers

There is limited published research in modeling of vehicle maneuvers using finite elements, even fewer using elastic components as most simulations are done using rigid body formulations. As mentioned earlier, Hellman [7] does begin to look at modeling vehicle maneuvers using a substructured Volvo frame and using connector elements to model the suspension joints. Hellman did not have an accurate tire model, so he was limited to straight line dynamics and bump analysis.

Grujicic [6] did do some research on vehicle maneuvers with finite elements on military vehicles. They focused on building off an explicit model they developed earlier modeling tire-sand interaction and were successful in representing the maneuvers. In the work they compare the finite element results to multi-body simulations and found they were in agreement. Grujicic and Hellman have provided evidence that Abaqus can replicate the solutions from accepted multi-body software. The similarity in the solutions also shows the structures in the simulations can considered rigid bodies

In an Abaqus Technology Brief [23] simulating an aircraft landing gear using rigid bodies and connector elements using Abaqus finite element software was evaluated. Rigid components were later replaced with elastic components to build a flexible-body dynamic solution. In this analysis they were concerned with designing a particular component of the system and thus were able to make it elastic while the remaining components were rigid. This process allows for systematically incorporating elastic components into a dynamic simulation.

2.6 Connector Elements

In Abaqus there a few different ways to model kinematic relationships between nodes, multi-point constraints(MPC), springs/dampers, and connector elements. MPCs and springs/-dampers are generally used to specify basic relationships, whether they are simple elastic spring/damper or tied together. The advantage of using connector elements instead of the springs/dampers or MPCs is that unlike MPCs they do not delete nodes from the solution and they allow for complex relationships relative to a local coordinate system that moves with the model. This complexity does mean MPCs tend to be more computationally efficient than connector elements, but the utility of connector elements lies in the complex relationship between kinematic degrees of freedom of specific joints that can be effectively accounted for and included in a finite element model.

In simplest terms, connector elements define degrees of freedom that can have relative motion between two nodes relative to a particular coordinate system. These relative degrees of freedom can then be given properties like elastic stiffness, damping, friction, allowable range of motion, etc. For example a damper could be modeled as a connector element where the relative degree of freedom would be the 1-direction in a coordinate system where the 1-axis is the line connecting the two nodes. A damping constant can be prescribed as well as stops to mimic the amount of motion available in the real system. An example is shown in Figure 2.5 where nodes 11 and 12 represent the two ends of the of a shock.

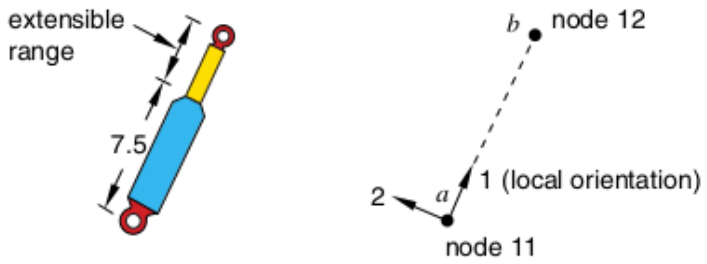

Figure 2.5: Figure of shock modeled as a connector element. From Abaqus 6.13 Documentation, Dassault Systemes, Providence, RI, USA, 2013 [25]. Used under fair use, 2014.

In a general Abaqus model when forces, boundary conditions, or other relationships are defined relative to a local coordinate system, other than the global system, they are defined relative to the initial orientation of the local coordinate system. The defined system does not move with the model, and a transformation matrix is established to map the initial orientation of the new coordinate system into the global system. With connector elements, the user can define the degrees of freedom the two nodes have defined in a relative local coordinate system that will move with the model. Connector elements provide a systematic and consistent method for modeling complex kinematic relationships that would be otherwise

difficult with multi-point constraints while allowing for relative local data to be exported into the results file.

Chapter 3

Chassis/Suspension Models

3.1 Coordinate System

In all models discussed the global coordinate system and positive directions are as follows:

- X-axis/U1 runs from the rear of the chassis to the front parallel to its centerline.
- Y-axis/U2 points to the driver's right.
- Z-axis/U3 points down towards the ground plane.
- 4-direction/Roll/UR1 is rotation about the 1-axis.
- 5-direction/Pitch/UR2 is rotation about the 2-axis.
- 6-direction/Yaw/UR3 is rotation about the 3-axis.

The above list only details the global coordinate system. The connector elements discussed later also have local coordinate systems that will be defined using the same nomenclature as above. Figure 3.1 shows the coordinate system in more detail. If no designation is given, the assumption is the direction is in the global coordinate system. All the chassis figures to follow have the coordinate system arrows in the lower left of the image.

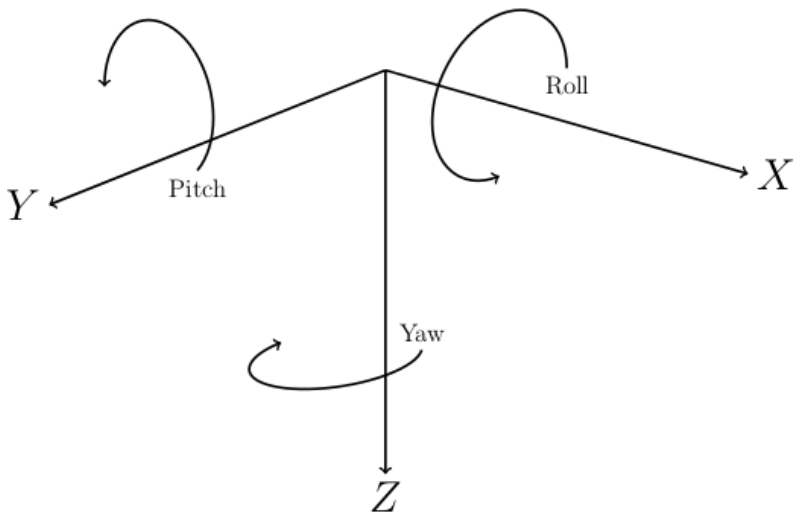

Figure 3.1: Iso view of coordinate system

3.2 Base Chassis Models

3.2.1 Base Model

The base chassis model was the 2012 VT FSAE 4130 steel space frame chassis without any composite structure shown in Figures 3.2 and 3.3. The geometry was extracted from NX5, a computer-aided-design software package, as points and lines in comma-separated (CSV) files as follows:

- Node File – contains node numbers and coordinates.
- Connectivity File – contains how the nodes are connected together to form the structure. This file also contains the section property keys for the tubes.

Each node, tube/line, and group of nodes and lines were given set names. Sets in Abaqus are containers for geometry, nodes, surfaces, and other such items that are grouped together with a name and are used as references for section properties, boundary conditions and loads among others. The set names were used to establish connectivity for the lines in the chassis. Python scripts were written to build this geometry and the suspension geometry to follow in Abaqus using its Python scripting interface and editing Abaqus input files. An example of the node and connectivity files as well as python scripts can be found in Appendix B.

The Abaqus input file (.inp) is a flexible format allowing for input from other .inps as well as using parameter definitions. Numerous chassis or other structural components can be created

independently and input into the main file when needed. An example is shown in Appendix B. By building the geometry and setting up the analysis parameters this way establishes a method for parametrization of the chassis design process allowing for any number of changes, geometrically, material, section, mesh density or anything else. This process allows for greater control of exploring the design and evaluating changes. For example, if the designer wanted to look at the structural effect of moving the front roll hoop closer to the front bulkhead without a parameterized model, the designer would need to go back to the CAD software and regenerate the geometry files and import the updated geometry file back into Abaqus. The entire model would need to be setup again with the correct section properties and loading scenarios, but if the nodes and connectivity are parameterized the parameter controlling the distance between the two would just need to be changed and run the script to update the model. It generates a little more work up front creating the scripts, but saves times in the long run and allows for exploring the solutions and details of the models as well as optimization.

In the base model all the tubes are modeled as beam elements. Beam elements are used for the tubes of the chassis because the cross-sectional geometry of tubes is small compared to the dimensions along the length. The assumption that large amounts of bending or axial deformation does not occur is also important when considering beam elements. The preferred beam element in Abaqus is B32. B32 is the element code in Abaqus for a 3-D quadratic shear-flexible Timoshenko beam element developed using a hybrid element formulation [25]. Quadratic beam elements use quadratic LaGrange interpolation functions versus the linear function of linear elements allowing for more deformation shapes per beam. Quadratic beam elements also require a midpoint node definition thus adding more degrees of freedom to the model. More degrees of freedom means the elastic response of the chassis will not be hindered from overly stiff linear elements. Curved sections of the chassis are modeled as a series of straight lines, as beam elements can not be initially curved. The number of elements needed to represent the curve depends on the radius of the curve.

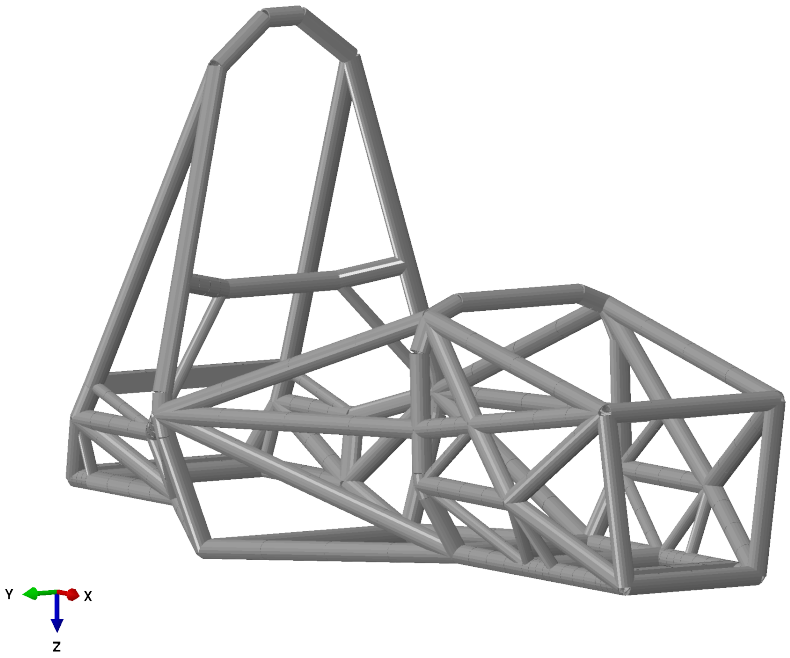

Figure 3.2: Angled view of base chassis.

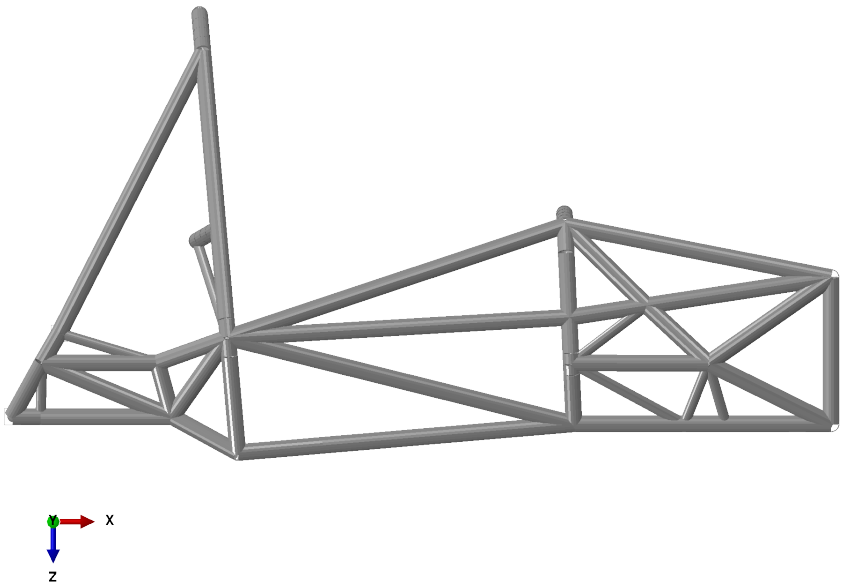

Figure 3.3: Side view of base chassis.

3.2.2 Rigid Model

The rigid model was the same geometry as the base model except the elastic modulus was increased. Based on observation an order of magnitude was enough for the beam element to become effectively rigid when considering the static twisting stiffness and modal analysis to follow. Increasing the elastic modulus too much can create solver issues because the analysis requires taking the inverse of the stiffness matrix. A rigid body definition was not used because elastic deformation was still needed. The structure only needed to act rigid when compared to the base model. The rigid model was used in both the static twist analysis and modal analysis as a comparison model.

3.3 Composite Models

The following section introduces the composite chassis models. These models are not true integrated composite structures, as they were not initially designed to have the composite structure carry load. The models represent closeout structures already attached to the 2012 chassis with clips and other non-permanent methods, and creating a more rigid structure. The composites in the following models only constitute a preliminary design where the composite layup was only designed to have stiffness aligned in particular directions to limit deflection shapes. They are not designed against a particular load or amount of deflection. The thicknesses of the composites are loosely based on structures already in use on the chassis. For these reasons the models can be thought of as a minimum performance for an integrated composite structure chassis and with proper design the performance metrics should only improve.

3.3.1 Composite Panels

The composite panels used on the composite chassis models are carbon fiber sandwich construction panels. Appendix A contains the material properties for the AS4 carbon fiber used, as well as for the Hexcel A1-64-6 honeycomb core. In the layup strings in the following sections the letter "c" will stand for core with the number following representing the thickness of the core in mm. For example, "c6.35", is a 6.35 mm honeycomb layer. When the symmetric designation is given the core layer it is only ignored for the second instance of the material. The symmetric layup is symmetric about the 6.35 mm core – $[45/-45/0/90/\text{c}6.35]_S$ would be $[45/-45/0/90/\text{c}6.35/90/0/-45/45]$. Also the following terms are used to designate different panels:

- Floor Driver – section in the cockpit where the driver sits, from the main to the front hoop.

- Floor Feet – section of the floor forward of the front roll hoop.
- Side Driver – side impact structure in the cockpit.
- Side Suspension – area forward of the front hoop where the suspension arms are mounted.
- Firewall – section in the main roll hoop separating the driver from the engine bay.
- Top Panel – section above the Floor Feet panel.

The composite panels are modeled using Abaqus S8R elements. S8R elements are 3-D doubly curved reduced integration shell elements with 6 degrees of freedom per node. The doubly curved shell element with reduced integration elements use a lower-integration element stiffness formulation, which reduces the amount of integration points within the element and therefore reduces the run time associated with the elements. Full integration is usually only needed when accurate stress gradients are required throughout the element, but the stresses and strains are not being evaluated. Therefore reduced integration provides accurate displacement shapes while reducing the model run time. A tie constraint is used to attach the panels to the chassis. The tie constraint represents an idealized attachment mechanism where the panel is permanently bonded to the chassis tubes, resulting in no losses in load transfer between the two structures.

The panel outline geometry is extracted from the chassis geometry and built using the loft tools in Abaqus. Lofting is a method to create complex sweeps where cross-sections at the beginning of the sweep paths does not have to match the cross-section at the end. This tool is especially useful when considering the panels like the top panel shown in Figure 3.4, the cross-section at one end of the panel is different than at the other end.

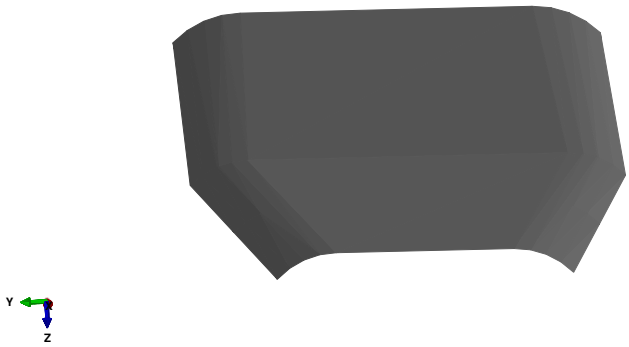

Figure 3.4: Figure showing the geometry of the top panel from the *Semi-monocoque* model.

3.3.2 Chassis Models

2012 Chassis

The 2012 Chassis model was the 2012 VT FSAE chassis as built. It was the same welded frame as the base model, except with a carbon composite floor. The geometry is shown in Figure 3.5. Some liberty has been taken with this model as the composite material used in model was different from what was actually installed on the chassis. The FSAE did not have the material data sheets and the carbon fiber was a bidirectional fabric rather than the unidirectional composite used in the rest of the models. This chassis will be referred to as *C2012*. The layup was as follows:

- Floor Driver – $[45/-45/0/90/45/-45/0/90/\text{c}12.7]_S$
- Floor Feet – $[45/-45/0/90/45/-45/\text{c}12.7]_S$

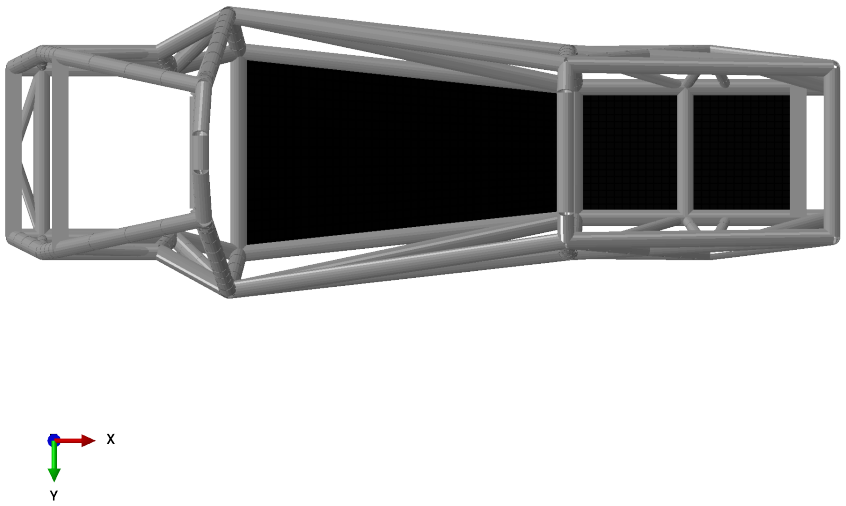

Figure 3.5: Top view of *C2012* model. Black section represents the composite structure.

Attached Composite Panels Chassis

The Attached Composite Panels Chassis model was the same geometry as the *C2012* chassis with the steel side impact structure replaced with a carbon composite sandwich structure, a different sandwich construction for the floor, and carbon composite sandwich structures have been added as a firewall and a closeout in the large open area above the driver's legs. The geometry for this model is shown in Figure 3.6. The 2012 vehicle does have a carbon composite firewall, but it was not used as a structural component of the chassis nor was it rigidly mounted to the chassis and the top panel was part the non-structural nose cone. Other than replacing the side impact structure, this model can be thought of as replacing the large open areas forward of the engine bay that are normally covered with closeouts with composite sandwich structure rigidly attached to the frame. From here on this chassis will be referred to as *Attached*. The layup was as follows:

- Floor Driver – $[45/-45/0/45/-45/0/90/0/\text{c}12.7]_S$
- Floor Feet – $[45/-45/0/45/-45/0/90/0/\text{c}6.35]_S$
- Side Driver – $[0/45/-45/45/-45/0/90/0/0/\text{c}12.7]_S$
- Firewall – $[45/-45/0/45/-45/90/0/90/\text{c}12.7]_S$

- Top Panel – $[45/-45/45/-45/0/0/0/\text{c}6.35]_S$

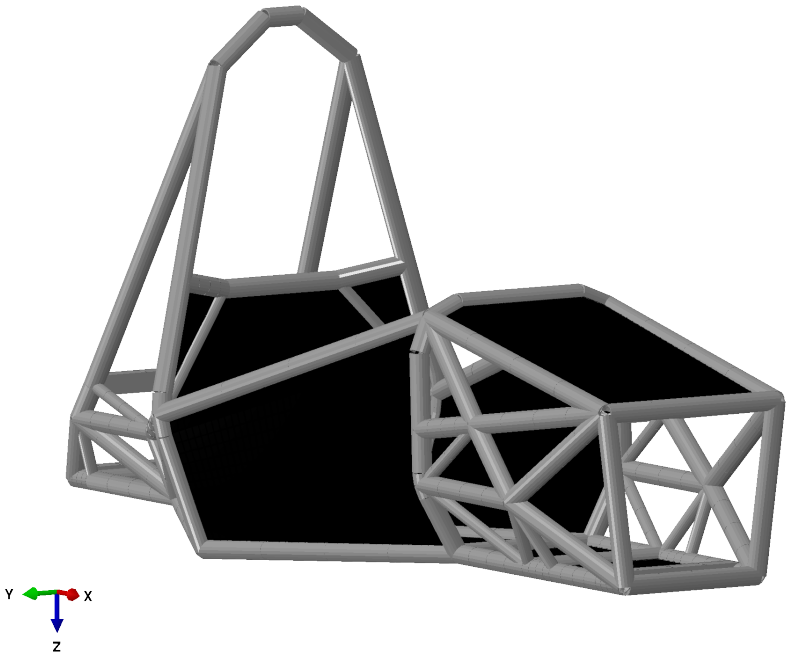

Figure 3.6: Iso view of Attached Composite Panel Model. Black section represents the composite structure.

Semi-monocoque

The *Semi-monocoque* Chassis model is similar to the structure in the driver's cell as the Attached model, but features a simple redesign of the structure forward of the front roll hoop. This structure was replaced with a series of bulkheads with the open areas filled with carbon composite sandwich structure. The front bulkhead was redesigned with a horseshoe shape to reduce sharp edges in the composite. Another bulkhead was added where the forward front control arms are mounted to the frame. There are then steel tubes to connect the bulkheads and give the overall shape. The open areas are then filled with the composite except for the small area to allow for the tie rods to pass. The geometry for this model is shown in Figure 3.7. The *Semi-monocoque* model was not analyzed to determine whether this structure was strong enough to handle loads from the suspension or not, but rather an exercise in creating more integrated structure to compare from a stiffness/natural frequency point of view. The only design consideration was to ensure the driver leg section would pass the template specification given by the FSAE rules. The suspension bulkhead was the same tube section as the front bulkhead and the connecting tubes are the same as used on the *C2012* chassis. This was done to create a heavier structure than was likely required,

and focus on minimum performance value. Part of the goal from this study was to show the minimum performance of the integrated structure was better than the maximum performance of the non-integrated composite steel frame chassis design. From here on this chassis will be referred to as *Semi-monocoque*. The layup was as follows:

- Floor Driver – $[45/-45/0/45/-45/0/90/0/\text{c}12.7]_S$
- Floor Feet – $[45/-45/0/45/-45/0/90/0/\text{c}6.35]_S$
- Side Driver – $[0/45/-45/45/-45/0/90/0/0/\text{c}12.7]_S$
- Side Suspension – $[0/45/-45/45/-45/0/90/0/0/\text{c}12.7]_S$
- Firewall – $[45/-45/0/45/-45/90/0/90/\text{c}12.7]_S$
- Top Panel – $[45/-45/45/-45/0/0/0/\text{c}6.35]_S$

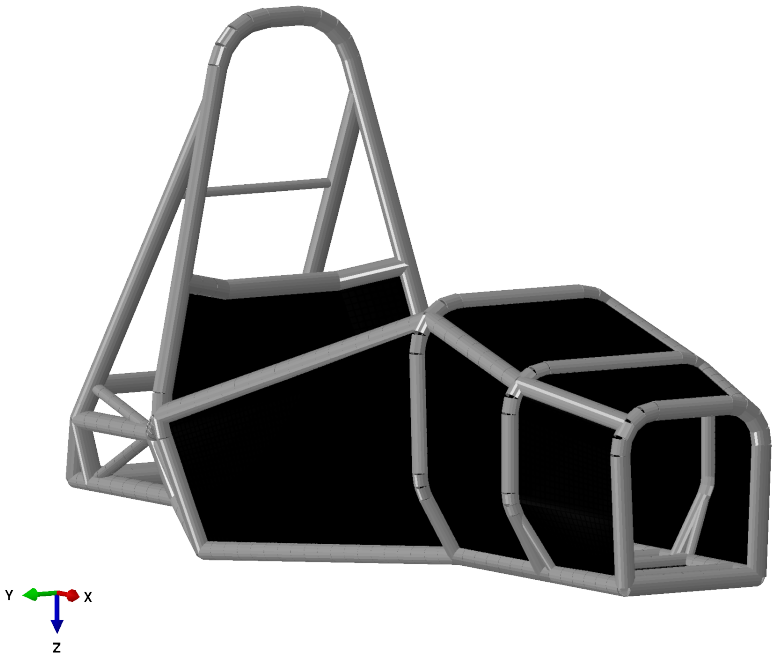

Figure 3.7: Iso view of *Semi-monocoque* Model. Black section represents the composite structure.

3.4 Suspension

The following section outlines the modeling techniques for the suspension components of the model. This includes both the physical components as well and the connector element joints.

Figures 3.8 and 3.9 show the overview of the front and rear suspension systems respectively. For Figures 3.8 and 3.9 and the figures to follow in this section the following shows the color codes used in the figures:

- White – Chassis
- Gray – Upright
- Blue – Control Arms
- Orange – Tie/Toe Rods
- Green – Pull Rods
- Red – Bell Cranks
- Purple – Steering Rack
- Yellow – Connector Elements

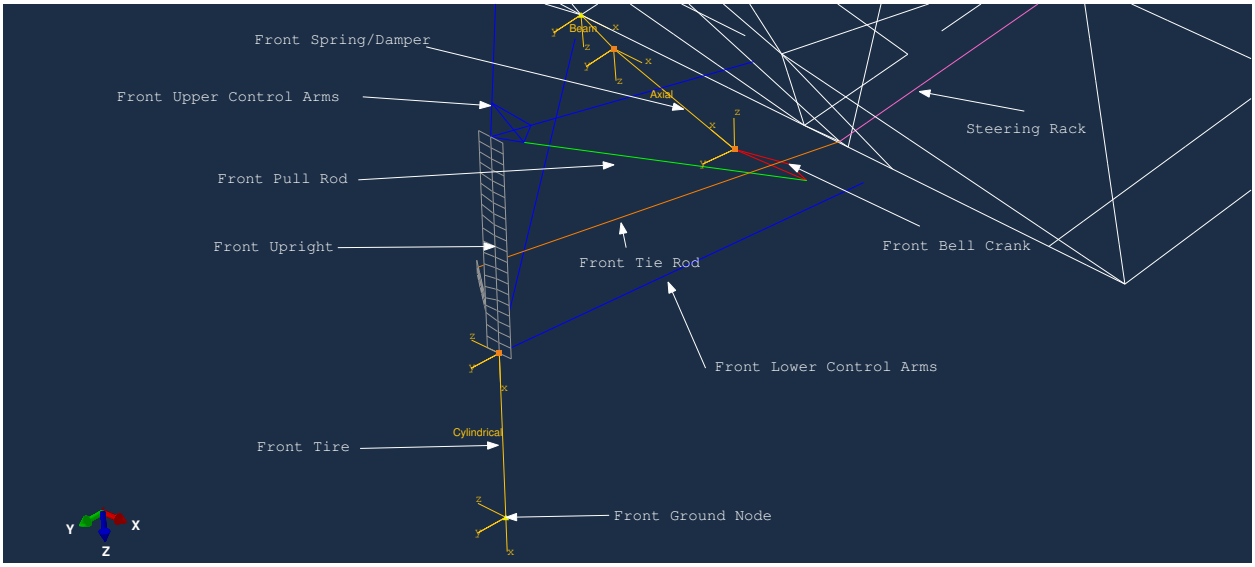

Figure 3.8: Front suspension overview.

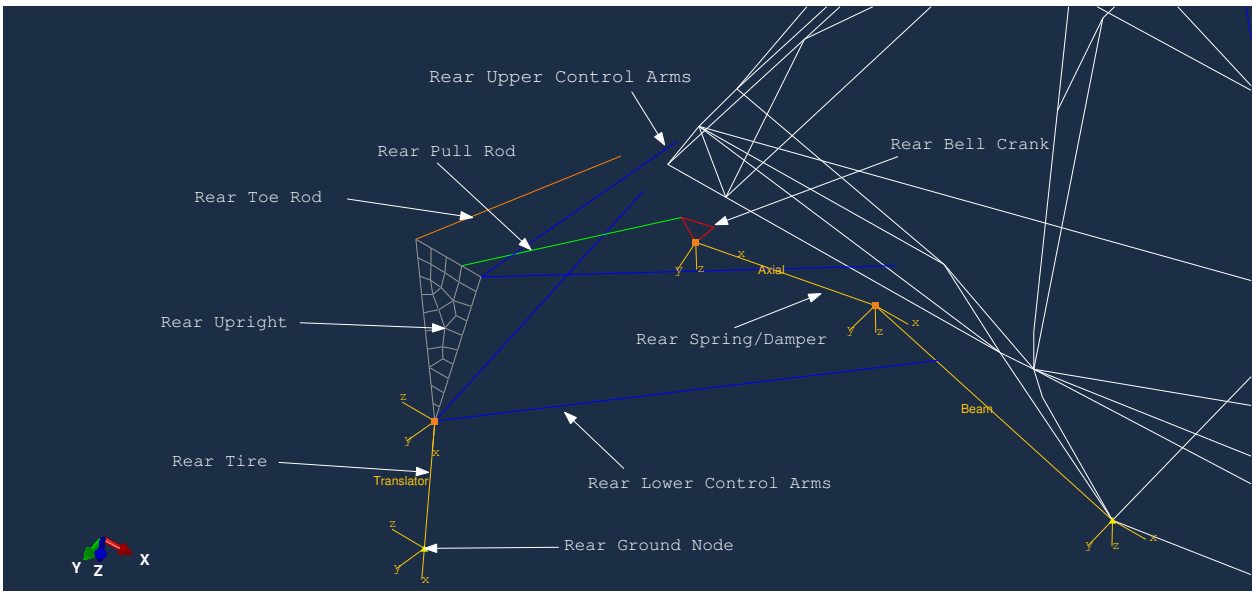

Figure 3.9: Rear suspension overview.

3.4.1 Suspension Arms

The goal in modeling the suspension was to create as simple a model as possible while still retaining the details needed to accurately create and react load. The suspension arms are modeled as pairs of elastic steel beams with linear 3-D beam elements (B31). By sharing the outboard point in the model, the pair of arms act as though they are welded together. Figures 3.10 and 3.11 show the geometry for the front upper and lower control arms. The rear control arms are modeled in a similar manner. Beam elements allow for bending and torsional deflection shapes necessary in the suspension members, while the linear elements reduce the number of degrees of freedom in the model. The suspension arms include the control arms, pull rods, and tie/toe rods with section properties of those used on the 2012 car.

Figure 3.10: Geometry of Front Upper Control Arms (FUCA)

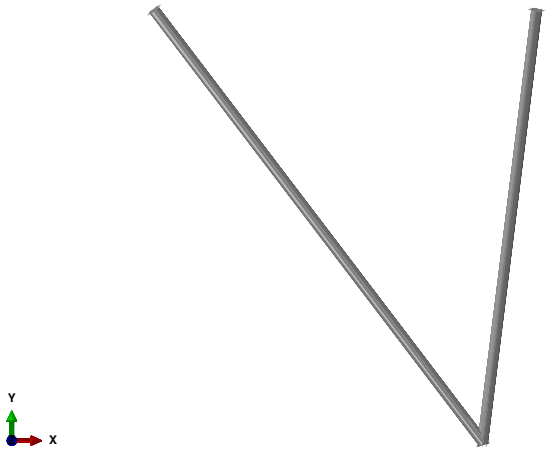

Figure 3.11: Geometry of Front Lower Control Arms (FLCA)

3.4.2 Bell Cranks

The bell cranks are modeled using solid rectangular beams, B31, by connecting the inboard pull rod point, outboard spring point, and the pivot. Figure 3.12 shows the bell crank geometry in more detail. The beam section reflects the overall thickness of the solid bell crank while ignoring small details in the design. In this case beams can reasonably reproduce the section properties needed and use less nodes/DOFs than a solid. Material properties are specified for an equivalent mass while maintaining the aluminum elastic properties.

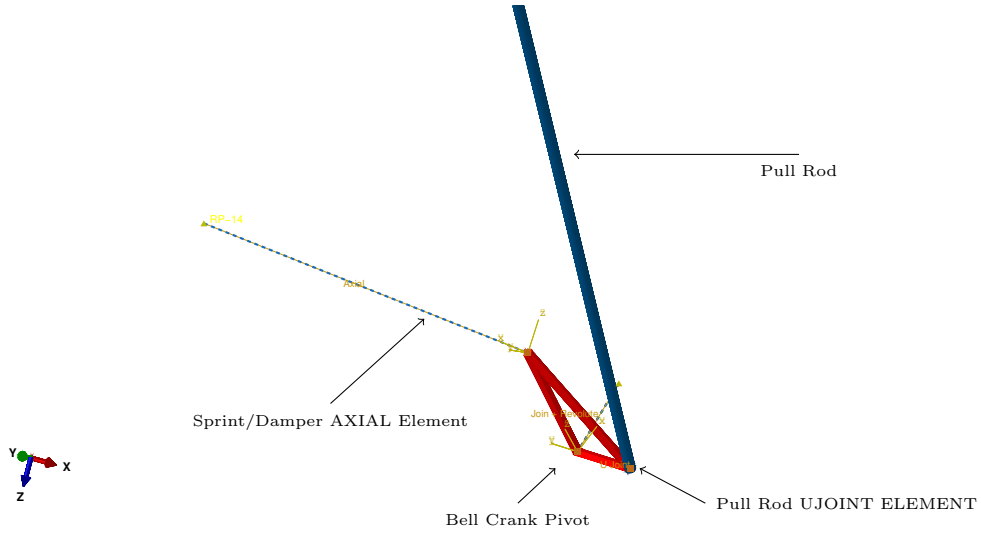

Figure 3.12: Front right bell crank geometry. Blue is the pull rod and the red triangle shape is the bell crank. The third node on the bell crank represents the pivot.

3.4.3 Springs/Dampers

Springs and dampers are modeled with AXIAL connector elements with a coordinate system created to orient the local x-axis along the line connecting the bell crank and chassis with degrees of freedom definition in Table 3.1. These elements are defined with nodes at the bell crank pickup points and the points in space where they are mounted. In Figure 3.12 the spring/damper is the AXIAL element on the left side of the bell crank. The AXIAL connector elements are given elastic and damping properties reflecting springs/dampers on the vehicle with limits on their relative displacement. Table 3.2 outlines the spring/damper properties. Limits on relative displacement for the connector elements are prescribed based on initial relative distance between nodes. Therefore when the stops are specified the initial distance between the nodes needs to be calculated and then added or subtracted to the allowable movement. For example the allowable movement for the springs in the model is 25.4 mm and the initial front distance between bell crank and spring mount is 169.39 mm. The stops for the connector would be defined as 143.96 and 194.76 mm.

Table 3.1: AXIAL Connector Element Definition

Available Degrees of Freedom	U1
Constrained Degrees of Freedom	N/A

Table 3.2: Spring/Damper AXIAL connector properties

Front Spring Constant	16.81 $\frac{N}{mm}$
Front Damper Constant	1.576 $\frac{Ns}{mm}$
Front Spring Limit	$\pm$25.4 mm
Rear Spring Constant	22.41 $\frac{N}{mm}$
Rear Damper Constant	1.978 $\frac{Ns}{mm}$
Rear Spring Limit	$\pm$25.4 mm

Table 3.1 shows the only available degree of freedom is the local x-direction with no constrained degrees of freedom. The connector element definitions to follow for the bell crank and spring attachment point will account for the restriction of motion needed. With no constrained degrees of freedom there can still be relative motion between the nodes, but only the local x-direction can be assigned properties.

3.4.4 Steering

The steering rack was modeled as a 3-D beam, B31, with elastic properties that make the section act as a rigid body. The beam is connected to the chassis using TRANSLATOR connector elements on both sides of the chassis with a local coordinate system such that the local x-axis points along the global y-axis at the start of the analysis. Figure 3.13 shows the details of the steering rack geometry and connection to the chassis. TRANSLATOR degrees of freedom definition is in Table 3.3. A connector behavior is defined to put stops on the rack movement and also some small elastic stiffness to keep Abaqus from actuating a displacement that does not have any stiffness. Table 3.4 details the properties used. Actual connector behavior values for the rack are not important for models, but is put in place for completeness as in future models they will be updated with system values.

Table 3.3: TRANSLATOR Connector Element Definition

Available Degrees of Freedom	U1
Constrained Degrees of Freedom	U2, U3, UR1, UR2, UR3

Table 3.4: Steering TRANSLATOR connector properties

Elastic Constant	10 $\frac{N}{mm}$
Rack Movement Limit	$\pm$76.2 mm

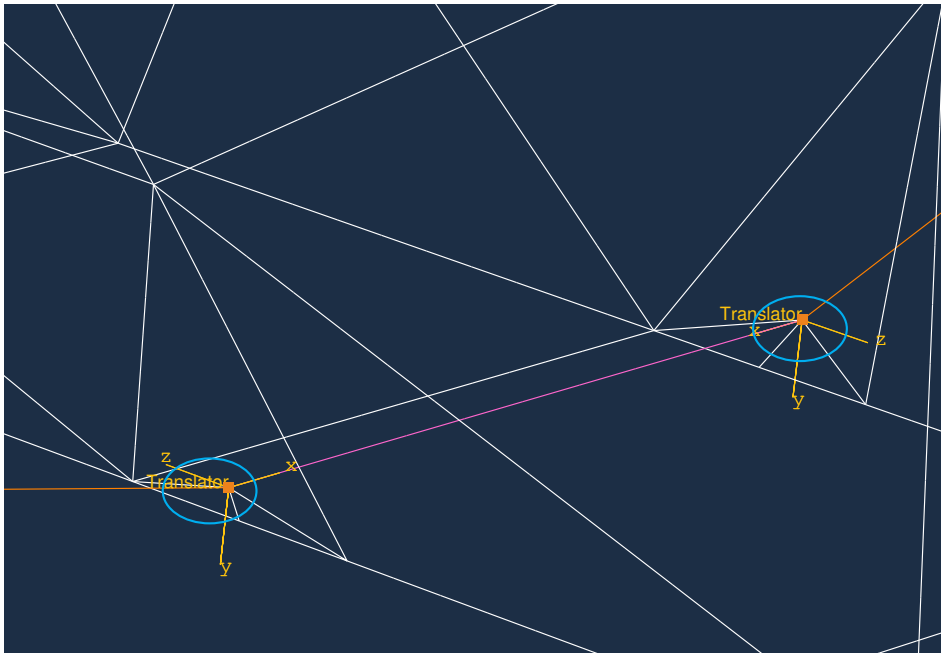

Figure 3.13: Figure showing the steering rack (purple) geometry and the connection to the chassis.

3.4.5 Uprights

The uprights are modeled as rigid bodies with a geometry that was defined by the outline of the control arms and toe/tie/pull rod pickup points as show in Figures 3.14-3.15. The upright assembly was assumed to be rigid compared to the suspension and the geometry was small relative to the rest of the system so the details of the upright geometry are not important. The mass for the tire and wheel assembly was accounted for by adding NONSTRUCTURAL

MASS elements to the upright geometry distributed evenly throughout the upright.

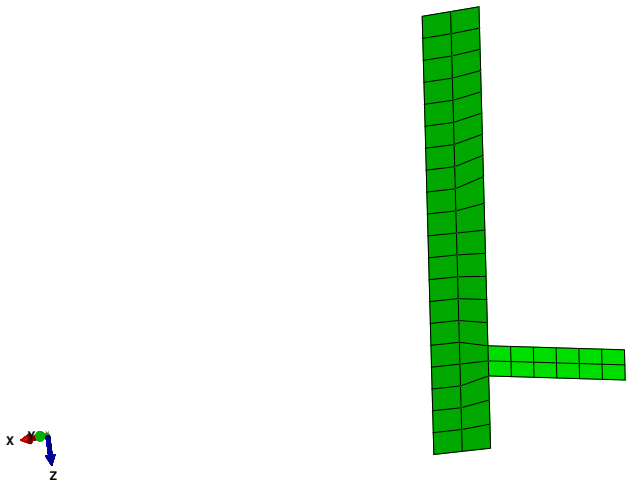

Figure 3.14: Figure of front upright geometry

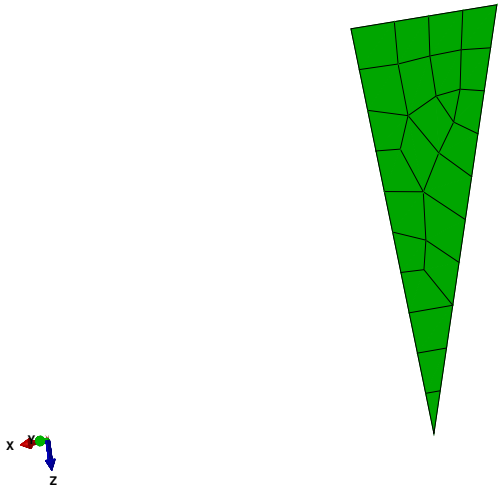

Figure 3.15: Figure of rear upright geometry

3.4.6 Tires

The front tires are modeled as CYLINDRICAL connector elements as found in Table 3.5, while the rear tires are modeled as TRANSLATOR connector elements as shown in Figure 3.16. The need for different elements was that the front tires need to be able to be activated by the steering rack. Both of these elements are defined with local coordinate systems with the local x-axis pointing along the kingpin inclination axis, or the vector that connects the

two outboard control arm points projected through the ground. Both of these elements also have connector behavior defined with elastic and damping properties in the local x-direction.

Table 3.5: CYLINDRICAL Connector Element Definition

Available Degrees of Freedom	U1, UR1
Constrained Degrees of Freedom	U2, U3, UR2, UR3

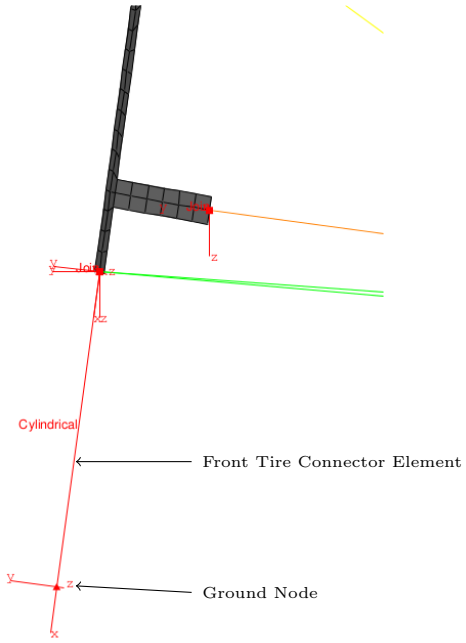

Figure 3.16: Figure showing the front tire connector geometry. The rear is the same setup except a TRANSLATOR element is used instead of CYLINDRICAL.

3.5 Full Suspension System

The full suspension system was also attached to the chassis using connector elements. Using scripts similar to those with the chassis, the suspension geometry was built to be independent of the chassis geometry. Scripting the assembly of the suspension to the chassis is very beneficial with connector elements because Abaqus defines them similarly to "normal" elements by referring to explicit node numbers rather than sets. Therefore, if the chassis model were to change and the node numbers were altered the suspension would no longer assemble the same. This can be overcome either by forcing the chassis model to keep attachment

node numbers the same, or use the scripts "knowledge" of sets to update the attachment configuration. While some hard-coding is inevitable, when parameterizing models as little hard-coding should be used as possible especially when using a relative definition does not require much effort. So, the approach to pre-build the chassis and suspension in separate scripts with an interface script to combine the two with relative definitions makes the most sense. By approaching the model this way it allows for a more modular design approach as the other components designs can be evaluated by loading the different components without having to completely redo the model.

3.5.1 Connections

Referring back to Figures 3.8 and 3.9 as an overview of the fully assembled suspension, the following section will go into more detail about how the suspension structures are connected to each other as well as the chassis.

Control Arms

The control arms are connected to the chassis and uprights at their specified pickup points with JOIN connector elements defined in Table 3.6. The JOIN elements represent spherical bearings that exist on the 2012 car restricting all translational degrees of freedom while allowing all rotational degrees of freedom. Because the JOIN element has all relative rotational degrees of freedom available a local coordinate system definition was not required and the global system was used instead. Figure 3.17 shows the front control arms connected to the chassis and Figure 3.18 shows the controls arms attached to the upright.

Table 3.6: JOIN Connector Element Definition

Available Degrees of Freedom	UR1, UR2, UR3
Constrained Degrees of Freedom	U1, U2, U3

The rear suspension was connected the same as the front except with different geometry. Figure 3.19 shows the rear upright connections with JOIN elements and coordinate systems.

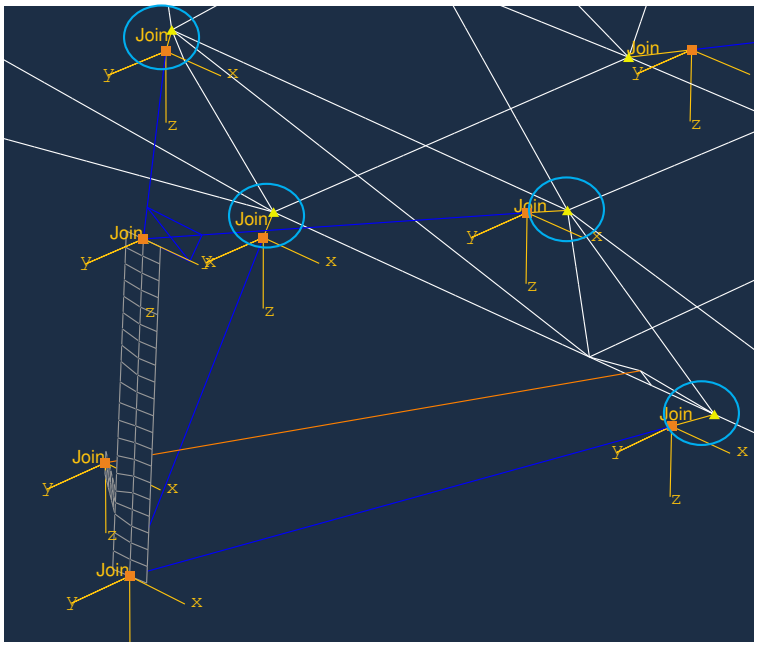

Figure 3.17: Figure showing the front control arms (blue) JOIN connections to the chassis, highlighted with cyan circles.

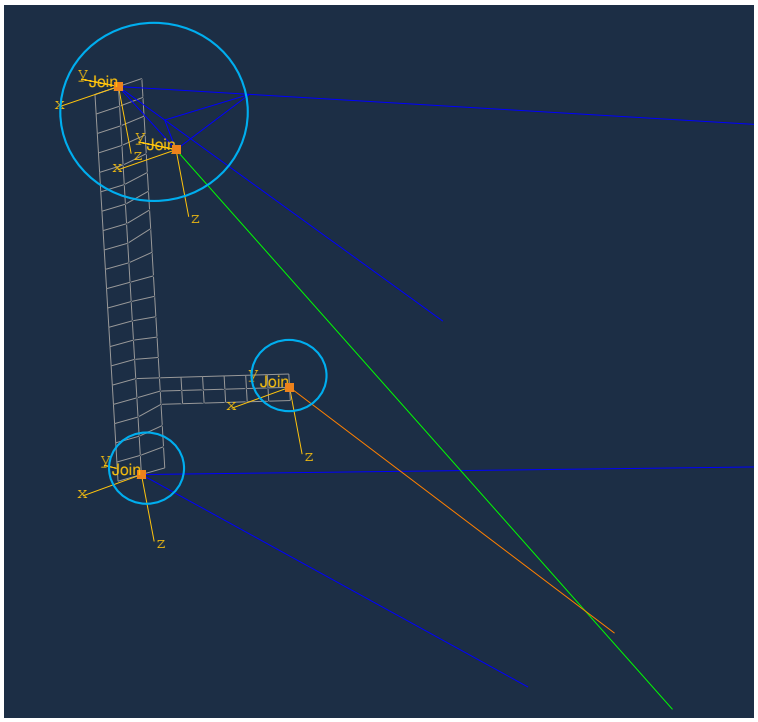

Figure 3.18: Figure showing the front control arms (blue) and tie rod (orange) JOIN connections to the upright. The pull rod (green) connection to the upper control arm is also shown.

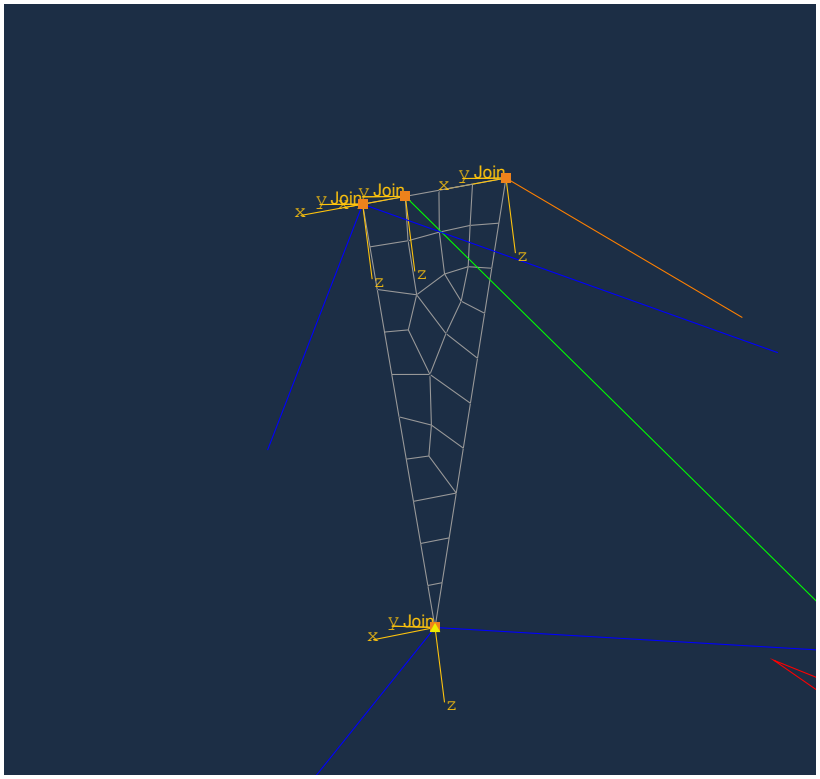

Figure 3.19: Figure showing the rear control arms (blue), pull rod (green), and toe rod (orange) to the rear upright.

Pull Rods/Bell Cranks/Springs and Dampers

The pull rods are attached to the uprights using the same JOIN connector elements, while UJOINT connector elements, defined in Table 3.7, are used at the bell crank pickups. A local coordinate system was created such that the local y-axis pointed along the axis of the pull rods. While the joint in the real system is not considered a universal joint, it does provide the necessary restrictions on the degrees of freedom to prevent the pull rods from spinning about their axis. In a JOIN element were used all rotational degrees of freedom would be available at both ends of the pull rod allowing the pull rod to rotate freely about its own axis. A UJOINT connector element with a local y-axis along the pull rod centerline the pull rod can no longer spin. Figures 3.20 shows the JOIN and UJOINT connector elements of the pull rod as well as the coordinate system for the UJOINT connector.

Table 3.7: UJOINT Connector Element Definition

Available Degrees of Freedom	UR1, UR3
Constrained Degrees of Freedom	1, 2, 3, 5

Figure 3.20 also shows the front spring/damper connection with the bell crank using the AXIAL connector element with its local coordinate system. The BEAM connector element, defined in Table 3.8, shown in Figure 3.20, connects the inboard side of the spring/damper to the chassis. The BEAM connector element eliminates the relative degrees of freedom between nodes negating the need for a local system. The bell crank was attached to the

Table 3.8: BEAM Connector Element Definition

Available Degrees of Freedom	N/A
Constrained Degrees of Freedom	U1, U2, U3, UR1, UR2, UR3

chassis using a JOIN plus a REVOLUTE connector element defined in Table 3.9. The local coordinate system was defined with the local x-axis connecting the bell crank pivot node and the mounting point on the chassis. This allows the bell crank pivot node to only rotate relative to the corresponding chassis node about the axis that connects them. Figure 3.21 shows the connection and the local coordinate system.

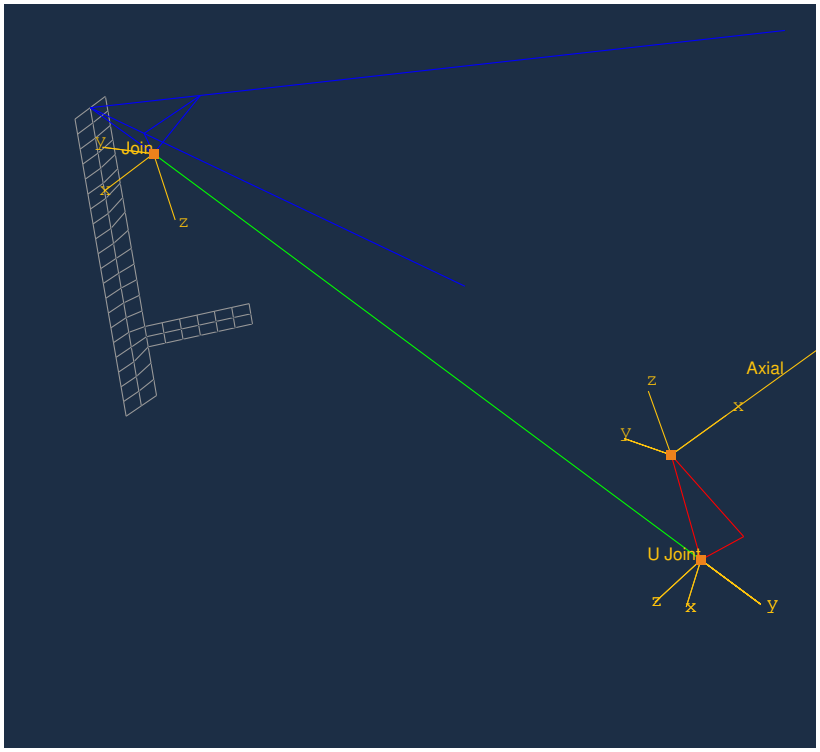

Figure 3.20: Figure showing the pull rod (green) and spring (yellow) connection to the bell crank.

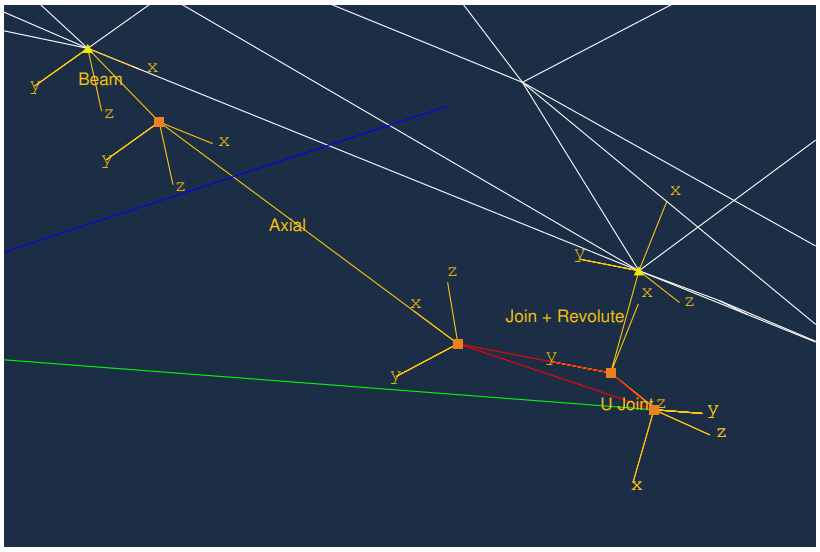

Figure 3.21: Figure showing the JOIN plus REVOLUTE connector element between the bell crank (purple) and the chassis (black).

Table 3.9: JOIN + REVOLUTE Connector Element Definition

Available Degrees of Freedom	UR1
Constrained Degrees of Freedom	U1, U2, U3, UR2, UR3

Toe/Tie Rods

The rear toe rod was connected to the rear uprights using a JOIN element, shown back in Figure 3.19, but a BEAM connector element connects the inboard node with the inboard node of the upper control arm. Figure 3.22 shows the BEAM connection between the inboard toe rod and the rear upper aft control arm. On the 2012 car these two points share a mounting location on the chassis.

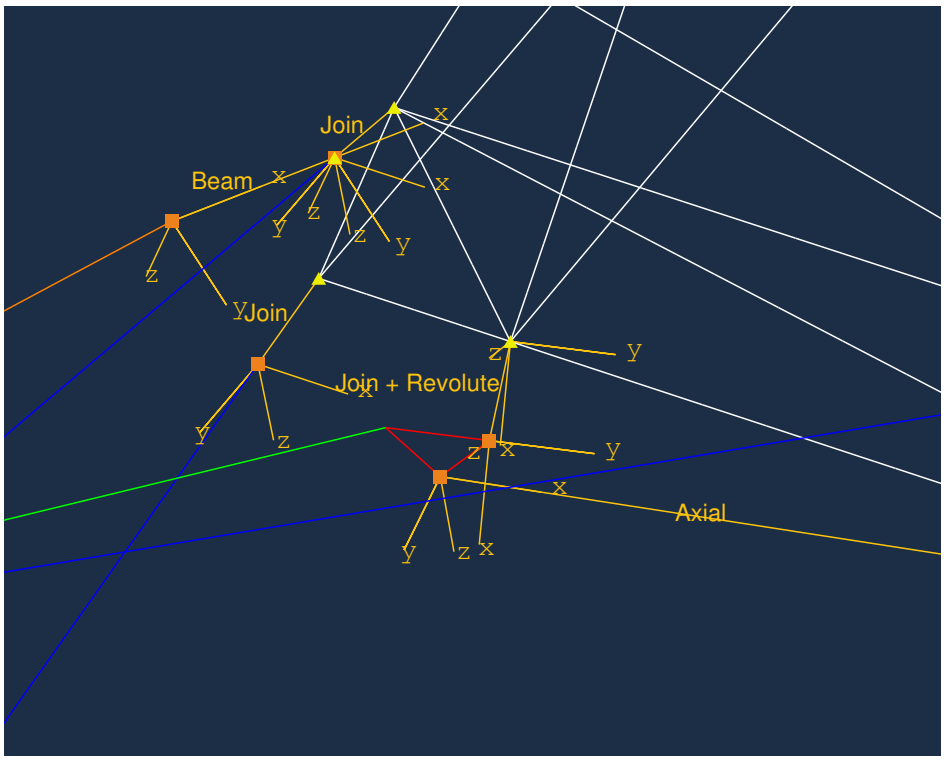

Figure 3.22: Figure showing the BEAM connection between the rear toe rod (orange) and the rear upper control arm (blue).

The front tie rod was connected to the steering beam using a UJOINT connector element for the same reason as the pull rods above, and the outboard node was connected to the

uprights using JOIN elements. The JOIN connection can be seen back in Figure 3.18, while the UJOINT connection and local coordinate system is shown in Figure 3.23.

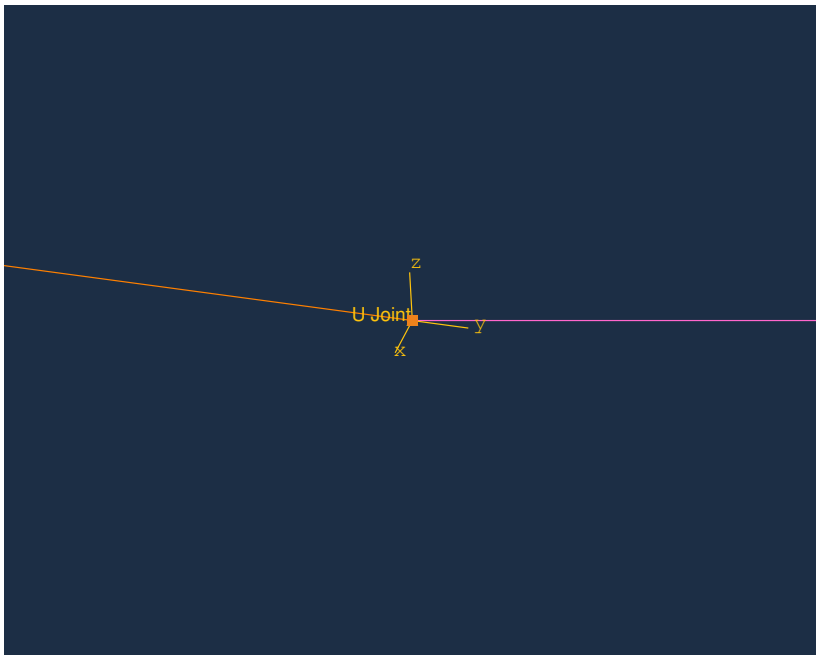

Figure 3.23: Figure showing the UJOINT connection between the front left and right tie rods (orange) and the steering rack (purple).

3.5.2 Rolling Tire

The rolling tire model is developed with the exact same suspension setup as the full system except a shell outline of the tire was introduced. Figure 3.24 shows the overall model with the tire geometry, chassis and ground. The tire is a rigid shell with a rigid body node at its center connected to the rigid body node for the uprights using the same JOIN and REVOLUTE connector element as the bell crank with a coordinate system between the two nodes. This allows for the tire to rotate relative to the upright assembly about the axis connecting them, effectively taking the place of a rigid spindle. The detail of the connection is shown in Figure 3.25.

The ground was modeled as a flat rigid shell geometry large enough to contain the entire maneuver. A contact definition was defined between the tires and the ground using friction to allow the vehicle to move. The friction coefficient, 4.5, was determined by slowly increasing the value until the overall vehicle speed was consistent with the rotational speed of the wheel.

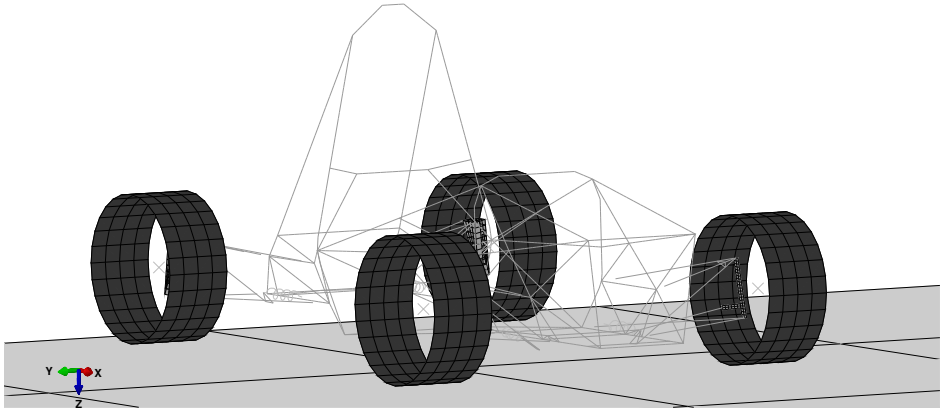

Figure 3.24: Figure showing the overall rolling tire model including the ground shell.

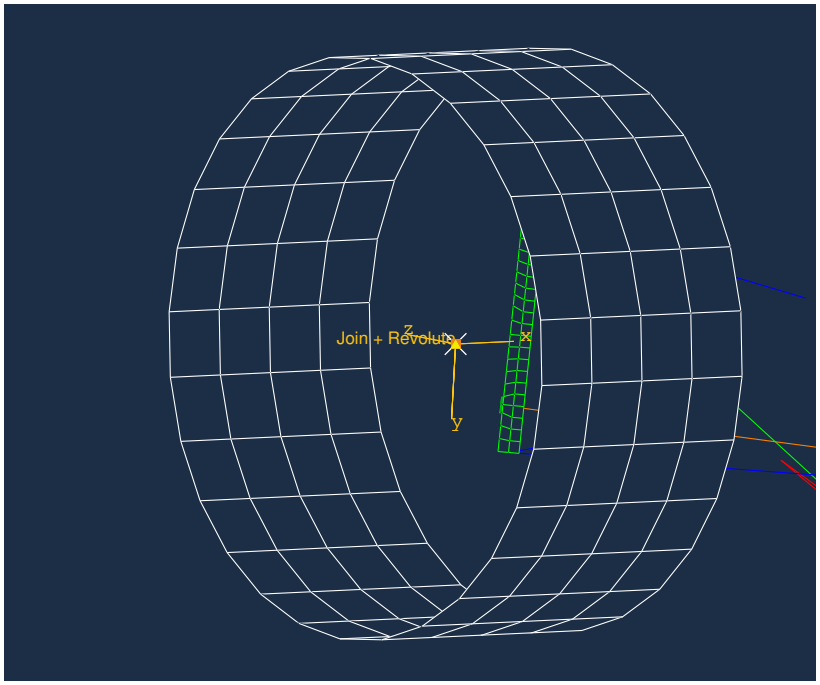

Figure 3.25: Figure showing the tire shell connected to the front upright using a JOIN and REVOLUTE connector element with the local coordinate system.

3.5.3 Modeling Scope

The scope of the modeling detail is shown graphically in Figure 3.26. In Figure 3.26 the green boxes represent the level of detail included in the previously detailed models. Also represented is a quick look at alternative modeling methods or details not included in the models.

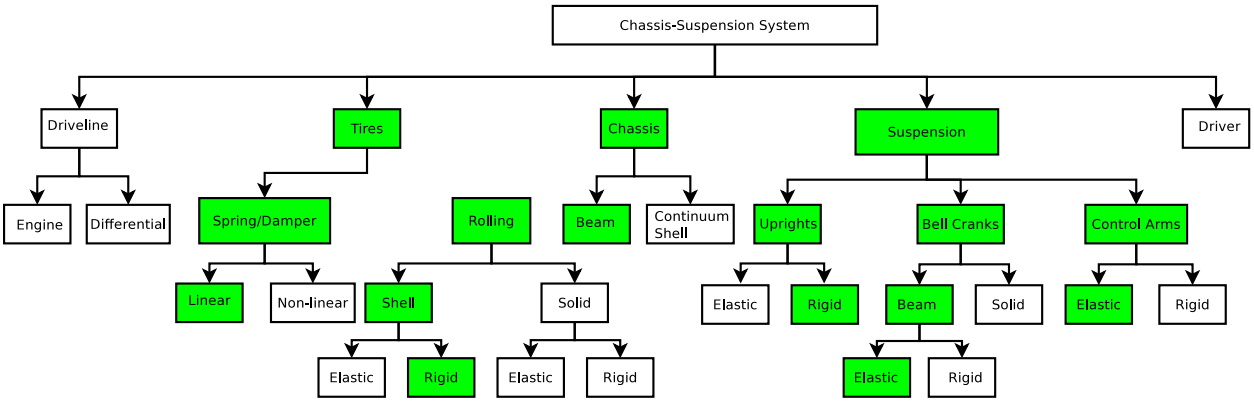

Figure 3.26: Scope of modeling detail. Green represents what is included in the models.

Chapter 4

Static Loading

4.1 Static Suspension Actuation

The following section covers the static actuation of the suspension to verify that the suspension as modeled with the connector elements moves as designed by moving the ground node vertically and measuring the spring displacement. The ratio between the amount of spring displacement to wheel displacement is defined as the motion ratio, the 2012 VT FSAE vehicle goal was a 0.8 motion ratio. The Abaqus model was a static step, with the chassis-suspension model was stripped down to a single suspension corner. The chassis points where the suspension connects were retained as assembly nodes that were fixed with the connector elements still mapped to the same points. The ground node was then displaced 25.4 mm in the negative z-direction and history data were recorded for the relative connector motion for the spring. Figure 4.1 shows the plots of the wheel displacement and relative spring displacement throughout the step as well as the motion ratio. The spring displacement is plotted as negative, meaning the relative motion between the two ends of the spring are moving closer together. The motion ratio for this model was approximately 0.76 and nearly constant throughout the entire motion. Constant motion ratios are desired when designing the suspension as they simplify the relationships used when selecting the springs/dampers needed.

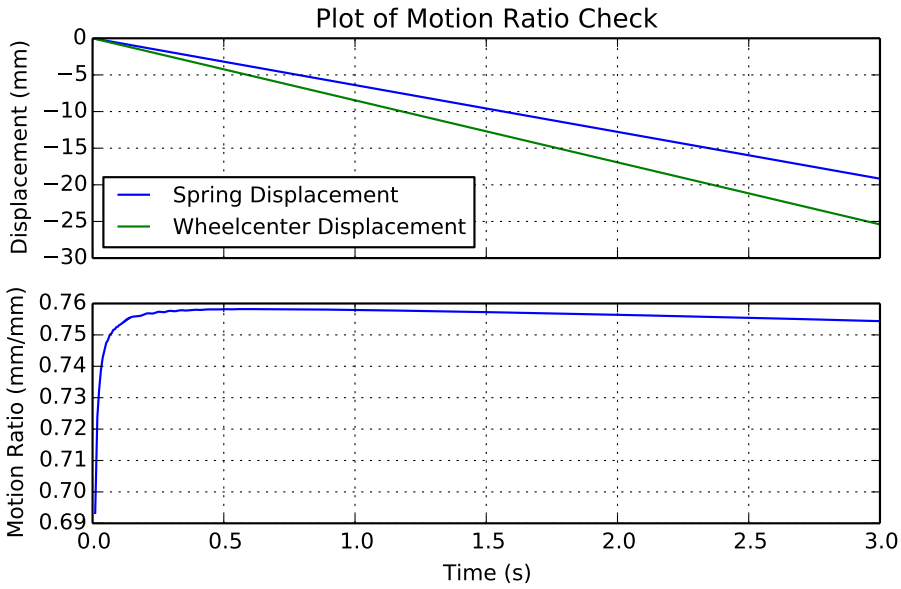

Figure 4.1: Plot of wheel displacement and relative spring displacement.

4.2 Loading

4.2.1 Abaqus Outline

An outline of the Abaqus analysis steps and parameters are provided below:

- Abaqus Implicit Solver
- Static General Step (1 second) – allows for nonlinear deformation
- Apply all boundary conditions in same step

4.2.2 Twist Details

The static twist loading scenario tests the twisting stiffness of the chassis under static load. In the static twist analysis the full system, chassis and suspension, are modeled not including the tire springs. Only the chassis stiffness was of concern therefore the tires are not needed, the suspension components are used to transfer the load to the chassis. The static twist the analysis was setup to mimic a welded tube in torsion with the rear of the vehicle fixed in all degrees of freedom and equal vertical loads applied in opposite directions at the front wheel centers. The boundary conditions and applied loads are shown in Table 4.1 and visually in Figure 4.2.

Table 4.1: Boundary conditions and applied loads for static twist.

Boundary Conditions		
Node	**DOF**	**Value**
LR	U1, U2, U3, UR1, UR2, UR3	0
RR	U1, U2, U3, UR1, UR2, UR3	0
LF	UR3	0
RF	UR3	0
Applied Loads		
LF	F3	Fz
RF	F3	-Fz

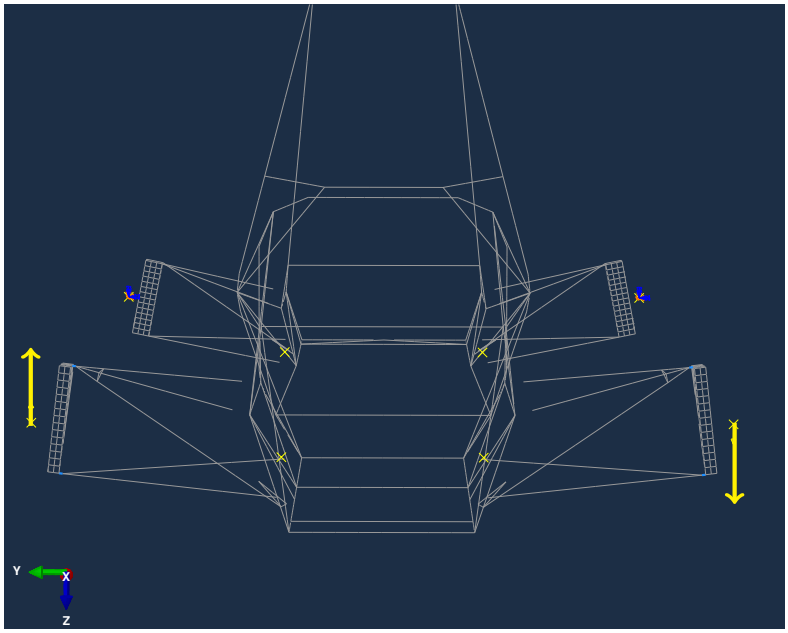

Figure 4.2: Figure showing the chassis and suspension system (gray), the boundary conditions (blue) at the rear wheel centers, and the applied torque (yellow) at the front wheel centers.

Table 4.1 shows the rear wheel centers are fixed in all directions. The limits on rotation of the front wheel centers keep the uprights from rotating about the z-axis. Equal forces are applied in opposite directions at the front wheel center nodes, applying a torque without

introducing bending. The applied load was varied from 50 N to 600 N in increments of 50 N to verify the assumption that the twisting stiffness was linear in nature. The vertical displacements at nodes on the bottom frame rails on both sides of the chassis are used to calculate the twist angle using Equation 4.1:

$$\theta = \arcsin(\frac{u_{zr} + u_{zl}}{l}) \tag{4.1}$$

where l is the distance between the two points on the chassis and u_z was the vertical deflection of the points on the left and right side of the chassis. Equation 4.1 assumes that the deflections are small, the distance between points does not change significantly, and rotation exists only about the longitudinal axis of the chassis.

4.3 Static Twist Results

The results from the Static Twist analysis and the other loading scenarios to follow were extracted from the Abaqus output databases (.odb files) using python scripts to extract the values of interest. The goal of this analysis was to show whether the chassis has enough static twisting stiffness to perform well with the suspension design. Figure 4.3 shows the *Base* model with the key points on the chassis rails used in the twist calculations. Figure 4.4 shows the twist angle at different points along the chassis as a function of the applied load. The angle of twist at every point increases linearly with increased applied load which is important. Because if simple chassis models are made at a later date linear spring elements can be used in place of the chassis.

The next step was to look at the twist along the chassis due to particular loads to determine relatively weak sections and to also compare the *Base* model to the *Rigid* model. Looking at the twist along the chassis for relatively weak sections gives the design team sections of the chassis to look at for improvement. With time working against FSAE teams, knowing where the most improvement can be made is important. By comparing the *Base* to the *Rigid* model allows the team to have a performance goal to strive for; a goal not rooted in rules of thumb, but quantified next to a *Rigid* model. The plots for the two extreme cases, 50 and 600 N applied load, are shown in Figures 4.5 and 4.6.

In Figures 4.5 and 4.6 the roll angles are plotted relative to their physical location on the chassis, so the distances between sections on the plot are to scale. The *Rigid* model maintains almost zero change in angle of twist from front to rear. This validates the assumption that increasing the elastic modulus an order of magnitude would result in an effectively rigid chassis. A single number was not given for a global stiffness of the chassis because a single number does not accurately describe the stiffness of the structure. In reality there are a series of "springs" that make up the chassis that need to be coupled with the suspension. Rather than a single value of stiffness it was determined that viewing the static twist case

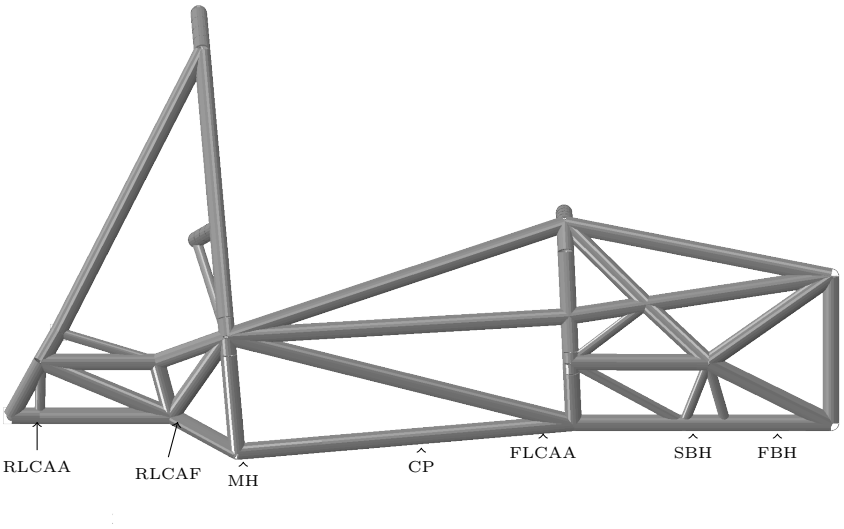

Figure 4.3: Figure of *Base* model with key points for twist calculations

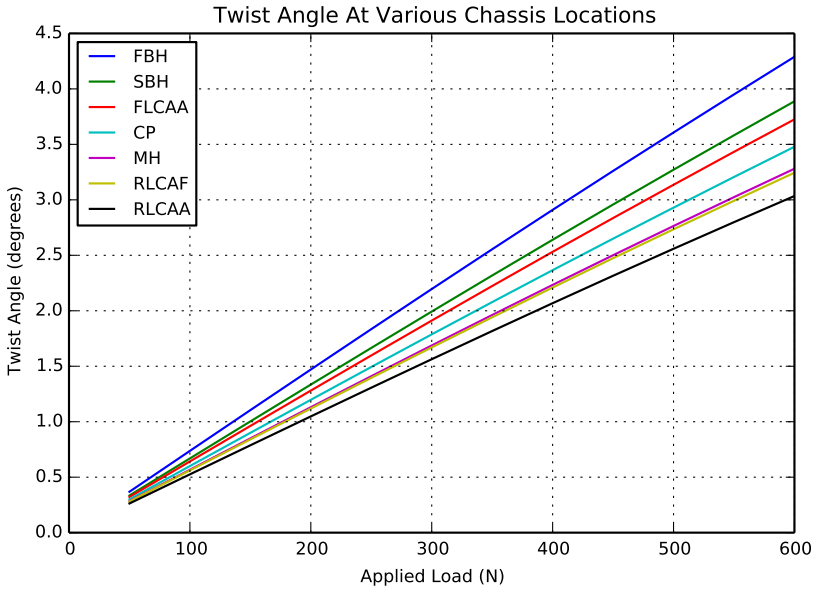

Figure 4.4: Plot of chassis roll angle as a function of applied load at different chassis locations.

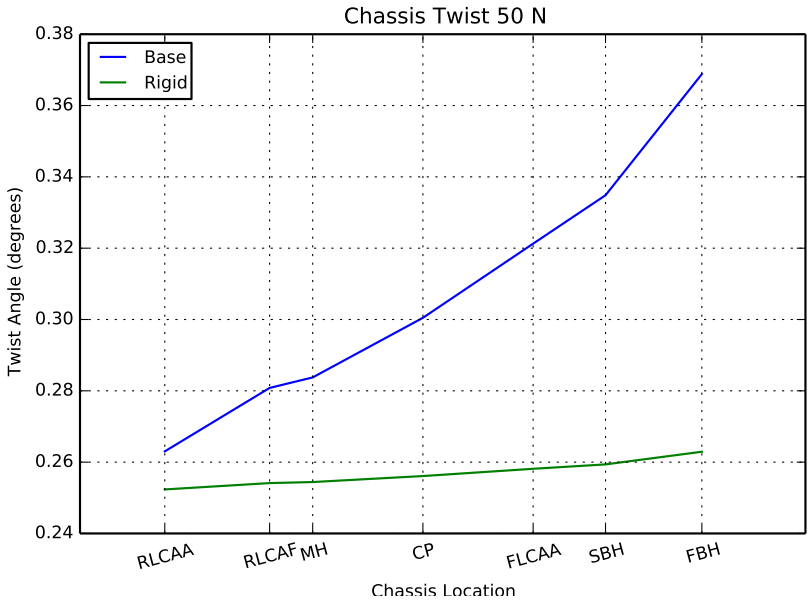

Figure 4.5: Plot of chassis roll angle along the *Base* and *Rigid* chassis for applied load of 50 N.

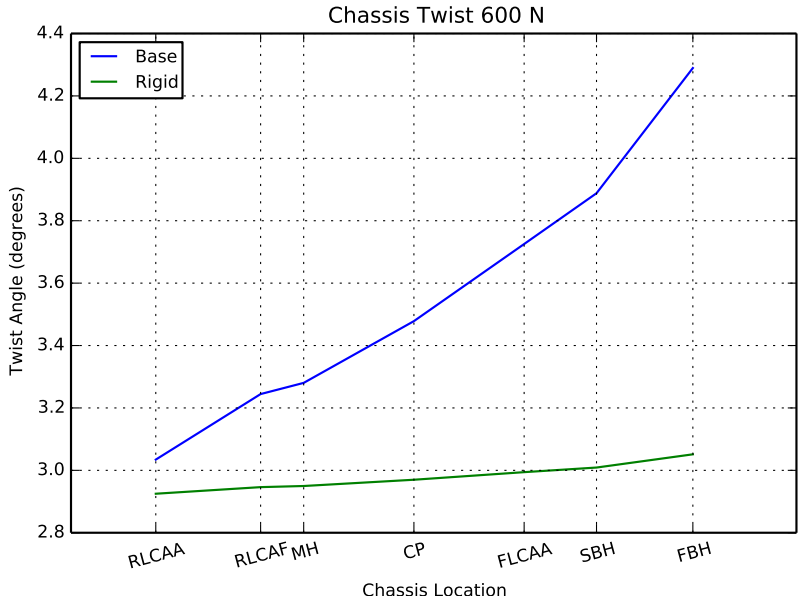

Figure 4.6: Plot of chassis roll angle along the *Base* and *Rigid* chassis for applied load of 600 N.

as a distribution was a better approach. By focusing on the twist angle distribution rather than a single number the design team can compare chassis models together at their common points and determine if the chassis was stiff enough or needs to be stiffer in the areas of concern. A simple example of the value would be to only increase the stiffness of the rear section of the chassis. While this will increase the static stiffness value for the chassis, the twist angle plot would not look much different as the rear was already stiff when compared to the sections forward of the main roll hoop.

4.4 Composite Model Results

The same static twist analysis was run on the composite models as the *Base* and *Rigid* model. Figures 4.8 and 4.9 show the results from all the models due to the 50 N and 600 N applied loads. In Figures 4.8 and 4.9 the rear of the chassis, where no composite structure was added, was similar for all models. Beginning with the cockpit section, between MH and FLCAA, was where significant gains were achieved from the composite models. The *C2012* model did show improvement even without being designed specifically for torsion. The *Attached* and *Semi-monocoque* models were almost identical in twist angles along the chassis. The only significant difference between the two models being the reworked front suspension section, most of the increased stiffness from the *C2012* model was from the top panel. Structurally the composite in the suspension area for the *Semi-monocoque* was as stiff as the steel structure. If the steel tubes were retained closeouts would still need to be used adding to the material used. The composite in this case is providing at least the same stiffness as the steel while also performing the close out duty. This reaffirms the desire to close out large open sections, previously covered with body panels, with structural panels. The composite panels add considerable stiffness without adding much in material than was already used. Figure 4.3 has been reproduced in Figure 4.4 to provide reference to the points on the chassis evaluated in the static twist analysis.

The results also show that except the rear, the *Attached* and *Semi-monocoque* models have a similar slope in twist angle to that of the *Rigid* model with only an offset from the steel rear section as the primary difference. With a proper integration of the composite structures, these models show a high likely-hood of approaching an effectively rigid state for static torsion. The rear of the chassis would receive an increase in stiffness from mounting the drive line systems, and would likely require more effort than stiffness gained to integrate composites permanently.

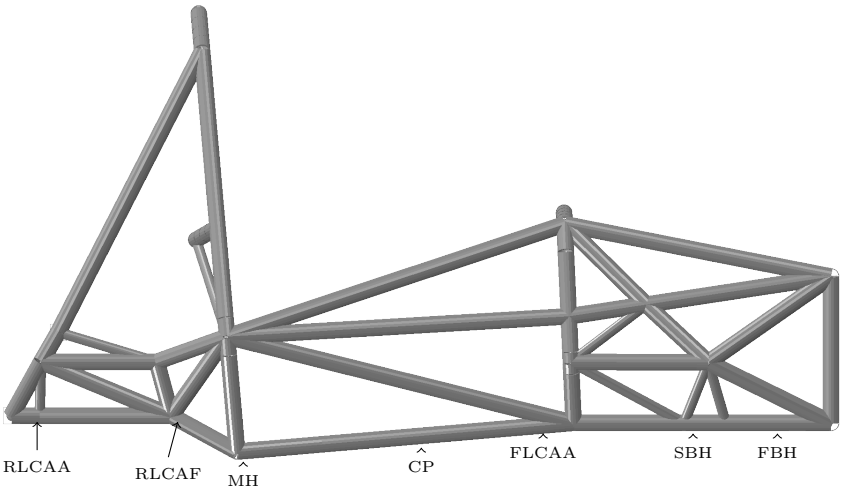

Figure 4.7: Figure of *Base* model with key points for twist calculations

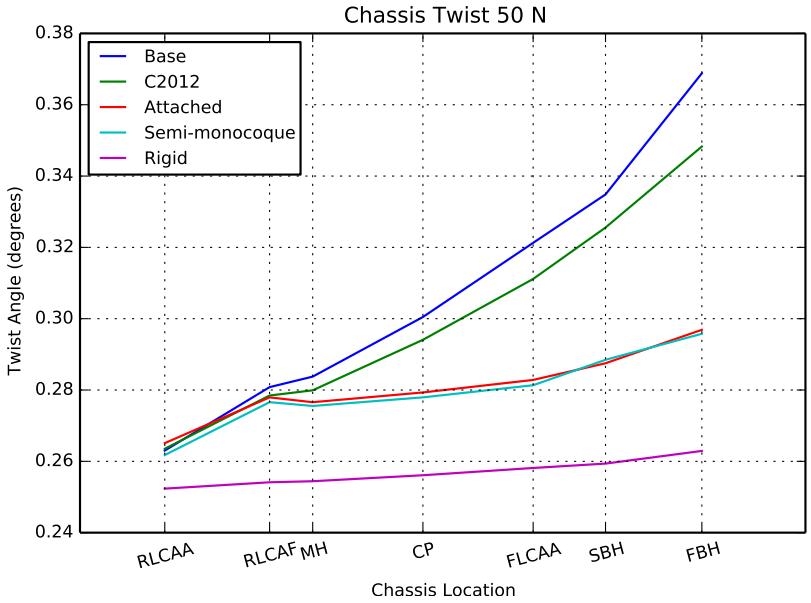

Figure 4.8: Plot of chassis roll angle for all chassis models for applied load of 50 N.

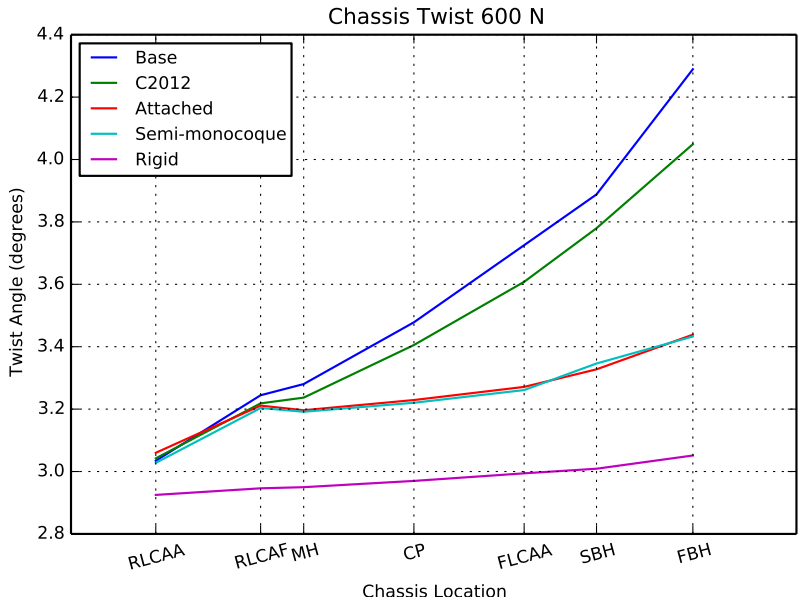

Figure 4.9: Plot of chassis roll angle for all chassis models for applied load of 600 N.

4.5 Conclusions

The modeling technique of using connector elements to attach the suspension components to the chassis does a good job of capturing the kinematics and degrees of freedom associated with the motion of the suspension. The motion ratio for the suspension was very close to the designed ratio, and the static twist analysis showed the difficulties and inaccuracies of using the static twist test to not only design from, but to boil down to a single stiffness value. Unless all sections of the chassis have a similar stiffness, a single value cannot accurately describe the twist of the chassis. While the composite chassis models did show a significant increase in stiffness, even approaching the *Rigid* model, the static twist test provides no value when determining whether the structure can stand up to loads developed from driving the car. These loads are extremely important in general and essential when designing integrated composite structures and need to be developed and applied in a dynamic analysis.

Chapter 5

Modal Analysis

This chapter presents the model setup, results and conclusions from the modal analysis. All chassis models (base, rigid, composite) were analyzed with and without the attached suspension to evaluate their individual behavior as well as interaction with the suspension.

5.1 Modal Analysis Setup

5.1.1 Abaqus Outline

An outline of the Abaqus analysis steps and parameters are provided below:

- Abaqus Implicit Solver
- Frequency Step – requested first 20 modes

5.1.2 Chassis Details

The modal analysis step for the chassis only model has no boundary conditions applied resulting in the first six frequencies as rigid body nodes, also known as free-free modal analysis. Twenty modes were requested, but only first torsion, bending, and lateral bending modes are of interest.

5.1.3 Chassis/Suspension Details

The modal analysis for the chassis-suspension models has the ground nodes pinned as shown in Table 5.1 allows for the suspension modes to be activated as well as the interaction between

the chassis and suspension. The first twenty modes are also extracted as this provides enough modes to characterize the suspension modes as well as the first chassis-suspension interaction modes.

Table 5.1: Boundary conditions for modal analysis of chassis-suspension system.

Boundary Conditions		
Node	**DOF**	**Value**
GROUND-LR	U1,U2,U3	0
GROUND-RR	U1,U2,U3	0
GROUND-LF	U1,U2,U3	0
GROUND-RF	U1,U2,U3	0

5.2 Results

5.2.1 Chassis Results

The important modes to look at are first torsion, first bending, and first lateral bending. Lateral bending is the mode with rotation about the z-axis, and bending was about the y-axis. The first modes of torsion, bending, and lateral bending are of interest because they represent the primary deflection shapes of the chassis under load, and only the first modes are important, typically, because the goal of modal design is to separate these modes far away from the suspension modes. If the first modes are far enough away from the suspension modes, the modes after that will also be far enough away. For the free-free modal analysis of the chassis Table 5.2 shows the natural frequencies for the *Base* and *Rigid* models, while Figures 5.1-5.3 show the mode shapes.

The significantly larger natural frequencies for bending show that the structure was far less efficient in torsion. This was not unexpected as Milliken [15] showed that when the chassis has sufficient torsional stiffness the chassis also has enough bending stiffness. The large open sections on the chassis make increasing the torsional stiffness difficult. Table 5.2 also shows how much stiffer the *Rigid* model was compared to the *Base* model with a $\sqrt{10}$ difference between every mode. It is not likely that the FSAE chassis will be able to reach the frequencies of the *Rigid* model, but combined with the static results it does show that the *Base* model was far from effectively rigid.

When designing future chassis, comparing natural frequencies of chassis with similar mass,

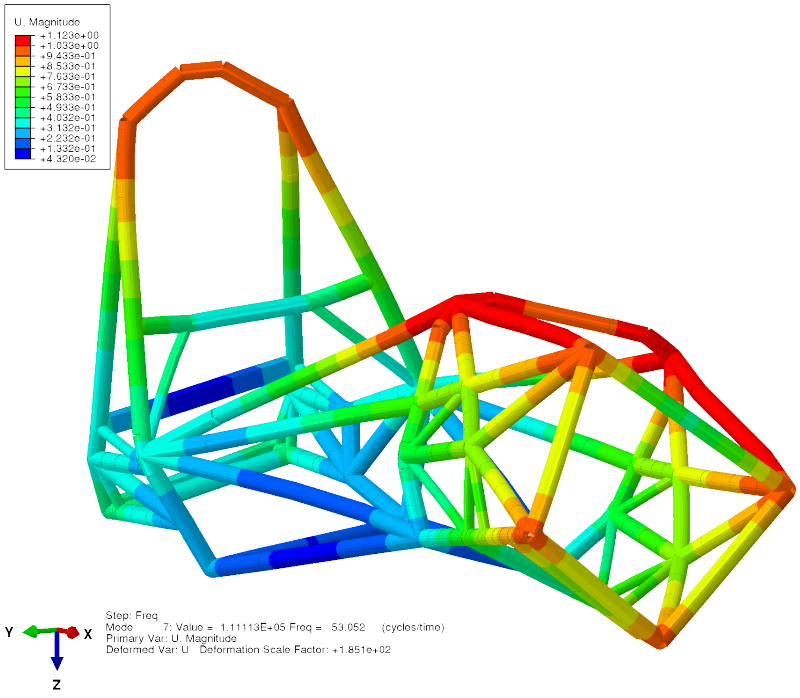

Figure 5.1: The first torsion mode for the *Base* chassis at 53 Hz.

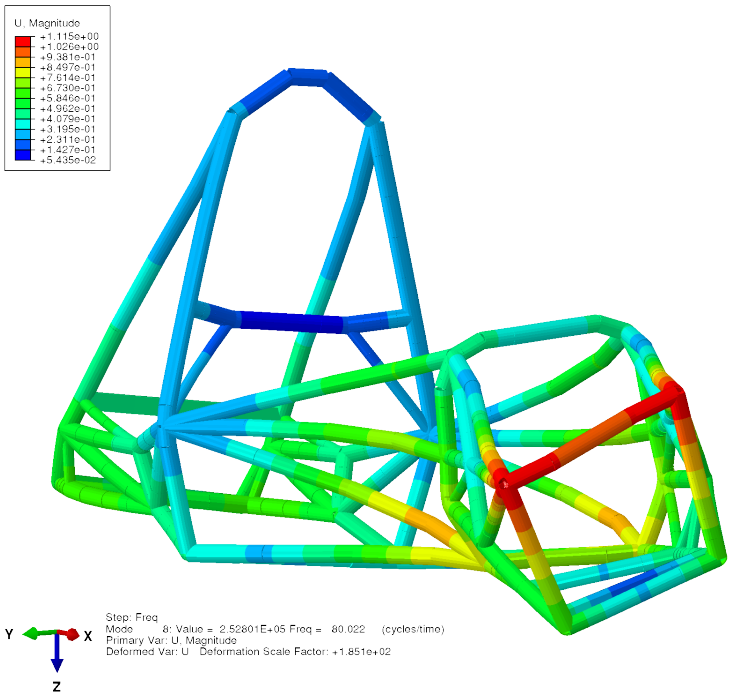

Figure 5.2: The first lateral bending mode for the *Base* chassis at 80 Hz.

Table 5.2: Modal results of base and rigid chassis model

Mode	**Base**	**Rigid**
Twisting Frequency (Hz)	53.0	167.3
Lateral Bending Frequency (Hz)	80.0	251.7
Bending Frequency (Hz)	84.7	262.6

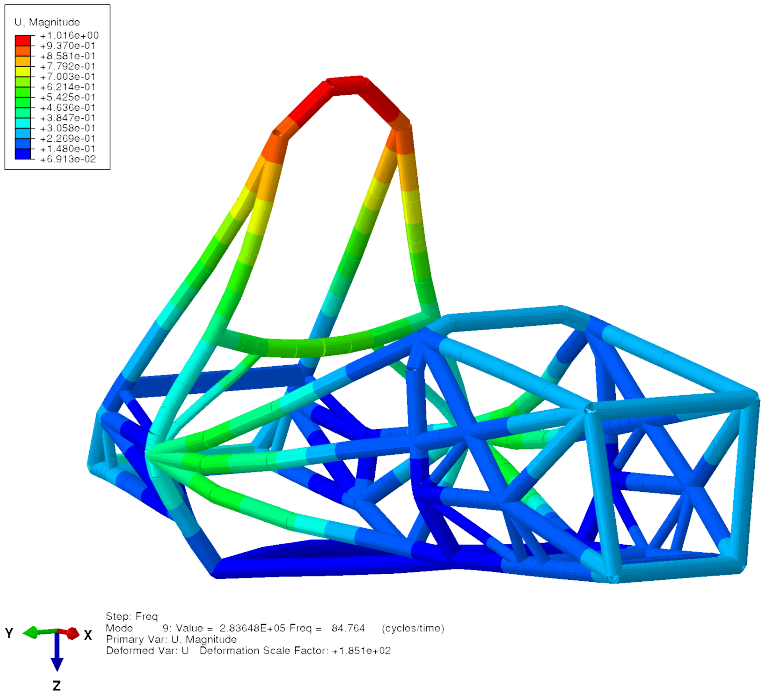

Figure 5.3: The first bending mode for the *Base* chassis at 84.7 Hz.

it can easily be seen if the adjustments to the structure are providing additional stiffness without adding too much mass. It will be important to keep the overall mass of the structure in mind when comparing modal models since the same natural frequency will only mean that the stiffness to mass ratio will be the same and not necessarily the stiffness in general.

The natural frequencies can be scaled by the total mass to give a "scaled" stiffness value to use as a comparison between models. But it is important to remember that this stiffness value does not represent the actual stiffness of the model. Abaqus does provide a generalized mass value for each mode which gives the mass value for a single degree of freedom system. This value is not unique and is dependent on how the modal matrices are scaled with eigenvectors.

Without a unique mass value a unique stiffness cannot be determined.

Even without a single value for stiffness the modal results contain useful information. They provide a natural optimization problem and a better method for validating the physical chassis structure. As the following section will show, it was easier and more repeatable to reproduce the free-free boundary conditions of the modal analysis than it would be to recreate the boundary conditions of the static twist.

Experimental Results

The following section presents the free-free modal experiment on the 2012 chassis to compare to the Abaqus results. An important detail from this test was the experiment was conducted after the carbon composite floor was installed while the Abaqus model does not have the carbon composite floor modeled. The experimental setup for the modal analysis consisted of hanging the chassis from the ceiling using bungee cords long enough so that the natural swinging period would not interfere with the natural frequencies of interest. Figure 5.4 shows the 2012 chassis hanging by the bungee cords as well as the overall setup.

Figure 5.4: Setup of the modal test on the 2012 chassis

Using bungs, small notched aluminum stock to create flat surfaces, accelerometers were attached to the chassis. Bungs are just small pieces of aluminum milled on one side to fit the chassis tube while the other side is flat to mount the accelerometers. The accelerometers

are bonded to the bung using accelerometer wax while the bung was attached to the chassis using high strength adhesive. A final bung was drilled and tapped to accommodate the shaker and force probe. A closeup of the setup from a different modal test is shown in Figure 5.5. The shaker was fed a periodic chirp input signal across a frequency band large enough to capture the frequencies of interest. A periodic chirp was used because it can deliver the same amount of energy at every frequency. The results from the probes were fed into an NI DAQ connected to MATLAB. Using fast Fourier transforms, Frequency Response Functions (FRF) were created from the data. The peaks in the magnitude plots of the FRFs represented the natural frequencies, while the phase response was used to determine the mode shapes. Table 5.3 has the results from the experiment along with the Abaqus results.

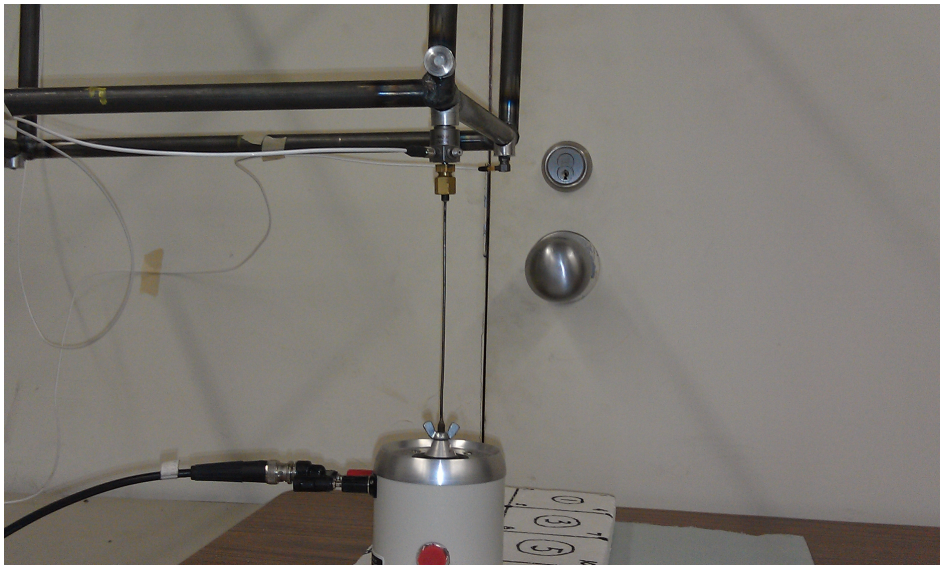

Figure 5.5: Closeup of the shaker and accelerometer setup with the attached bungs.

Table 5.3: Modal results of base chassis model.

Mode	**Abaqus**	**Experiment**
Twisting Frequency (Hz)	53.0	53.3
Lateral Bending Frequency (Hz)	80.0	N/A
Bending Frequency (Hz)	84.7	88.3

In the experimental results in Table 5.3, the twisting mode was not affected while the bending mode was higher in the experimental data. It will be discussed later, but even though the composite floor does add torsional stiffness it added the same amount of relative mass.

5.2.2 Chassis-Suspension Results

It was important to not only look at the chassis natural frequencies and static stiffness, but how the elastic chassis interacts with the suspension. By looking at the natural frequencies of the assembled system, the design team can begin to gage whether the chassis modes will become activated at or near suspension modes. If the chassis modes are too close to the suspension modes, there exists the possibility of exciting the chassis while the suspension is being loaded resulting in the chassis no longer being a rigid platform for the suspension. Table 5.4 shows the natural frequencies and mode shapes for the chassis-suspension model.

Table 5.4: Modal results of *Base* and *Rigid* chassis-suspension models.

Mode	**Base**	**Rigid**
Heave Mode (Hz)	6.6	6.7
Pitch Mode (Hz)	9.2	9.3
Roll Mode (Hz)	12.8	13.1
Lateral Bending Mode (Hz)	39.3	117.2
Twisting Mode (Hz)	52.0	148.0
Bending Mode (Hz)	80.2	243.6

The first suspension frequencies are between 6 and 12 Hz, while the first interaction mode doesn't occur until 39 Hz. The Abaqus results from the modes listed in Table 5.4 are shown in Figures 5.6-5.11.

The design team can begin to evaluate whether there is enough separation between suspension modes and the chassis modes. Only modes with similar mode shapes need to be compared to each other, as the twisting mode of the frame does not directly influence the bending interactions or the heave and pitch suspension modes. Unfortunately, there is not a standard value for determining whether two modes are separated "far enough". That value, like the global chassis torsional stiffness, is determined based on the system characteristics and experience. Given the general structure of the FSAE rules the prototypical steel space frame chassis will have similar mass, meaning the major differences in natural frequencies from design to design can be attributed to the stiffness of the chassis. While the previous statement was an extreme generalization, the typical ranges of chassis stiffness and mass mean it was more likely that the change in frequency was more directly a result of increased stiffness.

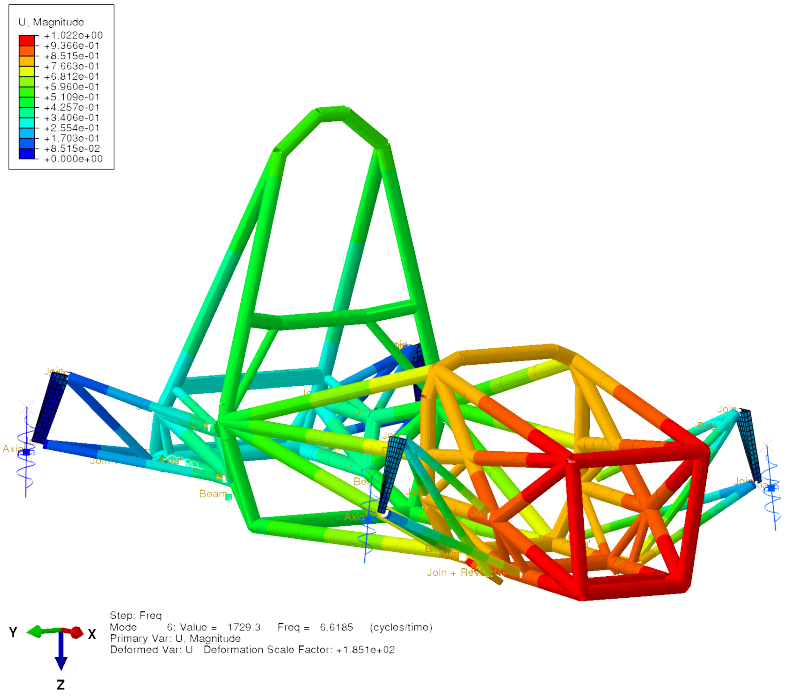

Figure 5.6: Heave mode for *Base* chassis-suspension model at 6.6 Hz.

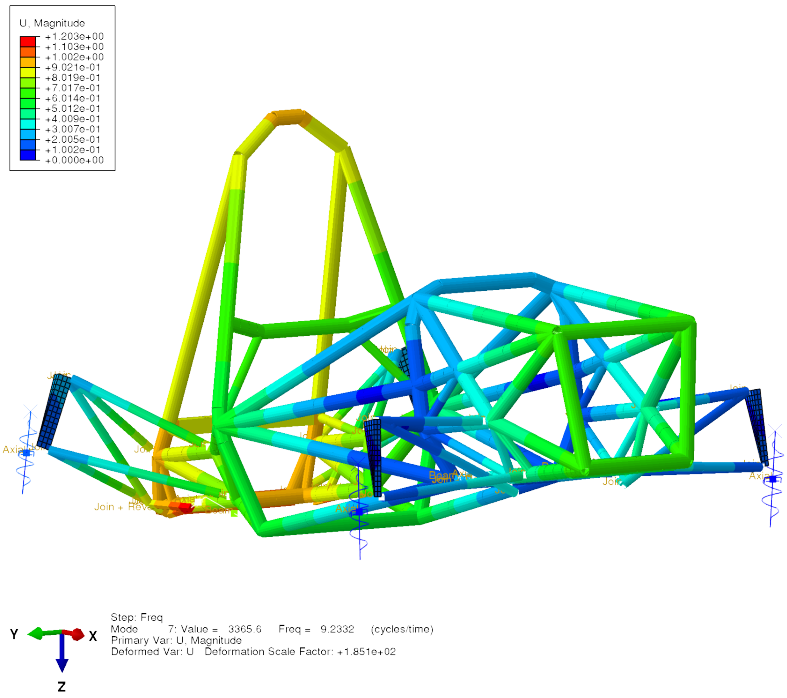

Figure 5.7: Pitch mode for *Base* chassis-suspension model at 9.2 Hz.

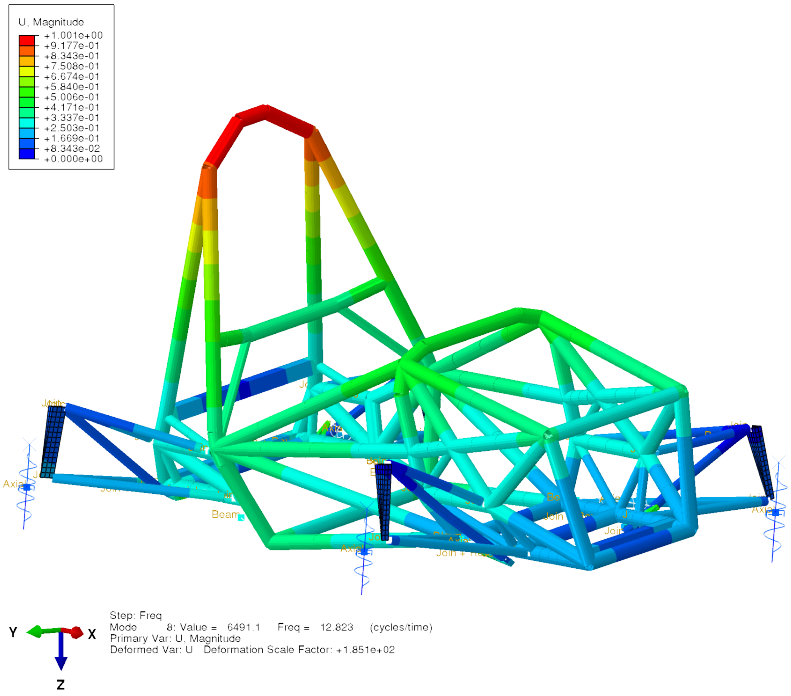

Figure 5.8: Roll mode for *Base* chassis-suspension model at 12.8 Hz.

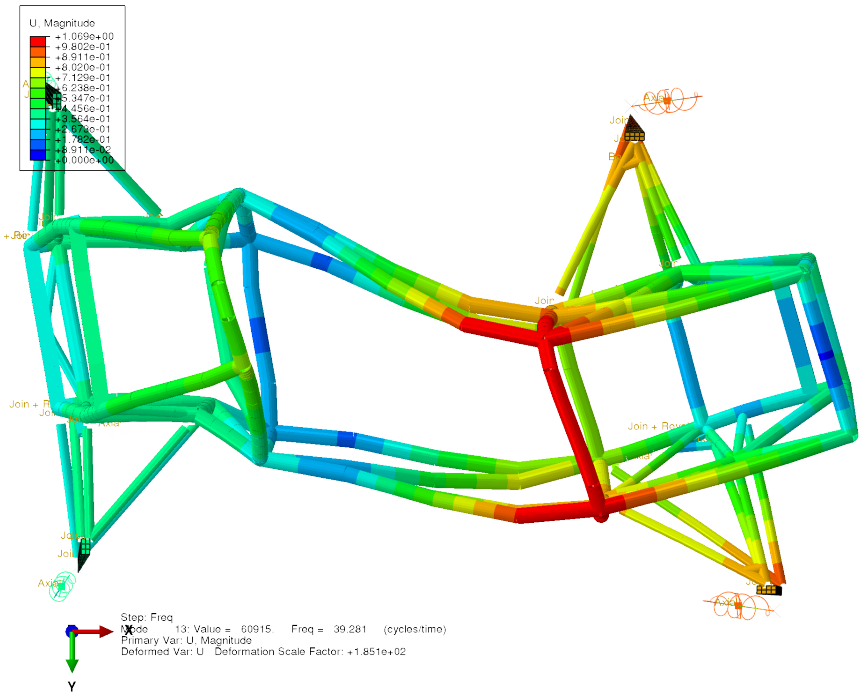

Figure 5.9: Lateral bending interaction mode for *Base* chassis-suspension model at 39.3 Hz.

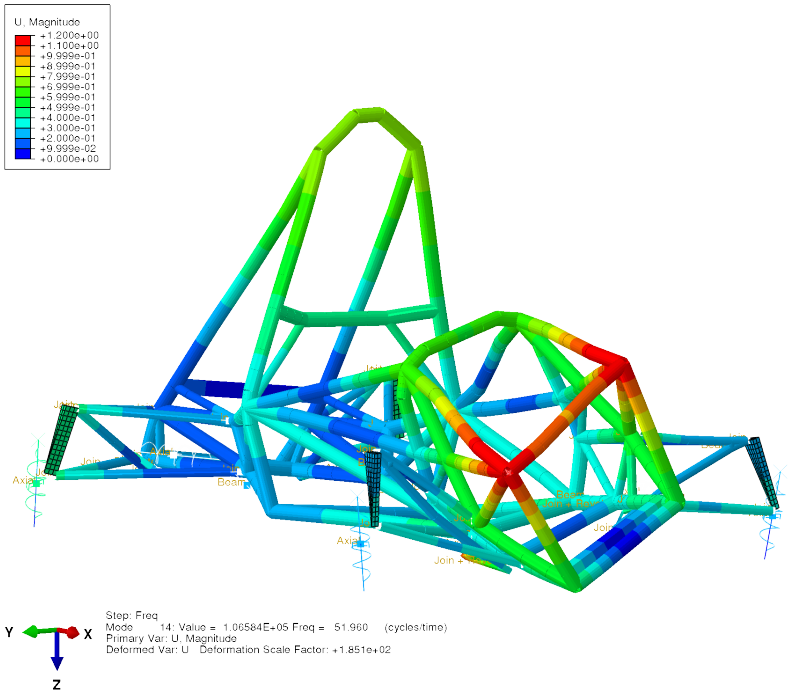

Figure 5.10: Twisting interaction mode for *Base* chassis-suspension model at 52.0 Hz.

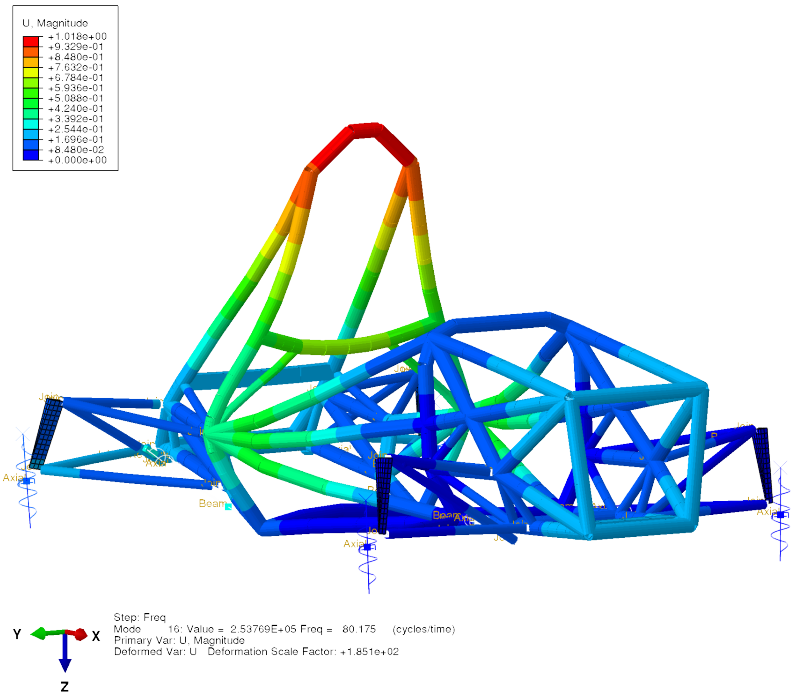

Figure 5.11: Bending interaction mode for *Base* chassis-suspension model at 80.2 Hz.

5.2.3 Base/Rigid Modal Analysis Conclusions

Modal analysis provides a better alternative to static stiffness as a performance metric. Natural frequencies naturally contain a stiffness to mass ratio in their definition, and a free-free modal test was easier to replicate in the lab than the static torsion boundary conditions. While this value is still no more useful to providing loading cases for design than the static case, when connected to the suspension the natural frequency response does provide an insight into how the chassis and suspension interact. Ideally the design should move the chassis frequencies as far from the suspension frequencies as possible.

5.2.4 Composite Results

Comparison of Abaqus model to literature data

Before running the modal analysis with the composite chassis models, the modeling technique for the composite panels in Abaqus was verified. Table 5.5 shows the results from Jenq [11] on natural frequencies of composite panels without cutouts compared to the Abaqus results.

Table 5.5: Comparison of Natural Frequency Data Between Jenq [11] and Abaqus.

	Paper	**Abaqus**
Mode 1	41.38 Hz	40.678 Hz
Mode 2	173.38 Hz	170.05 Hz
Mode 3	259.36 Hz	254.44 Hz

Jenq used cantilevered S-glass/epoxy unidirectional pre-preg tape (Fiberite, Hy-E 9134B) with a layup sequence of $[0/90/0/90/0/90/0/90/0/90/0/90/0/90/0]_T$ and panel dimensions of 6 cm x 17 cm x 1.5 cm. The same S8R elements were used to model the panel in Abaqus. Since the panels are predominately going to be used in modal analysis without any dynamic loads or failure analysis, these results show the panels as modeled are accurate enough to move forward with the analysis.

Composite Chassis Modal Results

Just as with the *Base* model, modal analysis was run for each of the composite models with and without the attached suspension. The results for the chassis without the suspension are

shown in Table 5.6. The mode shapes were similar to the base/rigid models.

Table 5.6: Natural frequency comparison between chassis models.

	Base	**Rigid**	**C2012**	**Attached**	**Semi-monocoque**
Mass (kg)	25.6	25.6	29.7	26.0	26.7
Twisting (Hz)	53.0	167.3	55.1	75.0	81.2
Lateral Bending (Hz)	80.0	251.7	109.3	N/A	120.5
Bending (Hz)	84.7	262.6	84.2	115.6	115.8

Table 5.6 shows that with the *Attached* and *Semi-monocoque* models there was a significant improvement in natural frequency response compared to the *Base* and *c2012* models. Meanwhile, other than in lateral bending there was very little improvement in the natural frequency response with the *c2012* model compared to the *Base* model. While the static tests show that the *c2012* model did improve on the stiffness of the chassis, the additional mass required was the same in proportion. With the similar stiffness to mass ratio for the *c2012* and *Base* models, it shows the composite floor was not an efficient design. The other two models show that when designed to have stiffness in particular directions the stiffness can be significantly increased without a large mass penalty. Another important aspect of Table 5.6 is that the mass values given for the *c2012* model reflects the mass of the chassis with the body coverings and closeouts attached to the frame. Without consideration of loading, the *Attached* model was approximately 4 kg lighter than the *c2012* while providing almost all the closeout structure needed while increasing performance in natural frequency and static twist. The performance gains carried over to the suspension interaction modes as well and are outlined in Table 5.7.

An important take away from these results was that the suspension modes remained the same frequency. This shows that even the *Base* system was stiff enough to not influence the pure suspension modes. It then becomes important to move the first interaction modes far enough away from their suspension counterparts. As Table 5.7 shows, the twisting interaction moved from 51.96 Hz in the *Base* model to 70.3 and 70.4 Hz in the *Attached* and *Semi-monocoque* models. When compared to the roll mode of the system, this moved the separation from about 40 Hz to almost 60 Hz. The bending modes also showed similar performance gains in mode separation.

Table 5.7: Natural frequency comparison between chassis-suspension models.

	Base	**Rigid**	**C2012**	**Attached**	**Semi-monocoque**
Heave (Hz)	6.6	6.7	6.4	6.3	6.5
Pitch (Hz)	9.2	9.3	9.1	9.1	9.3
Roll (Hz)	12.8	13.1	12.7	12.7	12.9
Twisting (Hz)	52.0	148.0	50.2	70.3	70.4
Lateral Bending (Hz)	39.3	117.2	63.6	62.9	62.1
Bending (Hz)	80.2	243.6	107.4	99.6	96.1

5.2.5 Composite Modal Conclusions

It would not be beneficial at this stage to run the composite models through the dynamic analysis, as the dynamic cases are not ready for design loads yet. But, as the static twist and modal analysis showed there are significant gains when the composites are properly designed. For the *Attached* and *Semi-monocoque* chassis the chassis only modes moved at least 20 Hz, while remaining relatively close in total mass to the *Base* model. With a more in-depth design the performance should only improve, although tailoring the composite to increase these frequencies should come second to tailoring to react load developed from dynamic maneuvers.

Chapter 6

Dynamic Maneuvers

This chapter outlines and presents results and conclusions from the dynamic vehicle maneuvers. First, the two-wheel bump case is investigated, followed by constant-speed-constant-radius turns. Also, in this chapter are simple model checks to verify the overall model responds well to the dynamic inputs.

6.1 Bump Maneuver

6.1.1 Abaqus Outline

An outline of the Abaqus analysis steps and parameters are provided below:

- Abaqus Implicit Solver
- Static General Step (1 second) – Initialize gravity in the model. Pinned ground nodes. Settle Vehicle.
- Implicit Dynamic Step – Get vehicle up to speed with amplitude curve. Ground nodes restricted only in the z direction.
- Implicit Dynamic Step – Amplitude curve for ground displacement. Manually specify time step.

6.1.2 Bump Details

The bump analysis contains the full chassis and suspension geometry with connector tire elements and represents the vehicle driving over a bump in the road to evaluate straight line

dynamics of the chassis-suspension system. The bump actuates both sides of the vehicle in-phase. Given the long time period of the simulation in real time, 11.5 seconds, an implicit solver was used as it is better suited for long time periods. While the explicit solver would work well for the bump section given the small time scales, it would require a restart analysis in Abaqus and transferring results. The process was very straight forward, but not all the options are available when transferring results containing connector elements.

The first step in the bump analysis was to apply a gravity load to the system to establish the static equilibrium position of the vehicle. The driver and engine masses are not included in this model. The gravity load only needs to be applied in the first step and will stay active throughout the following steps. Boundary conditions for the gravity step are detailed in Table 6.1.

Table 6.1: Boundary conditions for gravity step.

Boundary Conditions		
Node	**DOF**	**Value**
GROUND-LR	U1,U2,U3,UR3	0
GROUND-RR	U1,U2,U3,UR3	0
GROUND-LF	U1,U2,U3,UR3	0
GROUND-RF	U1,U2,U3,UR3	0
STEER NODE	U1	0
Applied Loads		
ALL MASS NODES	3	9810 kg*mm/s

Table 6.1 shows while the gravity load was applied, the steering input was set to zero and the ground nodes are restrained in the x and z direction. The z restriction represents the tires fixed to the ground while the x boundary condition represents the friction of the tires on the ground, keeping the vehicle from translating while the gravity load is applied. There are no loads in the x or y direction, but the vehicle would not be restrained from displacement in the x or y directions, rendering the system of equilibrium equations singular. The gravity load was applied over a period of 1 second to not abruptly load the structure and allow the system to settle.

After the gravity load the vehicle was brought up to speed, 11.18 m/s, using a linear amplitude curve to minimize acceleration. The final velocity was scaled against an amplitude curve to slowly bring the vehicle to a speed of 11.18 m/s (25 mph) over a period of 5 seconds and remain at 11.18 m/s for 4.5 seconds. The time periods used do not have significance in

magnitude as the purpose was to limit the acceleration in the velocity portion and to allow the vehicle to settle after reaching speed before the bump. Table 6.2 outlines the boundary conditions for the velocity step.

Table 6.2: Boundary conditions for velocity step.

Boundary Conditions		
Node	**DOF**	**Value**
GROUND-LR	U3,UR3	0
GROUND-RR	U3,UR3	0
GROUND-LF	U3,UR3	0
GROUND-RF	U3,UR3	0
STEER NODE	U1	0
CHASSIS	V1	11176 mm/s

After the vehicle has reached velocity and settled, the bump was initiated by controlling the z-displacement of the ground nodes. Each ground node was given a prescribed displacement of -1 mm, positive z is down, and scaled by amplitudes that defined the bump profile. Both the front and rear have the same profile, the rear was delayed by a time interval equal to the time necessary to travel one wheelbase length at velocity. Table 6.3 shows the boundary conditions for the bump step.

The bump profile was defined using equations designed for cam systems from Mabie [13] as it produces a curve with zero acceleration at the beginning and the end of the curve. The bump curve also minimizes the derivative of the acceleration, jerk, which also ensures a slow ramp up to velocity. Equation 6.1 outlines how to produce the profile. The time scales are determined by the time to travel the bump length at 11.18 m/s. The bump used has a height of 25.4 mm and a length of 101.6 mm (1 in by 4 in) and a shape shown in Figure 6.1. Given the small time period over which the bump occurs, the time increment the solver takes has to be specified. The solver looks up the current time in the amplitude table and interpolates the value, and if the time step was too large the entire bump could be skipped. The amplitude profile was defined with 100 linearly spaced values between the beginning and the end of the bump section. The order of magnitude of the steps between values in the

Table 6.3: Boundary conditions for bump step.

Boundary Conditions		
Node	**DOF**	**Value**
GROUND-LR	U3	-1
GROUND-RR	U3	-1
GROUND-LF	U3	-1
GROUND-RF	U3	-1
GROUND-LR	UR3	0
GROUND-RR	UR3	0
GROUND-LF	UR3	0
GROUND-RF	UR3	0

amplitude curve were chosen as the solver time interval, in this case 4.0E-5 seconds.

$$\begin{aligned} R &= \frac{T}{T_h} \\ b_{up} &= h_b \left(\frac{R-1}{2pi} \sin(2piR) \right) \\ b_{down} &= h_b \left(1 - \frac{R+1}{2pi} \sin(2piR) \right) \end{aligned} \tag{6.1}$$

where R is the ratio of the current time value (T) to the time value at the peak (T_h), b_{up} and b_{down} are the bump amplitudes for the way up and down, and h_b is the height of the bump. When b_{up} and b_{down} are combine at the peak of the bump they create entire profile. Figure 6.1 shows the bump profile as well as the velocities and accelerations of the profile.

So that there was not an abrupt change in model behavior at the start of the analysis step, a 0.25 second offset was used before the amplitude was started. This was accomplished by padding the beginning of the amplitude curve with zeros. The analysis was allowed to continue to run after the rear wheels returned to the ground for 0.5 seconds to allow the suspension to return to equilibrium.

The model also outputs the history data of particular variables of nodes and elements of interest, the relative spring and tire displacements for example. The history data were used to evaluate the important aspects of the results as it can be hard to tell what exactly was going on when just viewing the Abaqus Visualization Module.

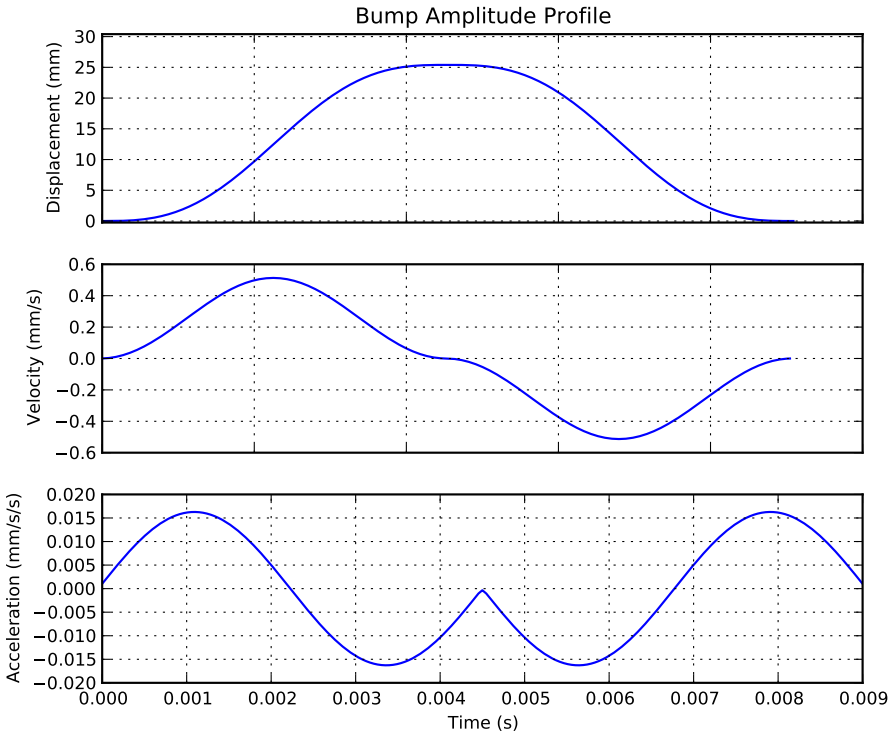

Figure 6.1: Plot showing the shape of the bump profile used.

6.1.3 Dynamic Model Checks

Without experimental results to compare to, intermediate steps need to be verified to be working properly before simulating the maneuvers. The first step in all the dynamic analysis was a static gravity step. Using the center of mass of the model, the reaction forces due to gravity can be determine using Equations 6.2 and 6.3 that are based on the load diagram in Figure 6.2.

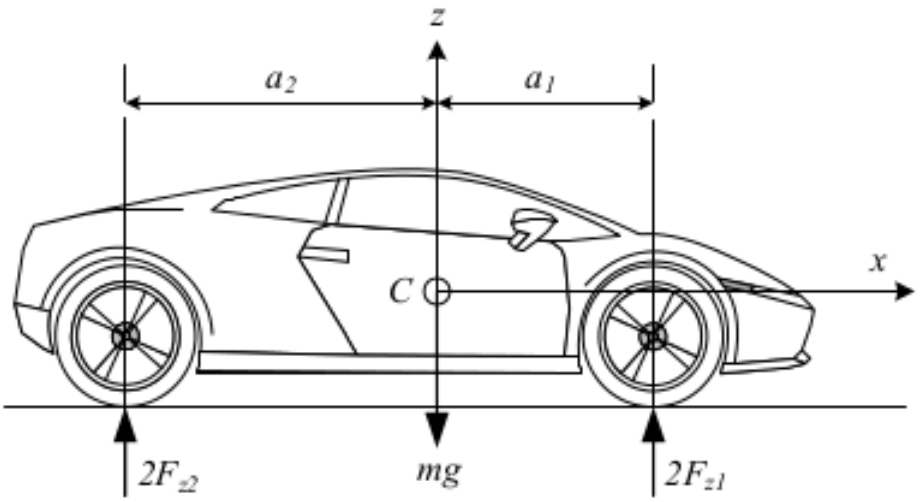

Figure 6.2: Figure showing tire reaction forces due to gravity. Reproduced from Vehicle Dynamics: Theory and Application, by R. N. Jazar, Copyright 2008, Springer Publishing with kind permission of Springer Science+Business Media [10]

$$F_{z_1} = \frac{1}{2} mg \frac{a_2}{l} \tag{6.2}$$

$$F_{z_2} = \frac{1}{2} mg \frac{a_1}{l} \tag{6.3}$$

where a_1 and a_2 are the distances from the center of gravity to the front and rear axles, F_{z_1} and F_{z_2} are the reaction forces at the front and rear tires, m is the mass, and g is the acceleration due to gravity. Using Equations 6.2 and 6.3 the expected reaction forces at the ground nodes is shown in Table 6.4, and the Abaqus plot of reaction forces is shown in Figure 6.3.

Table 6.4 shows that the calculated results are extremely close to the predicted values. This was the final step that could be verified with calculations and/or experimental data. The suspension's vertical actuation and the model's gravity response suggest the model was able to capture the motion of the suspension in under static loads. As such, the dynamic analysis can only be taken for their trends and relative displacement as the team does not currently have data to compare these results with.

Table 6.4: Reaction forces in the z direction due to gravity.

Location	Calculated	Abaqus
Ground-LF	146.10 N	145.98 N
Ground-RF	146.10 N	146.41 N
Ground-RR	131.66 N	131.78 N
Ground-LR	131.66 N	131.36 N

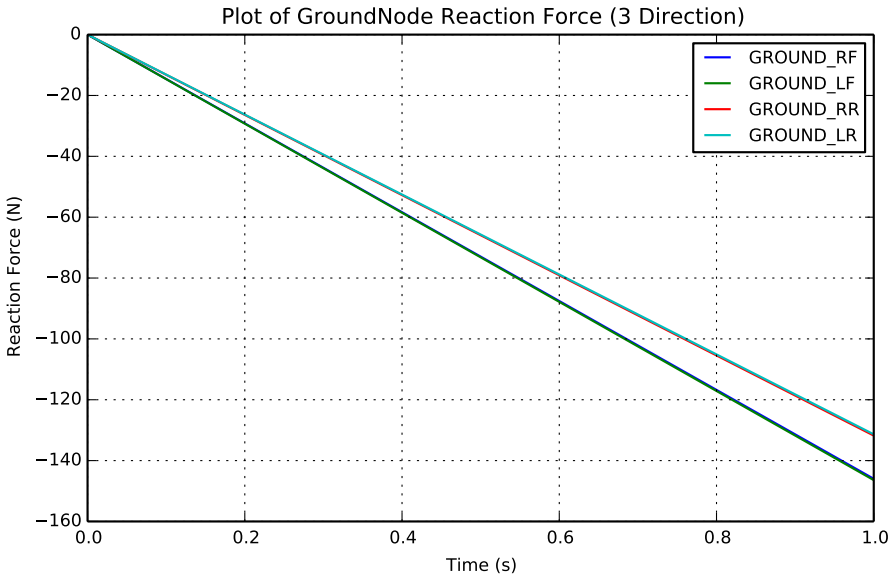

Figure 6.3: Plot of reaction force in the z-direction ground nodes due to gravity

The next step in the dynamic analysis was the velocity step. It will be discussed in more detail in the following sections, but the ramp up to speed was slow to keep out acceleration effects and focus on the bump/turn. Figures 6.4 and 6.5 show the velocity results of the chassis and wheel centers respectively. As both figures show, the velocity was slowly ramped up, and then held constant for 4.5 seconds to make sure the system was settled before entering the maneuvers. Figure 6.6 shows the spring displacement response through the velocity step of the analysis. After the gravity step there is no apparent change in spring displacement suggesting the acceleration is slow enough as to not cause the chassis to pitch.

Through the velocity steps in the dynamic models, the model was performing as expected. The reaction forces due to gravity were close to calculated and the vehicle accelerated slowly

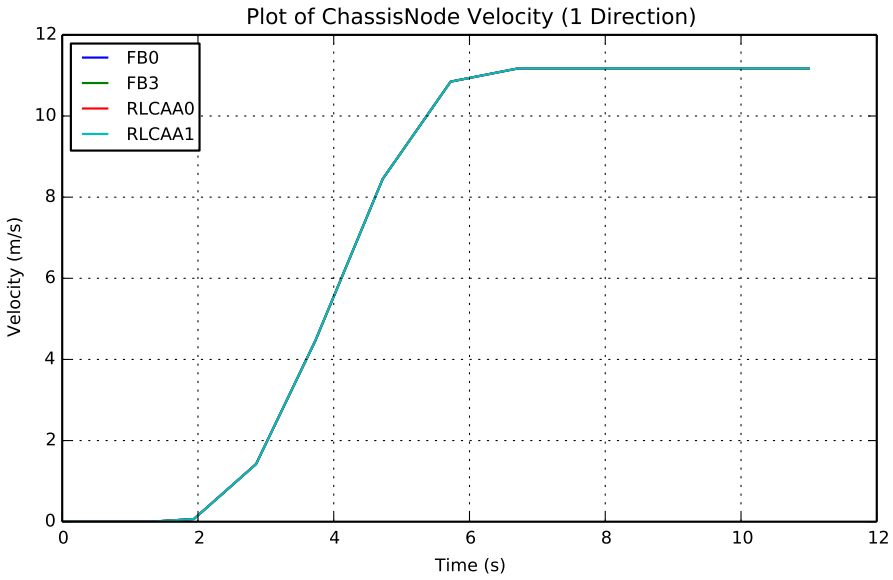

Figure 6.4: Plot of velocity in the 1-direction of chassis nodes through the velocity step.

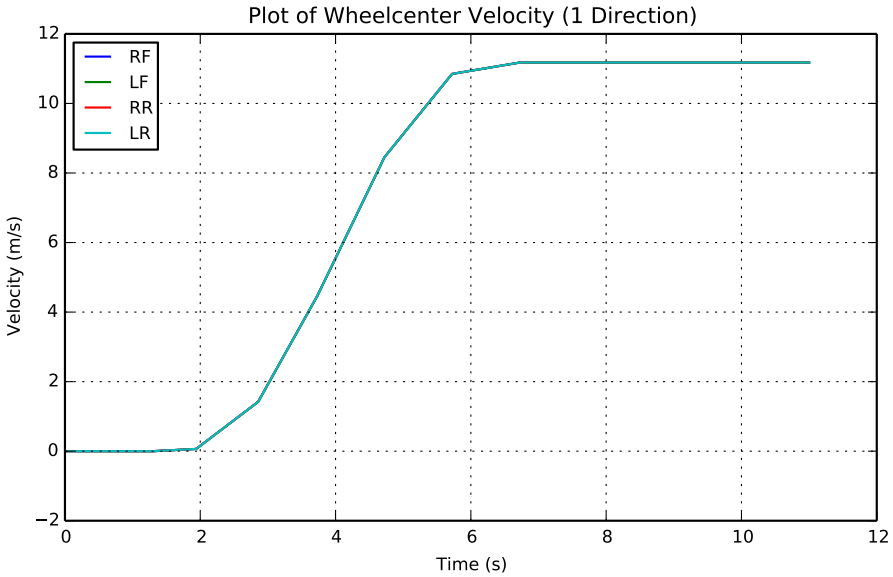

Figure 6.5: Plot of velocity in the 1-direction of wheel centers nodes through the velocity step.

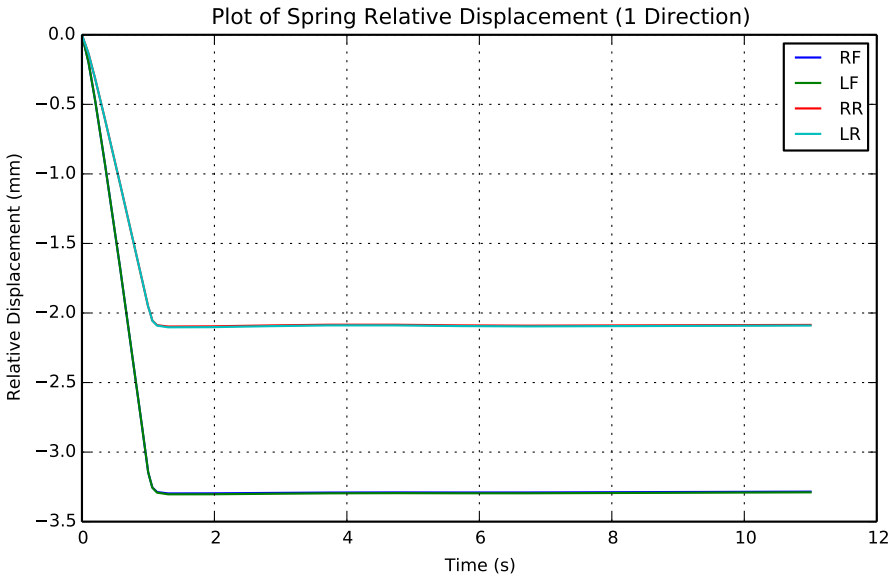

Figure 6.6: Plot of spring displacement through the velocity step.

up to speed without any noticeable pitching.

6.1.4 Bump Results

The important components evaluate in the bump analysis were the relative spring displacements and the overall response of the chassis-suspension system. Without data to compare to, it was important to look at the overall motion of the system and determine if enough of the details looked promising. Even if such data were available, the two systems would not be close enough together to compare data as the base model here does not have a driver, engine, or differential all of which are large mass components on the car. The first component looked at was the ground nodes to verify that they did displace as intended. The other important component to look at was the relative spring displacements. Figure 6.7 shows the plots of the two components plotted next to each other.

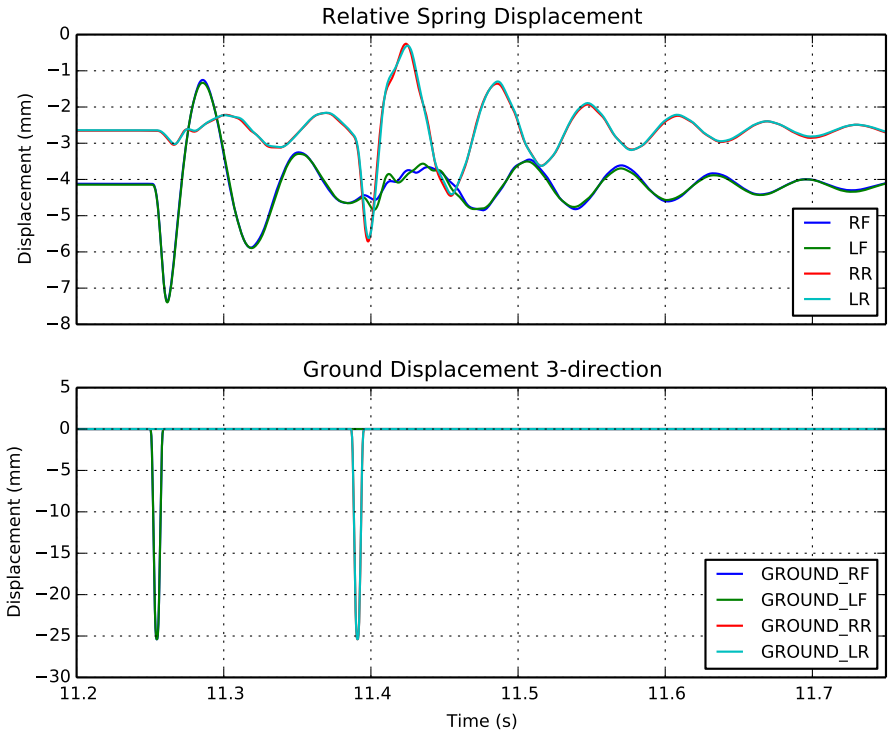

Figure 6.7: Plots showing relative spring displacement and ground z-displacement during bump analysis

The bump displacement begins at 11.25 seconds on the plot for the front wheels and at 11.38 seconds for the rear bump with each bump lasting 0.009 seconds. It only appears as though there two lines on each plot, when the left and right spring and ground node lines lie on top of each other. This was a good sign for the analysis given the two sides were activated in phase. With the lines on top of each other the kinematics on the left and right side of the vehicle are identical.

The spring displacements are also smooth in nature, a by-product of how the bump profile was defined without sharp changes in direction. Figure 6.7 also shows the springs, both front and rear, reaching their peak displacements after the ground node does. This delay in deflection was due to the connector tire element and its elastic/damping characteristics. Figure 6.8 shows the relative tire spring displacement along with the relative spring displacement from Figure 6.7.

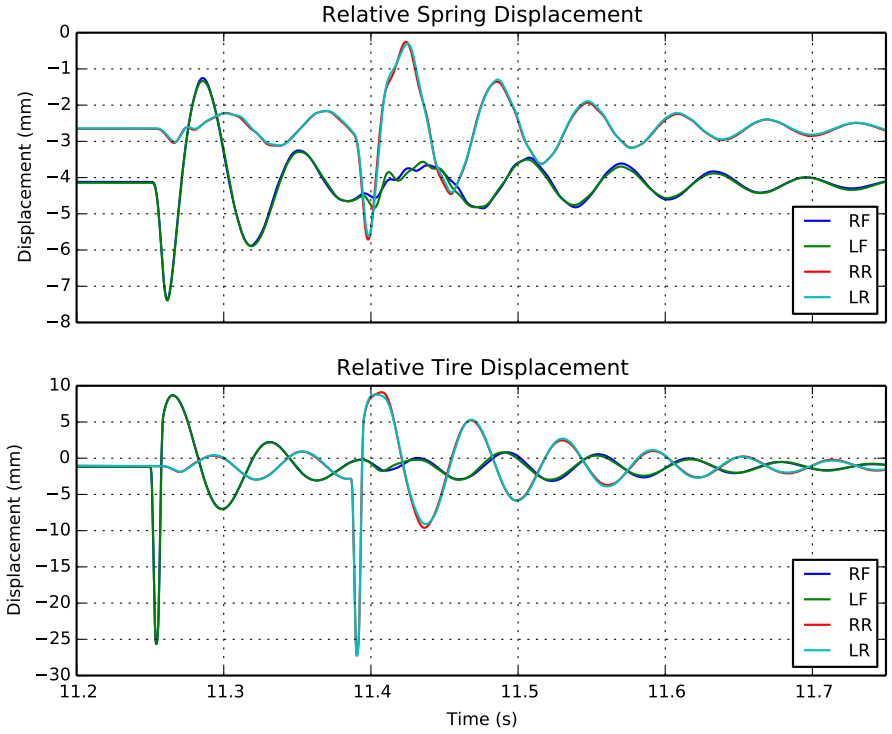

Figure 6.8: Plot of relative displacement of suspension springs and tires during bump analysis.

In Figure 6.8 it is clear that once the tire has displaced the spring begins to displace. The tire spring then goes through its equilibrium position and begins to extend. The extension is due to the bump boundary conditions. At the top of the bump profile the ground node was "pulled" back towards the ground, while the rest of the suspension assembly continued to move upwards. This caused the tire spring to expand as the ground node was moving down while the upright was still moving up. Without including an actual ground surface for the node to travel on or significantly increasing the stiffness/damping properties of the tire connector element, this motion will continue to exist, though it is likely some elements of tire compression exists in the real system.

Even considering the details of the tire connector motion, the overall behavior of the vehicle system was as expected. The suspension springs responded in a manner consistent with a

vehicle going over a bump. Figures 6.9-6.11 show, the chassis itself behaved as it should in a bump analysis. Figure 6.9 shows the 3-direction displacement of the lower nodes on the front and rear bulkheads. The plots show that once the front tires hit the bump the front and rear of the chassis remain out of phase with their displacements resulting in a pitching motion. The maximum displacement of the chassis was also under 25.4 mm which is expected given the bump was 25.4 mm high. The tires and suspension springs should and did absorb most of the displacement and should only be transmitting load into the chassis.

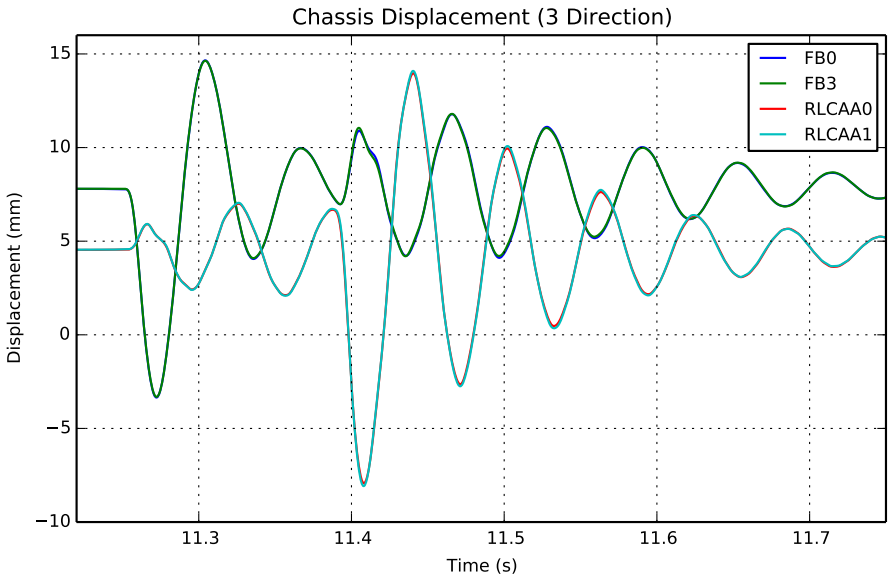

Figure 6.9: Plot of chassis displacement during bump analysis.

While the actual loads developed here are not representative of the full system, the structurally weak sections of the chassis can still be highlighted. Figures 6.10-6.11 both show the 2-direction displacement of the suspension pickup points on the chassis front and rear respectively. In the front, both upper control arm points saw the most displacement as they are the only points on the front suspension that do not have a cross brace attached at the node, resulting in a relatively weaker section. It cannot be known if it is too weak from this analysis only that it was weaker than the others. The rear had the two forward suspension points with high displacement. In this case, those points would have other sections attached to them which bolt the engine to the chassis. While the 2012 car does not use the engine as a stressed component, it does provide stiffness to the rear structure.

The magnitude of the displacement in Figures 6.10 and 6.11 are both under 1 mm of displacement, which given the low speed of the vehicle and the size of the bump, seems to make sense. It will be important to look at the displacement of the suspension nodes as well as the loads that are developed when analyzing future cars, especially at higher speeds and larger bumps. If these suspension points were to displace too far, the suspension geometry

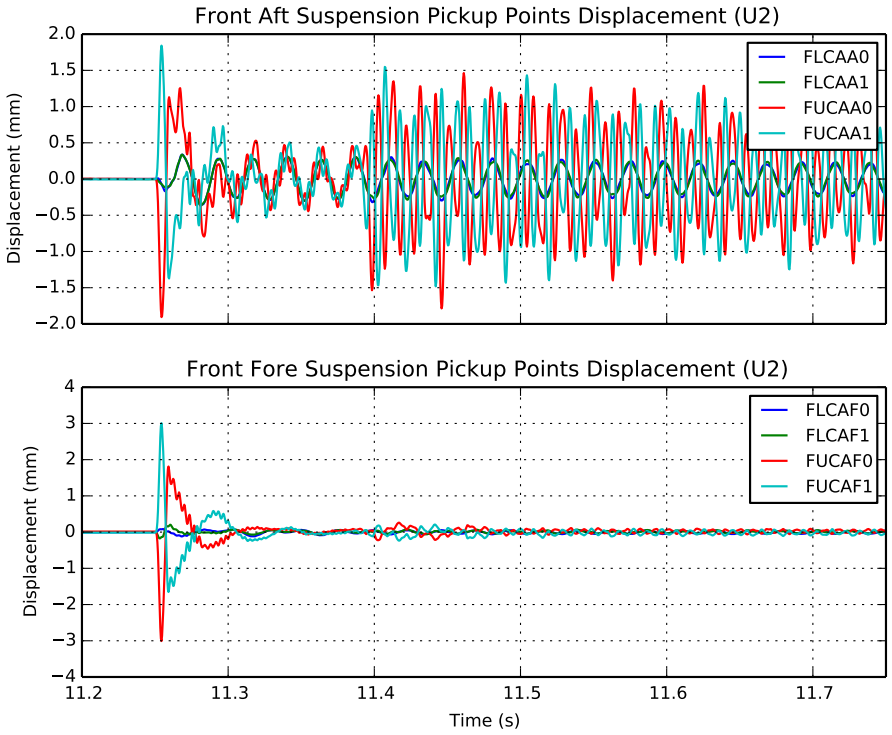

Figure 6.10: Plot of front suspension pickup displacement during bump analysis.

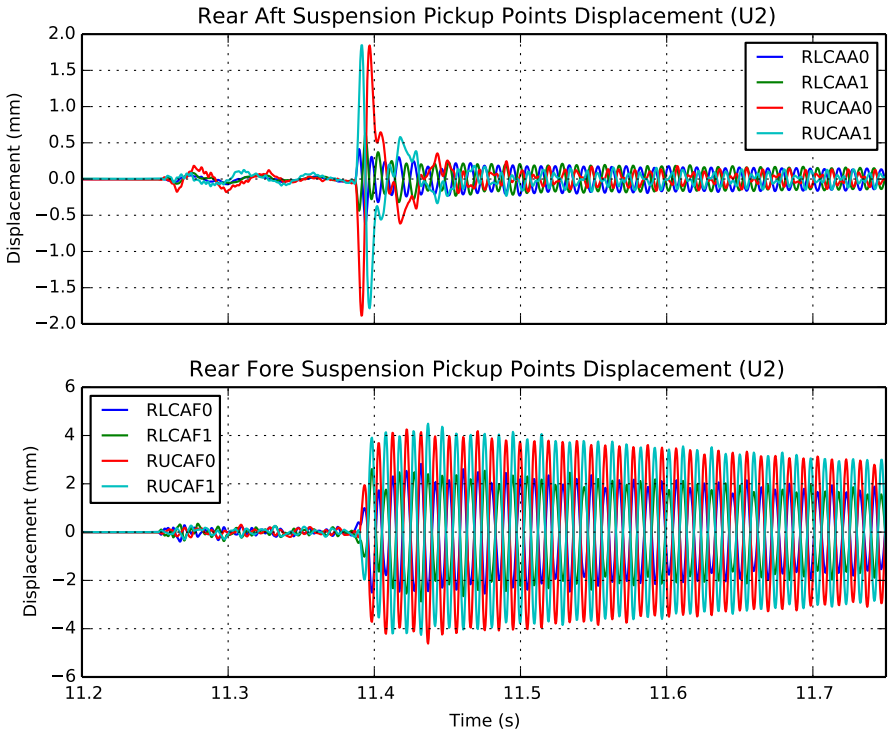

Figure 6.11: Plot of rear suspension pickup displacement during bump analysis.

then starts to change and would no longer perform as designed. Also, in the case of the rear points, it would be up to the design team to decide if the rear points should be able to survive and/or not displace too far without help from the engine.

6.1.5 Bump Maneuver Conclusions

Overall the motion of the vehicle in bump followed trends that would be expected in the real system. The spring and chassis motion reflected bump motion with the pitching motion back and forth as well as the majority of the displacement occurred in the suspension versus the chassis. The connector element representation of the tire seems to handle the straight line dynamics of the model as well as the vertical displacement of the suspension.

6.2 Turning Manuever

After looking at the bump analysis, the next step was to look at non-straight line maneuvers. A constant-speed-constant-radius turn was used. Similar to the bump analysis, only the trends and overall motion of the vehicle are of concern at this point. Without data, it would not be possible to determine if the loads or magnitude of displacement generated in the model were representative of the system. The loading profile and results are presented below.

6.2.1 Connector Tire

Abaqus Outline

An outline of the Abaqus analysis steps and parameters are provided below:

- Abaqus Implicit Solver
- Static General Step (1 second) – Initialize gravity in the model. Pinned ground nodes. Settle Vehicle.
- Implicit Dynamic Step – Get vehicle up to speed with amplitude curve. Ground nodes restricted only in the z direction. Steering input at end of step.
- Implicit Dynamic Step – Amplitude curve for ground node velocities in x and y directions.

Setup

The constant-speed-constant-radius turn using the connector tire was a first attempt at evaluating the system while performing a non-straight line dynamic maneuver. A constant low speed, low lateral acceleration turn provides a simple example to determine how the model reacts when no longer traveling in a straight line. The reason for using the connector tire model was it is simpler and fewer degrees of freedom than a rolling tire model, which was outside the scope of this thesis. The gravity and velocity steps are the same as the bump step before. The only difference is in the velocity step at the end, a steering input was applied as shown in Table 6.5.

Table 6.5: Boundary conditions for velocity with steering step.

Boundary Conditions		
Node	**DOF**	**Value**
GROUND-LR	U3,UR3	0
GROUND-RR	U3,UR3	0
GROUND-LF	U3,UR3	0
GROUND-RF	U3,UR3	0
STEER NODE	U1	steering input (mm)
CHASSIS	V1	velocity (mm/s)

Motion of the vehicle in the connector tire model was not tied to the orientation of the tires and the steering input was used to put the upright and tie rod in the position they would be during a turn. Steering input was calculated Figure 6.12 and Equation 6.4.

$$\delta = \frac{l}{R} \tag{6.4}$$

where δ was the average steering angle for a vehicle with a wheelbase l and a turn radius of R. By actuating the steering rack and measuring the angle of the connector tire elements a steering input can be calculated to correspond with Equation 6.4. Figure 6.13 shows a plot of steering angle at the wheel versus the steering input from the rack.

The turn step was applied at the end of the velocity step. At the beginning of the turn step the initial velocities are the same as the previous velocity step and the tire connector element motion in the local 4-direction was fixed and the restriction on the ground nodes in the global 6-direction are removed to allow the vehicle to yaw. Velocities of 1 mm/s are

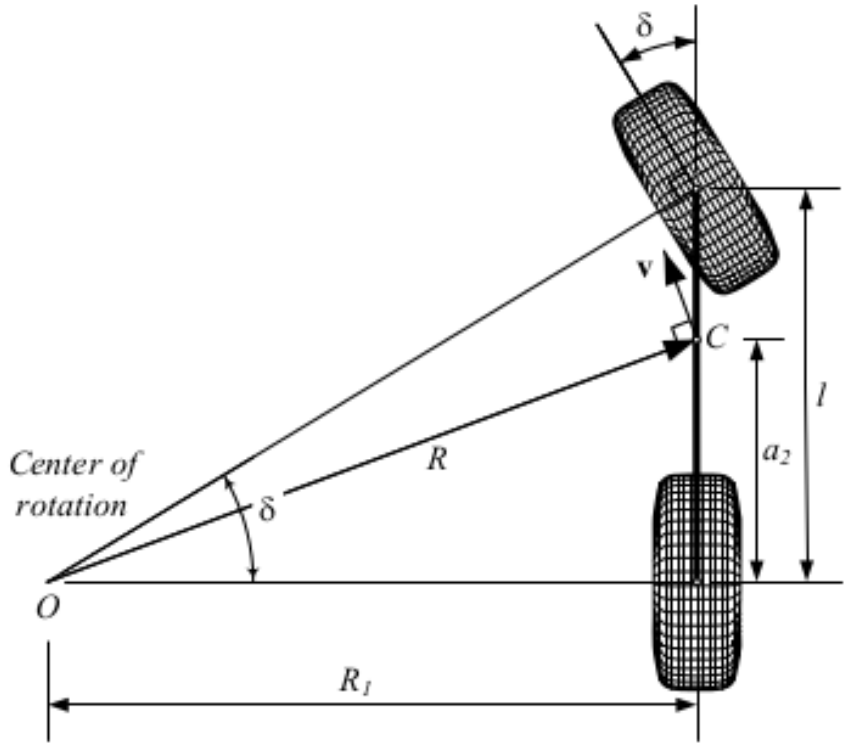

Figure 6.12: Bicycle model for steering angle. Reproduced from Vehicle Dynamics: Theory and Application, by R. N. Jazar, Copyright 2008, Springer Publishing with kind permission of Springer Science+Business [10]

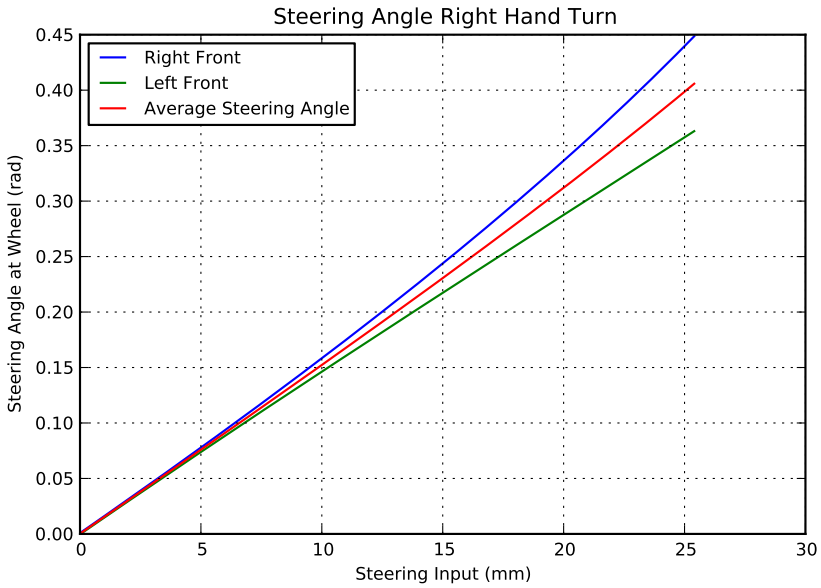

Figure 6.13: Steering angle at the wheel for different steering inputs.

applied to the two front ground nodes in the global 1- and 2-directions. The velocities are scaled with amplitudes corresponding to the x and y components of the tangential velocity going around a circle. The velocities are determined by calculating the radius of the turn and then adding/subtracting the half track width to get to the particular ground node as shown in Equations 6.5-6.9. The profile for the x and y velocities for the front right wheel during the turn is shown in Figure 6.14. The same history outputs from the bump analysis are requested for the turning analysis.

$$R = \frac{v^2}{a} \tag{6.5}$$

$$R_{wc} = R \pm \frac{T}{2} \tag{6.6}$$

$$v_{wc} = \sqrt{R_{wc} a} \tag{6.7}$$

$$V_x = v_{wc} \cos(\theta) \tag{6.8}$$

$$V_y = v_{wc} \sin(\theta) \tag{6.9}$$

where R is the radius of the turn, v is the velocity of the vehicle, a is the lateral acceleration, R_{wc} is the radius at the wheel center, v_{wc} is tangential velocity at the wheel center, θ is the angle on the circle, and V_x and V_y are the global x and y velocity components.

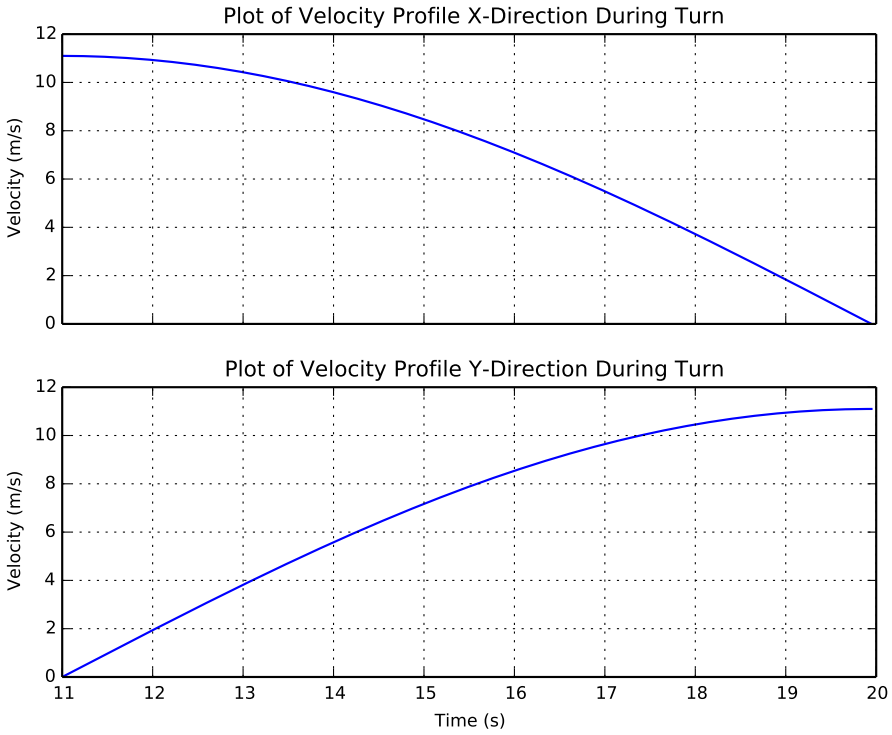

Figure 6.14: Plot of velocity profiles through the 90 degree turn.

Connector Tire Turning Results

As explained in Section 6.2.1, the constant-speed-constant-radius turn analysis was identical to the bump analysis through the velocity step. Figures 6.15 and 6.16 show the velocity of the ground nodes throughout the analysis in both the global 1- and 2-directions.

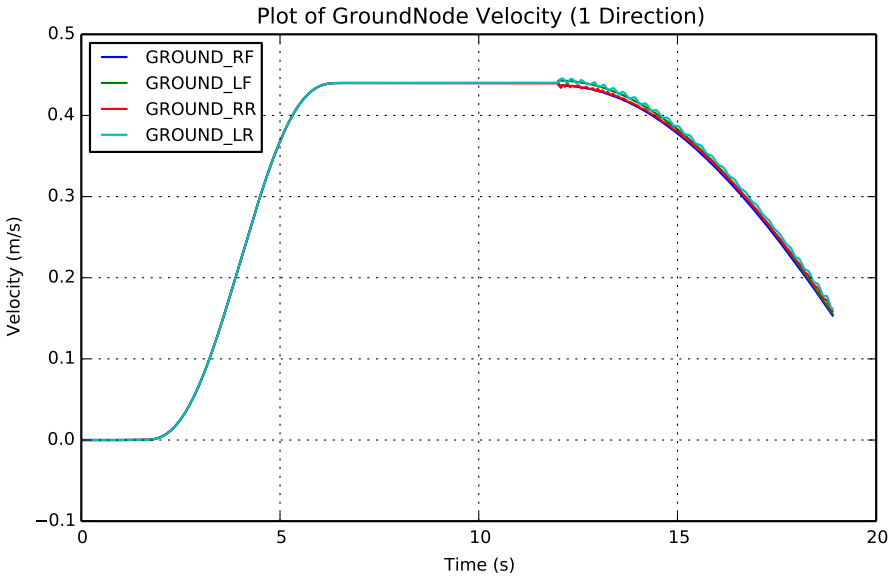

Figure 6.15: Plot of ground velocity in the 1-direction during turn analysis.

As Figure 6.15 shows the velocity profile before the turn was the same as in Figure 6.5. When the turn begins at 11 seconds, the outside ground node velocity magnitude increases while the inside ground node velocity magnitude decreases. There was some noise in the rear velocities because the rear velocities are not prescribed, but instead trail the front. This allowed for as little forced input into the system as possible, decreasing the possibility of over-constraining the model. After verifying that the ground nodes followed the prescribed velocities, the suspension spring displacements need to be checked. Figure 6.17 shows the relative displacement between the suspension springs.

At the beginning of the right turn step the left side springs, outside of the turn, had a negative relative motion (compression) from their position after the velocity step while the right side, inside of the turn, had a positive relative motion (extension). This displacement setup is characteristic of roll in the vehicle towards the left side of the vehicle. Roll to the left of the vehicle is characteristic of a right-hand turn and given the small amount of roll, the displacement is characteristic of a low-speed right-hand turn. However, as the turn progresses both front springs begin to expand maintaining their roll position while the rear holds constant. As Figures 6.18 and 6.19 show the front tires were compressing and the front chassis nodes are displaced upwards.

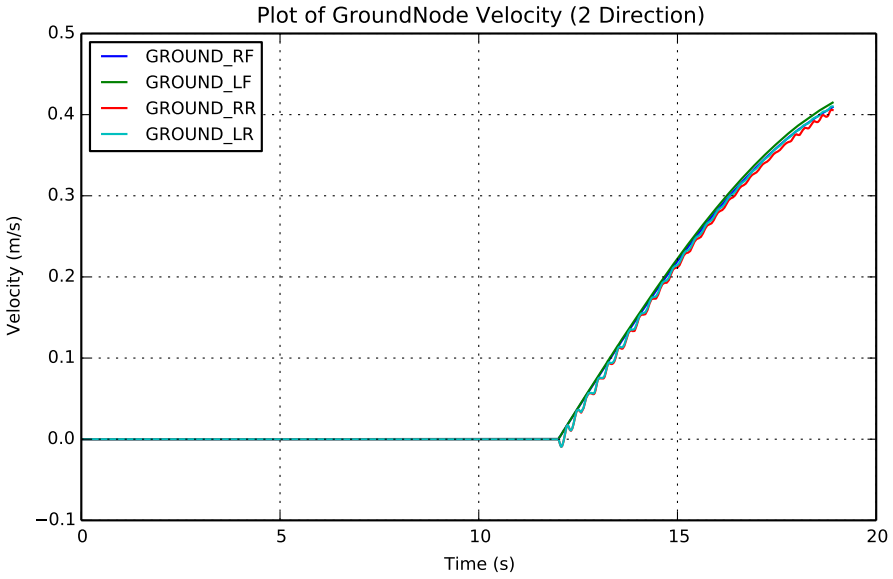

Figure 6.16: Plot of ground velocity in the 2-direction during turn analysis.

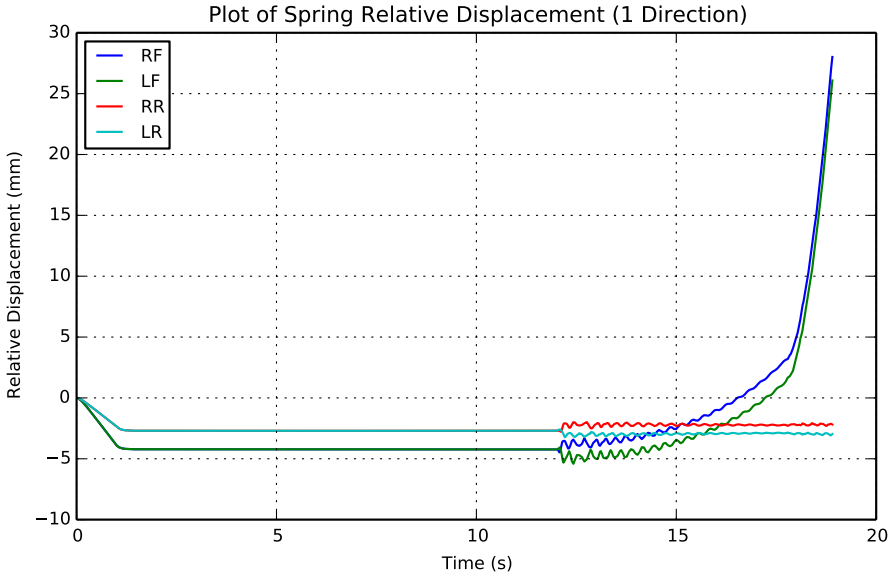

Figure 6.17: Plot of relative spring displacement during turn analysis.

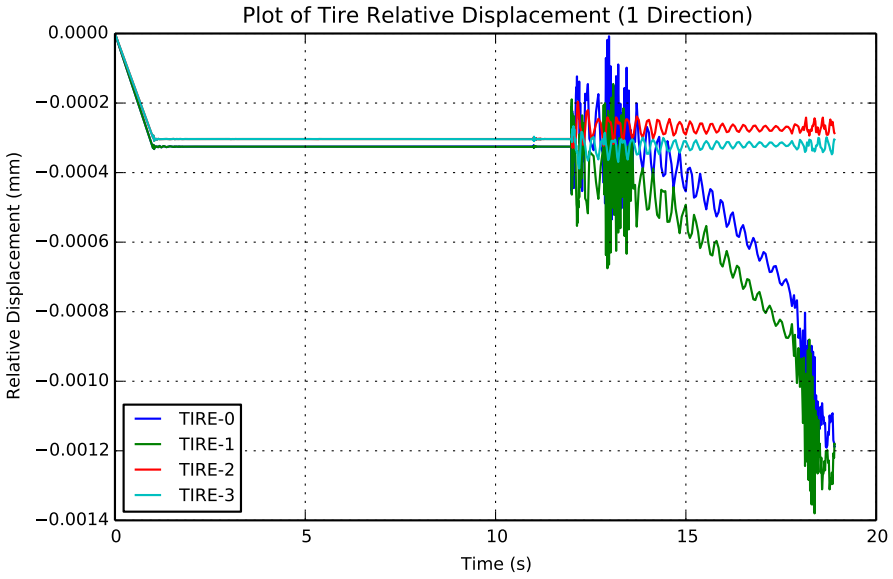

Figure 6.18: Plot of relative tire displacement during turn analysis.

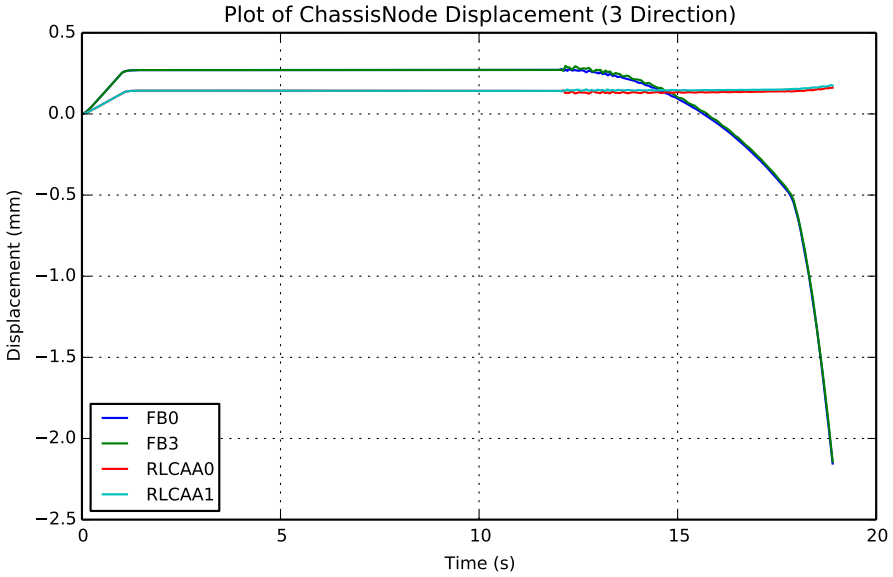

Figure 6.19: Plot of chassis displacement during turn analysis.

The initial roll at the beginning of the turn step was promising, it showed that the mass of the system was moving as expected and the boundary conditions seemed to describe the turn correctly. Unfortunately, as the simulation developed, it is likely the model could not react the loads developed at the ground nodes properly. A possible reason for the behavior could be that since the velocities have to be prescribed and are not developed, the outside and inside wheel velocities could be out of sync, leaving Abaqus to resolve dynamic equilibrium by pitching the chassis. Similar behavior also occurred in the rear when the velocities were prescribed in the rear instead of the front with the rear tires displacing and the rear pitching. This ruled out a modeling detail in the front suspension causing the problem.

The more likely reason for the failure of the connector tire model was that only one node without friction as the tire-ground interaction was not sufficient to handle the loads and deformation shapes needed. While in-plane forces are developed at the ground plane, they are due to the velocity boundary conditions. The simulation only had to keep the nodes at a velocity and not a particular track. Another limitation was that the upright assembly cannot change its camber without compressing the tire spring, therefore artificially adding camber stiffness to the system. In the real system the tire rolls about the longitudinal axis and changes its contact patch. While there would still be compression of the tire, it would be mostly due to the CG moving to add load to the tire and not from the upright changing orientation.

Connector Tire Turning Maneuver Conclusions

It is unlikely that changing to a displacement controlled simulation would yield different results as it would further restrict the motion of the system and would not help with addressing the camber issue in the upright and tire. The connector tire model showed promise at the beginning of the turn with the spring motion reflecting a small amount of roll which was to be expected for a low speed turn. After the initial roll the system began to deviate from the expected displacement shape when the lateral forces became larger, most likely due to the limitations of the connector tire representation. It appears that the connector tire representation does not allow the suspension to fully change camber angles and with only one node at the contact patch was unable to create and react the necessary forces to continue the turning maneuver. In order to accurately simulate and develop loading for vehicle maneuvers other than straight line motion, a rolling tire model would most likely need to be created. For straight line motion and simple vertical inputs to the suspension, the connector tire model can handle does seem to perform well.

6.2.2 Rolling Tire

Abaqus Outline

An outline of the Abaqus analysis steps and parameters are provided below:

- Abaqus Implicit Solver
- Static General Step (1 second) – Initialize gravity in the model. Pinned ground nodes. Settle Vehicle.
- Implicit Dynamic Step – Get vehicle up to speed with amplitude curve. Ground nodes restricted only in the z direction.
- Implicit Dynamic Step – Amplitude curve for steering input and wheel connector element relative velocities.

Setup

The connector tire model relies on specifying the resulting velocities in order to model how the vehicle takes the turn. With the rolling tire, it was a step towards modeling how the system actually behaves. The tire was modeled as a rigid shell element connected to the upright using connector elements. The relative rotational velocity between the tire and the upright coupled with friction at the surface interaction between the ground and tire causes the vehicle to move. When the steering input causes the orientation of the tires coupled with the change in wheel-speeds the vehicle changes direction. In the real system, the rear wheels are given a torque based on engine output and differential sensors, but those systems are not modeled here. Instead the front wheels are given the rotational velocities they are expected to have during the acceleration up to velocity and through the corner.

The steps for this model are similar to the connector tire model. Restriction on the z-displacement was modeled with the ground shell rather than boundary conditions in the connector tire model. The restriction on the global x-direction motion at the wheel centers was still used. In the velocity step either the wheel rotational velocities or the chassis velocity can be prescribed. The wheel rotational velocities were chosen because they will need to be applied in the turn step to initiate the turn.

After reaching velocity the turn step was started by ramping up the steering input calculated before. Over the same time interval the wheel rotational velocities are changed to what they are calculated to be during the turn. The amplitude curve for the steering input was linear from 0 to the final steer input. For each intermediate steering input value a turning radius was calculated and used in Equations 6.5-6.9 to calculate the intermediate vehicle speeds. The rotational velocities are calculated from the translational velocities of the connector tire

turn model and the radius of the tire shell as show in Equation 6.10. The steering input was held until the end of the simulation. Tables 6.6 through 6.8 outline the boundary conditions.

$$V_{rotation} = \frac{V_{translation}}{R} \tag{6.10}$$

Table 6.6: Boundary conditions for gravity step for rolling tire analysis.

Boundary Conditions		
Node	**DOF**	**Value**
LR	U1	0
RR	U1	0
LF	U1	0
RF	U1	0
STEER NODE	U1	0
Applied Loads		
ALL MASS NODES	3	9810 kg*mm/s

Table 6.7: Boundary conditions for velocity step for rolling tire analysis.

Boundary Conditions		
Node	**DOF**	**Value**
WHEEL-LF	VR1	velocity (rad/s)
WHEEL-RF	VR1	velocity (rad/s)
STEER NODE	U1	0

Table 6.8: Boundary conditions for turn step for rolling tire analysis.

Boundary Conditions		
Node	**DOF**	**Value**
WHEEL-LF	VR1	velocity (rad/s)
WHEEL-RF	VR1	velocity (rad/s)
STEER NODE	U1	steering input (mm)

Results

In order to more accurately model the turning maneuvers for the FSAE vehicle, a rolling tire model needed to developed, allowing for a more complete representation of the tire-ground interaction using friction. Using the conditions described in Section 6.2.2 the vehicle was brought up to speed and completed a constant speed turn. With the lack of accurate tire geometry and elastic models at the time of this research, rigid shells were used in place of the tires. This model was meant to begin to develop the framework for the process and mechanics of the analysis.

Using wheel speeds and a steering input the vehicle was able to get up to speed and perform a turning maneuver using the friction at the contact patch to change directions. Figures 6.20 to 6.23 to follow show a small time lapse of the beginning of the turn from above.

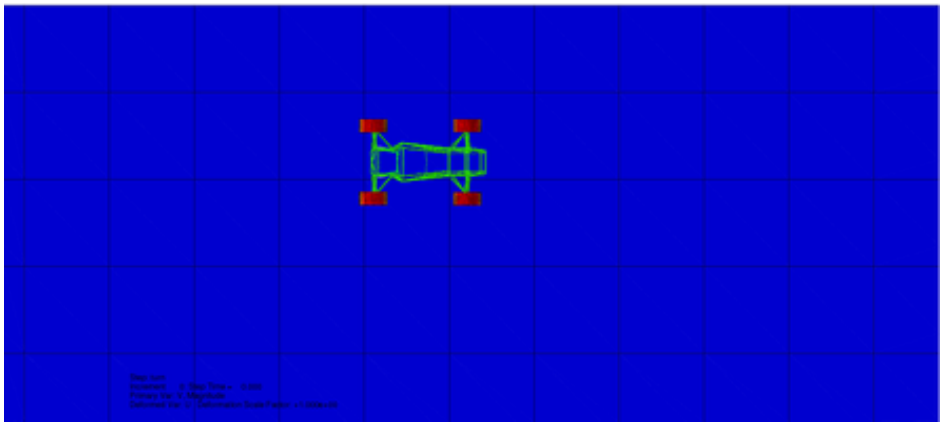

Figure 6.20: Rolling tire model at the beginning of the turn step.

As the front wheels turned and their rotational velocity was changed the vehicle began to turn in. Figures 6.24 and 6.25 show the wheel speeds and the spring displacement throughout the analysis. The front wheel speeds are as they were prescribed with the rear wheels developing

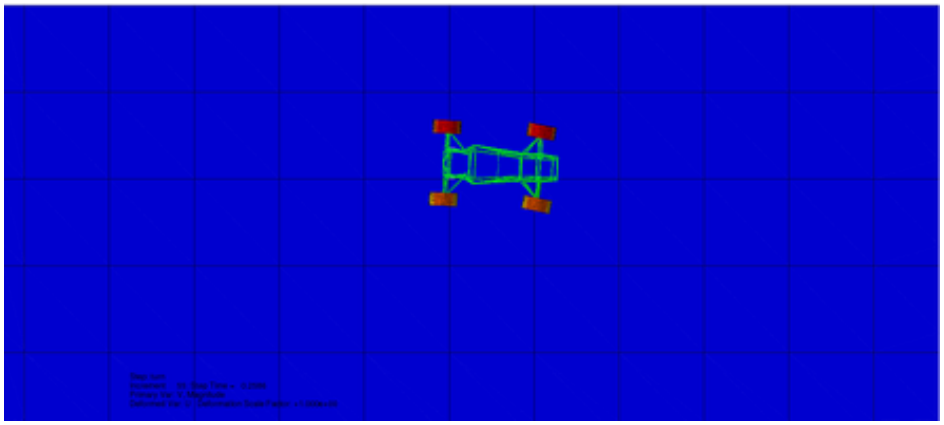

Figure 6.21: Rolling tire model 0.25 seconds into the turn.

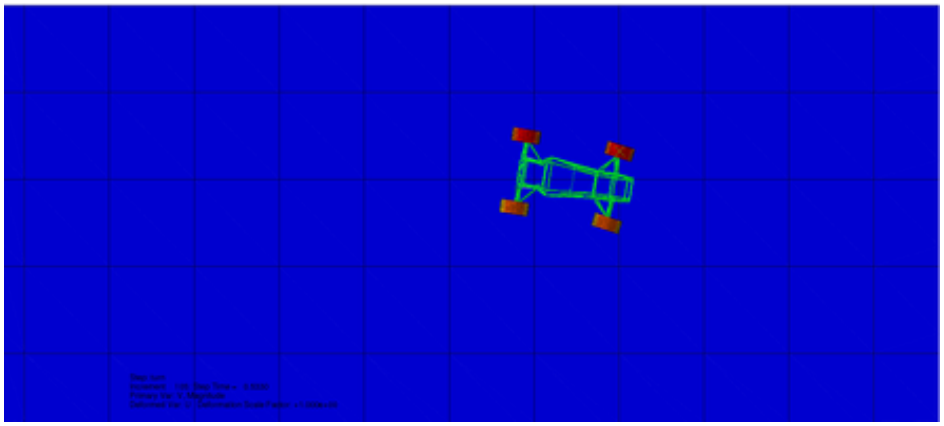

Figure 6.22: Rolling tire model 0.50 seconds into the turn step.

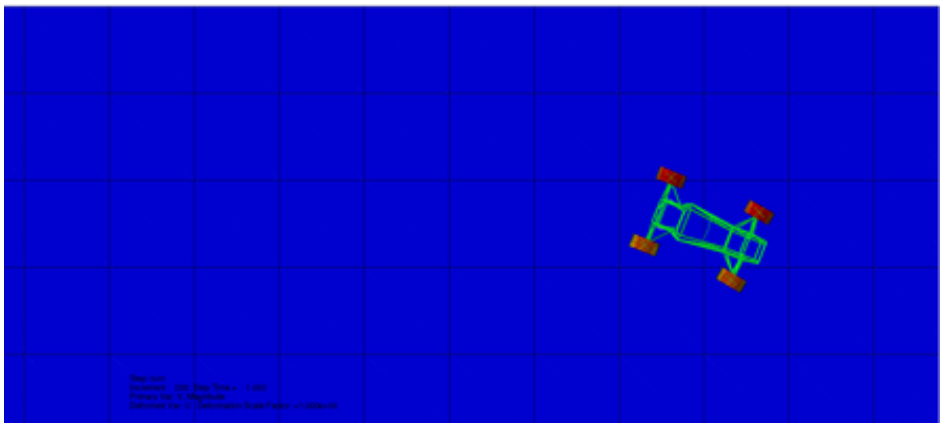

Figure 6.23: Rolling tire model 1.00 seconds into the turn step.

the wheel speeds necessary for the turn. As the rear wheels do not follow the same track as the front wheels through the turn, they shouldn't have the same velocity. The spring displacements show an initial roll state like the connector tire, but there was also a pitching motion at the beginning of the turn.

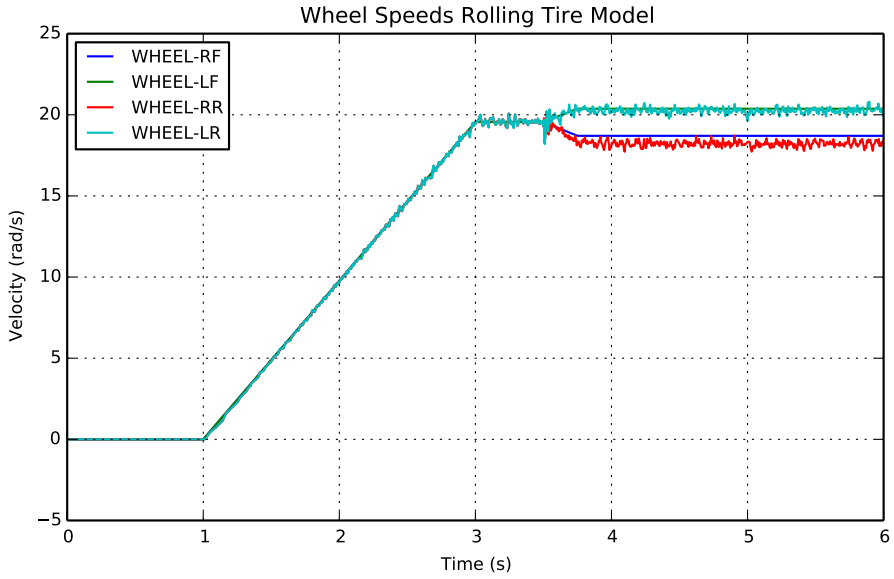

Figure 6.24: Rolling tire model rotational velocity.

The pitching motion comes from a slight dip in overall vehicle speed at the beginning of the turning maneuver when the wheel speeds are being changed. Figure 6.26 shows the overall vehicle speed throughout the analysis. The pitching motion was absent from the connector tire model because there was more direct control of vehicle speed in prescribed boundary conditions. In the connector model the velocities were explicitly prescribed at the ground nodes, where in the rolling model the rotational velocities of the wheels are prescribed.

In Senatore's [22] work he saw a slight change in vehicle speed and pitch angle during a constant speed double-lane-change maneuver. The beginning of the lane change maneuver and the turning maneuver are similar in nature. It is reasonable to assume that the overall vehicle reaction to the turning maneuver is consistent with what would happen in the real vehicle.

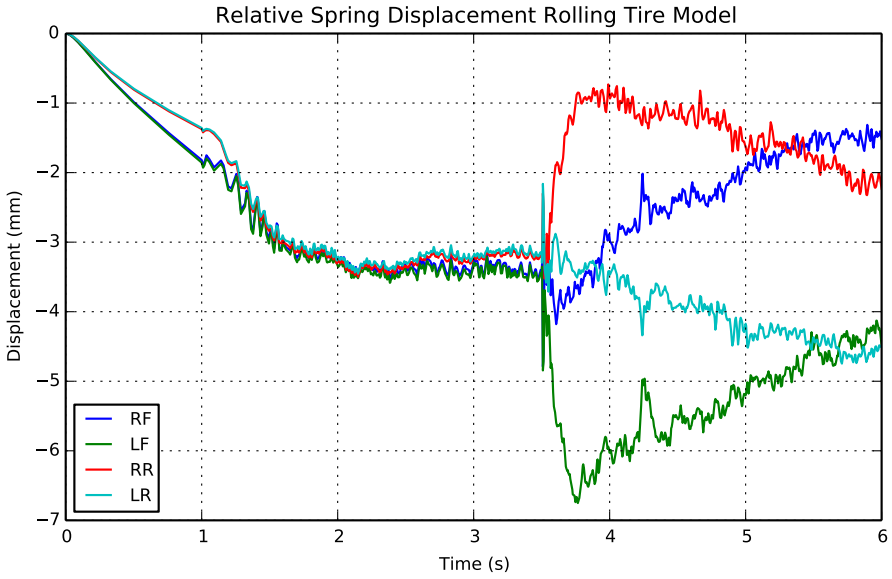

Figure 6.25: Rolling tire model relative spring motion.

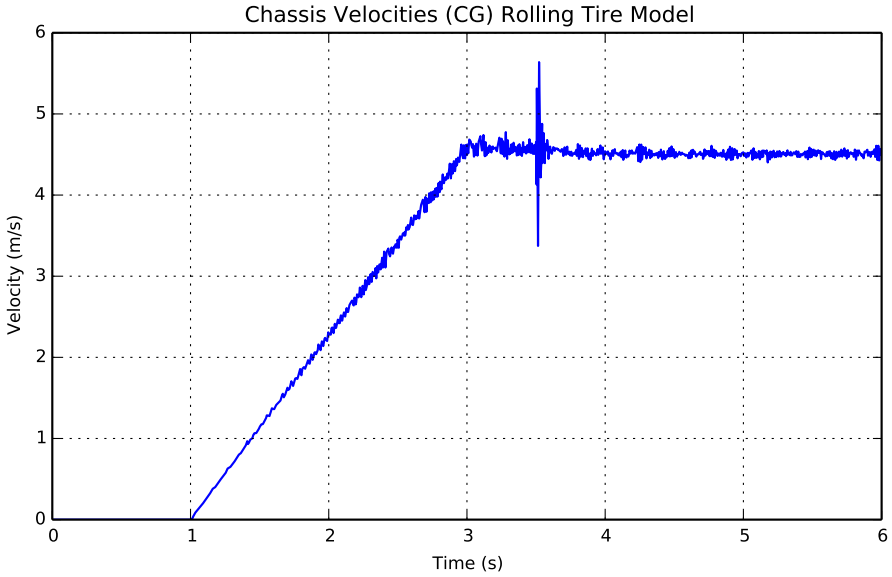

Figure 6.26: Rolling tire model vehicle speed.

Rolling Tire Turning Maneuver Conclusions

Currently the rolling tire model can accelerate up to speed using either prescribed rotational velocities at the tire or a prescribed straight line velocity for the chassis. Either approach produces the same result, but the turn rotational velocities need to be prescribed so it makes sense to use them for the acceleration step as well. The model can turn when given new rotational velocities at the inside/outside front wheels combined with a steering input. Without an engine/differential to develop the rotations, the wheel speeds need to be calculated and prescribed for the maneuver. From afar, as if standing watching the car on the track, the turning maneuver did what it should. The vehicle reached its speed and turned when the steering and velocity inputs were ramped on. The details of the solution show a pitching motion being developed along with the roll angle before becoming entirely roll. It is believed that this behavior is representative of the actual system because the vehicle is changing direction, resulting in a change in velocity and acceleration, leading to another acceleration, the pitching motion. The important part of this turning simulation is that the overall modeling structure is in place to begin getting accurate results. The model still needs a more detailed tire model and the mass and stiffness from the engine. Will also need a mass to represent the driver as the engine and driver make up the majority of the mass of the FSAE sprung mass. Overall the modeling system is in place to begin investigating the loading scenarios that the FSAE car experiences. With the more accurate loading scenarios, assumptions can be validated or invalidated as well as more efficient structures can be designed.

Chapter 7

Conclusions/Future Work

7.1 Conclusions

From the literature Riley and others have established a base for analyzing the FSAE chassis using static torsional stiffness, while evaluating the dynamics of the vehicle using rigid body simulation software. Efforts are made to derive solutions to determine when the chassis is considered "stiff enough" to be used in the software. However, there are no published data on evaluating the elastic chassis from loading scenarios developed from the vehicle maneuvers. While designing the steel space frame chassis with respect to vehicle maneuvers should be done, it is extremely important when considering integrated composite structures. As shown in Chapter 2, the orientation of the composite fibers has a dramatic impact on its ability to carry load.

In Chapter 4 the static and modal components of the chassis-suspension system were investigated. Static actuation of the suspension was performed in Abaqus to verify the suspension modeled with connector elements moved as designed using motion ratios. Chapter 4 also discusses how looking only at static torsional stiffness or torsional natural frequency does not provide enough information to design the chassis to carry loads from vehicle maneuvers. The static stiffness analysis did provide a good tool for evaluating the static stiffness of the chassis models when considered as a distribution rather than a single value. When compared to the distribution of the *Rigid* model, the design team has a goal to approach in each section of the chassis. The natural frequencies provide an estimate of the efficiency of the added stiffness in the chassis due to the mass/inertia components. The natural frequencies also provide an estimate of the interaction of the chassis and suspension components by evaluating the separation of similar mode shapes. Maximizing the separation is the goal in the modal design phase, though an exact amount of separation needed cannot be determined without testing.

Chapter 4 also shows how when tailored to a particular deflection shape, composite structures

can be much stiffer than classical materials. In Chapter 4 the composite chassis models began to approach the static stiffness of the *Rigid* model, while increasing the natural frequencies by at least 20 Hz at each mode. In the case of the *C2012* model, where the composite was not designed to be anything more than a quasi-isotropic panel, there was no change in torsional frequency, while it did increase the static torsional stiffness. By not tailoring the structure, the floor did add some stiffness, but added a proportional amount of mass, resulting in an inefficient use of material.

In Chapter 6 the framework was established to model the straight and non-straight line dynamics of the moving vehicle. Gravity and velocity responses were evaluated to verify that the vehicle was reacting loads appropriately and able to accelerate up to speed successfully. The gravity step was verified by comparing z-direction reaction forces at the ground nodes with calculations derived from statics. The velocity steps were evaluated on how well the vehicle followed the prescribed amplitude curve. The acceleration was designed to be extremely small and the spring results showed little to no pitching motion while accelerating to the prescribe velocity.

The bump model described in Section 6.1 represents the model's ability to actuate the suspension dynamically while moving the rest of the vehicle. The results showed that the suspension actuated as expected for a vehicle going over a bump and the chassis had the pitching motion associated with such an event. There was a delayed reaction in suspension behavior due to the limitations of the spring/damper formulation of the tire element in the bump model. In the real system there is likely this same delay on the initiation of the bump, though not as pronounced as in this model and the delay on the downward track of the bump likely does not occur. This behavior could likely be tweaked with changes made to the spring/damping coefficients and formulations for the tire, but the overall framework of the bump model replicated what would be expected in a bump situation.

While the bump model focused on the straight line dynamics Section 6.2 focused on turning maneuvers of the vehicle. It was determined that a slow constant-speed-constant-radius turn would be the best maneuver to start with. It provides an opportunity to evaluate the system, while turning without the need to develop a particular corner and line of attack. The first approach, in Section 6.2.1, built off the connector tire model found in the bump analysis with the x and y components of velocity throughout the turn specified at the front ground nodes. While the vehicle was able to perform the turn from a top view, the details of the solution were not representative. The initial portion of the turn looked promising with a small roll angle change when the velocity vectors changed, but the suspension was no longer able to develop the loads and deflection necessary as the chassis began to pitch up throughout the rest of the turn. This behavior was likely due to the simplicity of using a single ground node to represent the tire-ground interaction and could not accurately represent the needs of the model.

To combat the issue in the connector tire representation turning model, a simple rolling tire model was developed. A rigid shell tire geometry was connected to the existing suspension

using connector elements and friction interaction between the tire and the ground caused the vehicle to move. This setup represents a more accurate model of how the system behaves. In the rolling tire model the front wheels are given a rotational velocity profile to ramp up to speed like in the connector tire model. To initiate the turn, the rotational velocity of the outside wheel (left) was increased, while the inside wheel (right) was decreased combined with a steering input to change the orientation of the tires. Unlike in the connector tire model, there is a dip in straight line velocity at the start of the turn, causing the chassis to pitch in combination with roll. As the speed returns to normal the chassis levels out. There is some literature, Senatore [22], to support this drop in velocity, giving reason to believe this may happen in the real system.

Overall the models presented in the work showcase a framework for modeling FSAE vehicle maneuvers using finite elements, but also presents a design and analysis flow for the FSAE chassis. Using parameterized models can allow for a more in-depth look at particular cases for each model as well as add flexibility to the modeling process. It was also apparent that the static stiffness and modal analysis is important in the design of the chassis, but is only a beginning step. The detailed design needs to be developed from loading scenarios derived from the maneuvers the vehicle with experience. Without these loads the chassis, whether using integrated composites or not, will either be not as efficient as possible or worse, experience failure while driving.

7.2 Recommendations

7.2.1 Tire Geometry/Properties

The accuracy of loads developed using finite elements hinges on having a serviceable tire geometry, elastic properties, and ground interaction properties. The tires control all the movement of the vehicle and the load introduced into the other components. While a framework was presented in this work that can simulate the maneuvers of the vehicle, without accurate tire models the loads developed and small details of the model will not be correct.

7.2.2 Driver/Engine Mass

While the models presented here contain the framework to replace the rigid and simplified geometry with more accurate and elastic geometry, the addition of adding the driver and engine mass needs to be addressed. The engine and driver make up a large component of the system's mass and need to be included for accurate mass distribution and load generation. The engine would likely be the most straightforward to add to the model once the geometry is generated, as there is already structure in place on the chassis to accommodate the engine. The engine should also be considered a soft body for the purposes of the simulations as the

engine is not used as a stressed member. By modeling the engine as a soft body it will be unable to transfer load in the chassis, forcing the chassis design to be stiff around the engine to protect the engine from excessive load. A long term goal would be to accurately determine the elastic nature of the engine to better understand how it effects the chassis structure.

Incorporating the driver will likely be more difficult and will likely need to be defined using percentile body compositions found in the literature. Another obstacle will be how to restrain the driver in the model. The restriction of driver movement in the vehicle not only relies on the five-point racing harnesses but also the rigidity of the seat and the amount of room the driver has in the seat. This restriction is also limited mainly to the torso and does not restrict the arms, legs, or head of the driver. Fortunately, the typical chassis design tries to limit the amount of free space around the driver and/or the template specifying the minimum size of the driver area. The combination of restrictions means the driver mass is not likely to move far enough to significantly alter the loading scenarios and could be kept tied in its initial orientation. If movement was deemed critical, springs and dampers could be connected from the body to the chassis to allow the body geometry to move.

7.2.3 Test Data

The simulated maneuvers and the loads developed from them are not helpful until they are verified against data. Complex maneuvers will likely be the hardest to verify, therefore it might make more sense to evaluate each component separately. Using strain gages on suspension members as well as chassis members in combination with wheel speed sensors, motion potentiometers on the springs and steering rack, and using a GPS sensor near the car CG would likely be enough to correlate the simple maneuvers. Using the wheel speed and steering rack sensors skidpad, acceleration, single wheel bump and simple turns could be recreated in finite elements and compare the spring displacements and strains developed. Of course other sensors, like slip angle, could be incorporated into the tests and validate other details of the model. It will be important to coordinate the sensors used on the car during physical testing with those used in the model. It is important to compare the same type of data at the same locations. The same signal processing routines and methods used on the track data should be used on the finite element data as well, as both data sets are time series data sets.

7.2.4 Critical Maneuvers

The maneuvers presented in this work are not likely to be critical loading scenarios for the vehicle as it is unlikely the vehicle will drive straight over a bump with both wheels or the slow gradual turn will break the car. Other scenarios need to be run to determine the critical scenarios and design the car to handle those scenarios. There will not be enough time in the design phase to evaluate every vehicle in every possible scenario, but determining which

scenarios are the most critical will allow for faster design times by evaluating the vehicle against the most important scenarios.

When critical scenarios are identified, efforts will need to be made to break them down into dynamic load cases that can be used without the need to simulate the entire maneuver. The run times for the models presented here, are relatively small compared to accurate tire models with engine and driver mass, already can be computationally expensive making running every design possibility through the maneuvers impractical. Load cases need to be developed, that are rooted in the simulated maneuvers, to evaluate the designs until there are a few enough to run through the entire simulation.

7.2.5 Integrated Composites

When loading scenarios have been developed and verified, they can then be used to properly design integrated composite structures. The composites can be tailored to not only be stiff in twist and bending for natural frequency response, but also to transfer loads introduced into the chassis from the suspension. By designing the composite to handle the critical driving scenarios and load cases with some consideration to the minor cases, the composite will be more effective than trying to design the composite to handle every scenario equally.

The previously mentioned recommendations are for expanding and improving upon the vehicle maneuvers simulation, but there are some next steps and recommendations that apply directly to the use of integrated composite structure design. The following list represents the measures that need to be in place for effectively designing the composite structures:

1. Composite material characterization to build material models in finite elements.
2. Structural optimization routines.
3. Close the loop on the design and test.
4. Fabrication facilities and procedures.

All of the items listed above are important, but the material characterization would probably be considered the most important. Without material models for the composite structures, the entire design process falls apart. While there are material data sheets published, much can be learned from performing the tests. Verification of models in finite elements at the top of the list, but also a measure of installed properties. The installed properties ties into the fabrication facilities and procedures. The entire manufacturing process of the composite structures need to be standardized within the team structure to ensure not only quality structures are produced, but consistently as well. The team needs to be confident that structures they design will be built with the same properties the models have.

Structural optimization routines will become increasing beneficial when designing integrated composite structures. Everything from overall shape, to fiber orientations, and stack sequences will need to be investigated. Trade offs will need to be evaluated systematically and consistently. The structural optimization will become more effective when the loop on design and testing is closed. If the design is not or cannot be verified with testing, the optimization will suffer. The trade-offs the optimization routines evaluate rely on the accuracy of the data it uses to make decisions.

The process for improving the vehicle simulations and composite design methods can and should be done in parallel. The vehicle simulations will help with the design of any FSAE vehicle regardless of material used. Working towards a more complete composite structure design process will also aid the entire vehicle as it forces the design team to fully understand all the loads associated with the vehicle.

Bibliography

[1] MatWeb Material Property Data.

[2] L. T. Borg. An approach to using finite element models to predict suspension member loads in a formula sae vehicle. Master's thesis, Virginia Polytechnic Institute and State University, 2009.

[3] A. Crocombe, E. Sampe, and A. Somiotti. Chassis Torsional Stiffness: Analysis of the Influence on Vehicle Dynamics. *SAE 2010 World Congress & Exhibition*, 2010.

[4] I. M. Daniel, O. Ishai, I. M. Daniel, and I. Daniel. *Engineering mechanics of composite materials*, volume 2006. Oxford university press New York, 1994.

[5] D. J. Ewins. *Modal Testing: Theory and Practice (Engineering Dynamics)*. Research Studies Pr, 1984.

[6] M. Grujicic and H. Marvi. The effect of up-armoring of the high-mobility multi-purpose wheeled vehicle (HMMWV) on the off-road vehicle performance. *Multidiscipline Modeling in Materials and Structures*, 6(2), 2010.

[7] A. Hellman. Simulation of complete vehicle dynamics using FE code Abaqus. Master's thesis, LuleåUniversity of Technology, 2008.

[8] Hexcel. HexWeb® A1 and A10 Product Data.

[9] M. W. Hyer. *Stress analysis of fiber-reinforced composite materials*. DEStech Publications, Inc, 2009.

[10] R. N. Jazar. *Vehicle Dynamics: Theory and Application*. Springer, 2008.

[11] S. Jenq, G. Hwang, and S. Yang. The effect of square cut-outs on the natural frequencies and mode shapes of GRP cross-ply laminates. *Composites Science and Technology*, 47(1):91–101, Jan. 1993.

[12] C. Kassapoglou. *Design and Analysis of Composite Structures: With Applications to Aerospace Structures*. Aerospace Series. Wiley, 2011.

[13] H. H. Mabie and C. F. Reinholtz. *Mechanisms and dynamics of machinery*. Wiley, 1987.

[14] C. Michael and P. David. *Racing and Sports Car Chassis Design*. London, UK: BT Batsford Ltd, 1966.

[15] W. Milliken, D. Milliken, and L. Metz. *Race car vehicle dynamics*. Number v. 1 in R: Society of Automotive Engineers. Society of Automotive Engineers, 1995.

[16] R. Mueller. Full vehicle dynamics model of a formula SAE racecar using ADAMS/Car. Master's thesis, Texas A&M University, 2005.

[17] D. J. Peery and J. J. Azar. *Aircraft structures*. McGraw Hill, 1982.

[18] B. Riley. Design and Analysis of Vehicular Structures. Master's thesis, Cornell, 2000.

[19] W. B. Riley and A. R. George. Design, Analysis and Testing of a Formula SAE Car Chassis. Technical report, Dec. 2002.

[20] SAE International. 2013 Formula SAE Rules. 2013.

[21] G. Savage. Composite Materials Technology in Formula 1 Motor Racing. *f1-forecast.com*, 1(July 2008):1–31.

[22] C. Senatore. *Prediction of mobility, handling, and tractive efficiency of wheeled off-road vehicles*. PhD thesis, Virginia Polytechnic Institute and State University, 2010.

[23] Simulia. Abaqus Technology Brief Aircraft Landing Gear Simulation using Abaqus / Explicit. (December):1–4, 2010.

[24] W. W. T. Steed. Torsional Stiffness Measuring Machine (TSMM) and Automated Frame Design Tools. Master's thesis, University of Cincinnati, 2010.

[25] D. Systemes. 6.13 documentation. *Abaqus Documentation, Providence, RI, USA*, 2013.

[26] L. L. Thompson, P. H. Soni, S. Raju, and E. H. Law. The Effects of Chassis Flexibility on Roll Stiffness of a Winston Cup Race Car. Technical report, Nov. 1998.

Appendix A

Material Properties

Table A.1: AS-4 3501-6 Material Properties

E_1	147.0 GPa
E_2	10.30 GPa
E_3	10.30 GPa
ν_{12}	0.27
G_{23}	3.70 GPa
G_{13}	7.00 GPa
G_{12}	7.00 GPa
ρ	1.6E-6 kg/mm^3

Table A.2: Hexcel A1-64-6 Honeycomb Material Properties

E_1	2.0 MPa
E_2	2.0 MPa
E_3	190.0 MPa
ν_{23}	0.01
ν_{13}	0.01
ν_{12}	0.2
G_{23}	2.0 MPa
G_{13}	55.0 MPa
G_{12}	33.0 MPa
ρ	6.4E-8 kg/mm^3

Table A.3: Steel Material Properties

E	204774.283 MPa
ν	0.29
ρ	7.86E-06 kg/mm^3

Table A.4: Aluminum Material Properties

E	68947.570 MPa
ν	0.33
ρ	2.70E-06 kg/mm^3

Appendix B

Example Abaqus Scripting Code

```
** Front Bulkhead, name=FB
48.,  5.,   6.5
48.,  5.,  -6.5
48., -5.,  -6.5
48., -5.,   6.5
**-----------------------------------------
** Mid Bulkhead, name=FH
32.,  6,   7.
32.,  6,  -7.
32., -6,  -7.
32., -6,   7.
**-----------------------------------------
** Mid Bulkhead, name=MH
12.,  7.,   7.5
12.,  7.,  -7.5
12., -7.,  -7.5
12., -7.,   7.5
**-----------------------------------------
** Rear Bulkhead, name=RB
0.,  5.,   6.5
0.,  5.,  -6.5
0., -5.,  -6.5
0., -5.,   6.5
**-----------------------------------------
```

Figure B.1: Example chassis node file.

```
** Front Bulkhead, name=FB
FB,1,FB,2,625035
FB,2,FB,3,625035
FB,3,FB,4,625035
FB,4,FB,1,625035
**-----------------------------------------
** Front Hoop, name=FH
FH,1,FH,2,625035
FH,2,FH,3,625035
FH,3,FH,4,625035
FH,4,FH,1,625035
**-----------------------------------------
** Main Hoop name=MH
MH,1,MH,2,625035
MH,2,MH,3,625035
MH,3,MH,4,625035
MH,4,MH,1,625035
**-----------------------------------------
** Rear Bulkhead, name=RB
RB,1,RB,2,625035
RB,2,RB,3,625035
RB,3,RB,4,625035
RB,4,RB,1,625035
**-----------------------------------------
** Connection, name=CONNECT
FB,1,FH,1,625035
FB,2,FH,2,625035
FB,3,FH,3,625035
FB,4,FH,4,625035
FH,1,MH,1,625035
FH,2,MH,2,625035
FH,3,MH,3,625035
FH,4,MH,4,625035
MH,1,RB,1,625035
MH,2,RB,2,625035
RB,3,MH,3,625035
RB,4,MH,4,625035
**-----------------------------------------
```

Figure B.2: Example chassis line file.

Listing B.1: Example python function to build part of Abaqus model.

```
from abaqusConstants import *
import part, material, section
import os, sys, mathTools
import numpy as np

def drawLines(p,points,lines,sections):
        # p is the part
        # points is the dictionary of points.... points[name] = coords
        # lines is the dictionary of lines
        # lines[name] = [key1,point1,key2,point2,sectionKey]
        # sections is a dictionary of section names
        for j in lines:
                p1 = points[j[0]][j[1]]
                p2 = points[j[2]][j[3]]
                sectName = sections[j[-1]]
                vec = np.abs(np.array(p2)-np.array(p1))
                q = vec.argmin()
                if q==0:
                        bv = (1.,0.0,0.0)
                elif q==1:
                        bv = (0.0,1.0,0.0)
                else:
                        bv = (0.0,0.0,1.0)
                newEdge = p.WirePolyLine(mergeWire=OFF, meshable=ON, points=(p1,p2))
                m = p.getFeatureEdges(newEdge.name)
                a = map(str,j[0:-1])
                b = '_'.join(a)
                p.Set(name=b,edges=m)
                cR = p.sets[b]
                p.SectionAssignment(region=cR,sectionName=sectName)
                p.assignBeamSectionOrientation(region=cR,method=N1_COSINES,n1=bv)
                n1 = j[0]+str(j[1])
                n2 = j[2]+str(j[3])
                p.Set(name=n1,vertices=p.vertices.findAt((p1,)))
                p.Set(name=n2,vertices=p.vertices.findAt((p2,)))
        p.Set(name='All_Tubes',edges=p.edges)
        nodeSets = 'All_Tubes'
        return nodeSets
```

```
**------------------------------------------------------------------
** PARAMETERS
*include, input=../inps/parameters.inp
**------------------------------------------------------------------
** PARTS
*include, input=../inps/chassis_f_part.inp
*include, input=../inps/suspension_parts.inp
**------------------------------------------------------------------
** ASSEMBLY
*Assembly, name=Assembly
*include, input=../inps/chassis_instance.inp
*include, input=../inps/suspension_assembly_base.inp
*include, input=../inps/springs_visual.inp
*include, input=../inps/tire.inp
*include, input=../inps/tire_visual.inp
*End Assembly
**------------------------------------------------------------------
** MATERIALS
*include, input=../inps/materials.inp
**------------------------------------------------------------------
** AMPS
*include, input=../inps/vamps.inp
*include, input=turn_amps.inp
**include, input=../inps/rack_amp.inp
**------------------------------------------------------------------
** SUSPENSION BOUNDARY CONDITIONS
*include, input=../inps/connectorBehavior.inp
*include, input=../inps/tireBehavior.inp
**------------------------------------------------------------------
** STEPS
*include, input=../inps/gravity_step.inp
*include, input=../inps/steer_step.inp
*include, input=../inps/velo_turn_step.inp
```

Figure B.3: Example Abaqus input file.

Appendix C

Figure Permissions

VirginiaTech
Invent the Future

Nicholas Angelini <nangel@vt.edu>

WG: Request Permission to use figures in thesis

Essenpreis, Alice, Springer DE <Alice.Essenpreis@springer.com> Thu, Oct 31, 2013 at 9:27 AM
To: "nick.angelini@vt.edu" <nick.angelini@vt.edu>

DATE: October 31, 2013

SPRINGER REFERENCE

Vehicle Dynamics: Theory and Application. 2008
Authors: Reza N. Jazar
ISBN: 978-0-387-74243-4
Figures: 2.1, 2.7, 3.2, 3.3, 3.4, 7.1, 7.3, 7.3, 7.6, 7.7, 7.13

YOUR PROJECT
University:

Title: Simulating Vehicle Maneuvers With Finite Elements To Create Loading Scenarios For Design of Integrated Composite Structures On FSAE Chassis
Dissertation/Thesis

Hello,

With reference to your request to reuse material in which Springer Science+Business Media controls the copyright, our permission is granted free of charge under the following conditions:

Springer material
• represents original material which does not carry references to other sources (if material in question refers with a credit to another source, authorization from that source is required as well);
• requires full credit (book title, year of publication, page, chapter title, name(s) of author(s), original copyright notice) is given to the publication in which the material was originally published by adding: "With kind permission of Springer Science+Business Media";
• may not be altered in any manner. Any other abbreviations, additions, deletions and/or any other alterations shall be made only with prior written authorization of the author and/or Springer Science+Business Media.

This permission
• is non-exclusive;
• is valid for one-time use only for the purpose of defending your thesis and with a maximum of 100 extra copies in paper.
• includes use in an electronic form, provided it is an author-created version of the thesis on his/her own website and his/her university's repository, including UMI (according to the definition on the Sherpa website: http://www.sherpa.ac.uk/romeo/);
• is subject to courtesy information to the corresponding author;
• is personal to you and may not be sublicensed, assigned, or transferred by you to any other person without

VirginiaTech
Invent the Future

Nicholas Angelini <nangel@vt.edu>

RE: Form Submission- Contact Us

Anthony A. Deraco <aderaco@destechpub.com> Fri, Oct 18, 2013 at 3:55 PM
To: nick.angelini@vt.edu

Dear Nick:

We grant you permission to use the figures you requested for your Master's Thesis and ask that you list credit with each Figure used from the Book. The wording should include:

This figure reprinted from *Stress Analysis of Fiber-Reinforced Composite Materials*, by Michael Hyer. Copyright 2009. Lancaster, PA: DEStech Publications, Inc.

Regards,

Anthony A. Deraco

President

DEStech Publications, Inc.

439 North Duke Street

Lancaster, PA 17602-4967

Toll Free: 877-500-4337

Tel: 717-290-1660

Fax: 717-509-6100

E-Mail: aderaco@destechpub.com

From: Nick Angelini [mailto:nangel@vt.edu]
Sent: Friday, October 18, 2013 2:31 PM
To: Anthony A. Deraco
Subject: Re: Form Submission- Contact Us